

Numerical Modelling and Optimization of air gap Membrane Distillation

Martijn Bindels
Bart Medaer

Supervisor: Prof. Mekonnen G. Gebrehiwot

Co-supervisor: *Bart Nelemans MSc*

Master's Thesis submitted to obtain the
degree of Master of Science in Engineering
Technology: Electromechanical Engineering

Academic year 2018-2019

FACULTY OF ENGINEERING TECHNOLOGY

GROUP T LEUVEN CAMPUS

Numerical Modelling and Optimization of air gap Membrane Distillation

Martijn Bindels

Bart Medaer

Supervisor: Prof. Mekonnen G. Gebrehiwot

Co-supervisor: *Bart Nelemans MSc*

Master's Thesis submitted to obtain the
degree of Master of Science in Engineering
Technology: Electromechanical Engineering

Academic year 2018-2019

© Copyright KU Leuven

Without written permission of the supervisor(s) and the author(s) it is forbidden to reproduce or adapt in any form or by any means any part of this publication. Requests for obtaining the right to reproduce or utilise parts of this publication should be addressed to KU Leuven, Groep T Leuven Campus, Andreas Vesaliusstraat 13, B-3000 Leuven, +32 16 30 10 30 or via email fet.groept@kuleuven.be.

A written permission of the supervisor(s) is also required to use the methods, products, schematics and programs described in this work for industrial or commercial use, and for submitting this publication in scientific contests.

Acknowledgements

During a whole year we worked on this master thesis, the foam on top of our master program. We worked hard to achieve the result you can see here. However, this master thesis was not possible without some help. Therefore, we want to thank them.

The first person we want to thank is our promoter Prof. Mekonnen G. Gebrehiwot. In the beginning of our thesis we did not know each other. However, it quickly became clear that it was going to be pleasant to work with Mr Gebrehiwot. It was pleasing to see that he was enthusiastic and saw potential in the topic. Mr. Gebrehiwot started almost immediately reading about the topic which was nice for having discussions about our thesis. Another thing we want to thank Mr Gebrehiwot for is the freedom that he gave us. It was nice that he gave us time to work on interesting things.

The second person we want to thank is our co-promoter Mr Bart Nelemans. We are very grateful that he gave us the opportunity to work on this interesting topic. In addition, we want to thank him for the freedom that he gave us. For example, we were free to work on ourselves and had no intermediate deadlines. Thank you for your trust in us!

During the year we went a couple of times to Aqua|still in the Netherlands to discuss our work with Mr Nelemans. During the meeting you gave us critical comments on our work, which were correct and well explained. For us you were, as you said a couple of times not the devil's advocate, but an inspiration for us to constantly improve our work. Thank you for that!

Mr Nelemans is not the only one who helped us with our thesis at Aqua|still. Mr Niels Brand helped us to collect the data that was needed for the validation of the models. Actually, we want to thank everyone at Aqua|still! You guys are doing a fantastic job and we hope that Aqua|still can grow even further in the future.

We also want to thank our family. The last couple of years were very hard for us because we worked a lot for our studies. Therefore, we did not have a lot of time for our family. However, they always supported us with our decisions and helped us when it was needed. We want to thank you very much for always being there for us!

And as last but not least, we want to thank our friends that we made along the way. It would not be possible to have a fun education without them.

Abstract

De nood aan drinkbaar water gaat alleen maar stijgen door de toenemende wereldbevolking. Desondanks dat onze aardeoppervlak voor 70% uit water bestaat is slechts een beperkte hoeveelheid drinkbaar. Een mogelijke oplossing voor dit probleem is het ontzouten van zeewater. Een opkomende technologie hiervoor is membraandestillatie. In de meest eenvoudige configuratie wordt een warme oplossingsstroom gescheiden van een koude permeaat stroom door een hydrofoob membraan. Het temperatuurverschil zorgt voor een verschil in dampdruk over het membraan. Dit resulteert in een massatransport van waterdamp door het membraan. De waterdamp ontstaat door de verdamping van de warme stroom aan het membraan. Door de hydrofobe eigenschappen van het membraan kan enkel waterdamp door het membraan. Vervolgens gaat de damp condenseren in de koude permeaat stroom.

Deze thesis bestaat uit twee delen. Voor deze beide delen is er samengewerkt met Aqua|still.

In deel A is het doel om de procescondities en materiaaleigenschappen te vinden waarbij de destillaatproductie wordt gemaximaliseerd. De optimalisatie zorgt ervoor dat restwarmte van bijvoorbeeld een elektriciteitscentrale zo efficiënt mogelijk wordt benut. Vandaag wordt de laagwaardige warmte vaak niet meer gebruikt doordat het een laag Carnot rendement heeft. Voor het vinden van het globale optimum is er gebruik gemaakt van 'simulated annealing'.

De optimale proces condities voor membraan destillatie zijn 30.28°C , 90°C , 0 g/kg and 10 kPa voor de condenser toevoer temperatuur, membraan toevoer temperatuur, zoutconcentratie en de druk in de 'air gap'. De massa en warmteoverdracht parameters moeten verdubbeld worden om het optimum te bereiken. Dit is in tegenstelling tot de massa overdracht van de 'air gap' want deze moet gehalveerd worden om het optimum te bereiken.

In het tweede deel namelijk deel B is er een dynamisch model gebouwd. Met een dynamisch model is het mogelijk om de geproduceerde hoeveelheid destillaat te voorspellen wanneer de procescondities fluctueren. Veranderende procescondities ontstaan bijvoorbeeld wanneer er gebruik gemaakt wordt van hernieuwbare energiebronnen.

In deze thesis zijn drie mogelijke manieren van modelleren gekozen. De eerste manier van modelleren is gebaseerd op de regressieformule uit deel A. Hier worden de kortstondige effecten verwaarloosd om zo de hoeveelheid geproduceerd destillaat te berekenen voor kleine tijdstappen. De tweede manier van modelleren is gebaseerd op de analogie tussen thermische en elektrische netwerken. In voorgaand onderzoek is dit al toegepast op andere configuraties maar nu wordt het voor het eerst ook toegepast op 'air gap membrane distillation'. Het derde model maakt gebruik van partiële differentiaal en algebraïsche vergelijkingen. Dit is in het verleden al gebuikt maar nooit voldoende gevalideerd. In deze thesis is buiten de implementatie ook de validatie gedaan van de verschillende modellen. Het valideren van de modellen is zowel gedaan voor een statische ingang als voor een dynamische ingang.

De regressie en de energiebalans vergelijkingen geven de beste resultaten voor zowel statische als dynamische ingang. De thermische elektrische netwerken zorgen voor onnauwkeurige resultaten voor zowel een statische als dynamische ingangen. Hierdoor kan er geconcludeerd worden dat het regressie model het beste is door de eenvoud en door de accuraatheid van het model.

Extended Abstract

Water is used in many different domains. For example, the industry uses water to produce steel, tires and computers. Moreover, the agricultural sector is the biggest water consumer in the world. The current world population will grow by at least 30% in the next 30 years. Which will stress the current freshwater supply. Despite that the earth consist of 70% water, only a fraction of this is potable. A possible solution to water scarcity is seawater desalination. There are a lot of techniques to desalinate seawater. An upcoming technology to desalinate water is membrane distillation (MD). The simplest configuration is direct contact membrane distillation which consist of a hot liquid feed solution and a cold permeate solution which are separated by a hydrophobic semipermeable membrane. Due to the temperature difference of the two fluids there is a vapour pressure difference over the membrane. This results in mass transport of water vapour through the membrane. The vapour comes from the evaporation of the feed liquid at the boundary of the membrane. Due to the hydrophobic nature only water vapour can go through the membrane.

This thesis consists of two major parts. The purpose of part A is to identify the optimum process conditions and material properties to achieve the highest production of distillate. Due to the low Carnot efficiency there is low grade heat that is not used to produce electricity when using conventional power sources. However, the temperature of this waste heat is still high enough to produce water with membrane distillation. This results in a lower water footprint of the powerplant. To use this waste heat wisely the process conditions and the materials need to be as best as possible. There are two methods for finding the optimum process conditions and materials for a vacuum air gap membrane distillation module. The first methodology, response surface methodology, is better than the conventional experiments that change one parameter while the others are kept constant. Response surface methodology is better since it is less time consuming and exposes interaction effects between different parameters. On the other hand, it is hard to find a global optimum when there are a lot of parameters. Therefore, another methodology is needed.

In the first step, a design space with 12 parameters was created by using a space filling design method. Maximum projection method was chosen because this was found to be the best overall method. This design space was then used as an input for the existing Aqua|still model. The obtained flux gained output ratio, $Q_{heating}$ and $Q_{cooling}$ are used to create multiple second-order regression formula. After the creation of the regression formula, it was necessary to check the model adequacy to make sure that the regression correspond with the physical system. Residual analysis was used in this thesis to check the model adequacy as this is an effective method. Simulated annealing, an optimum seeking algorithm, was then used to find the optimum parameters for membrane distillation.

The optimum process conditions were found to be 30.28°C, 90°C, 0 g/kg and 10 kPa for the condenser inlet temperate, membrane inlet temperature, salinity and air gap pressure respectively. All of the mass and heat transfer parameters should increase two times to find the optimum. However, the mass transfer of the air gap should be halved to reach the optimum.

In part B, three dynamic models were made to predict the distillate production when the process is not steady state. This was done because MD can be used with green energy sources. For example, MD can be used in combination with solar pond, wind energy and geothermal energy. However, the prior mentioned energy sources do not have a constant

energy production. This results in a dynamic behaviour of the hot feed side. Consequently, there is a dynamic distillate output.

Three ways of modelling were chosen. The first way is based on the regression formula found in part A. This method neglects the transient effects because it can be assumed that these effects are insignificant. The second way of modelling was by using a thermal electrical network (TEN). An electrical network was developed where the electrical laws were used to model the system. The third method, the energy balances equation (EBE) model, uses energy balances and is based on the thermodynamic laws. After the creation of the models it is necessary to validate the models. Validation is done with steady state and dynamic data.

The steady state behaviour of the models was found to be sufficient. However, the dynamic behaviour of the systems shows good results with the regression and EBE-model but bad results in the thermal electrical network. The regression formula was found to be the best as it was the most simplistic to use and has a low error. During the modelling it was found that more research is needed to properly model the air gap.

Keywords: Membrane distillation, Regression, Simulated annealing, Modelling, Experiments

TABLE OF CONTENTS

Acknowledgements	iii
Abstract	v
Extended Abstract	vii
List of Symbols	xii
List of Acronyms	xv
1 Introduction	19
1.1 <i>Desalination by reverse osmosis</i>	19
1.2 <i>Desalination by membrane distillation</i>	20
1.3 <i>Applications of membrane distillation</i>	22
1.3.1 Low grade heat	22
1.3.2 Green energy	22
1.4 <i>Thesis goals</i>	23
1.5 <i>Overview of the thesis</i>	23
2 Introduction to membrane distillation	25
2.1 <i>Construction of a membrane distillation module</i>	25
2.1.1 Construction of a plate and frame module.....	25
2.1.2 Spiral wound modules.....	25
2.2 <i>Modelling of membrane distillation</i>	27
2.2.1 Introduction to the modelling of membrane distillation	28
2.2.2 Heat transfer	29
2.2.3 Mass transfer	32
Part A	37
3 Optimum seeking methods	39
3.1 <i>Response surface methodology</i>	39
3.1.1 Literature.....	39
3.2 <i>Methodology for finding the optimum</i>	40
3.2.1 Space filling designs	40
3.2.2 Data acquisition	43
3.2.3 Multiple second order regression model.....	43
3.2.4 Heuristics methods for finding the optimum.....	46
3.2.5 Conclusion	49

4	Optimum parameters of membrane distillation.....	51
4.1	<i>Space filling design</i>	51
4.2	<i>Regression model</i>	52
4.3	<i>Simulated annealing.....</i>	55
4.4	<i>Conclusions</i>	57
5	Conclusions part A	59
	Part B	61
6	Dynamic modelling of air gap membrane distillation	63
6.1	<i>Regression-based model</i>	63
6.2	<i>Thermal electrical networks.....</i>	64
6.3	<i>Energy balance model.....</i>	69
7	Validation of dynamic models.....	71
7.1	<i>Steady state data</i>	71
7.2	<i>Transient data</i>	72
	7.2.1 <i>Materials and methods.....</i>	72
8	Results and discussion	75
8.1	<i>Steady state validation</i>	75
	8.1.1 <i>Regression model</i>	75
	8.1.2 <i>Thermal electrical network</i>	76
	8.1.3 <i>Energy balance equations model</i>	77
8.2	<i>Dynamic validation</i>	78
	8.2.1 <i>Regression model</i>	78
	8.2.2 <i>Thermal electrical network</i>	80
	8.2.3 <i>Energy balance model</i>	81
8.3	<i>Benchmarking of the models.....</i>	83
8.4	<i>Conclusion</i>	83
9	Conclusion part B	85
10	Overall conclusion and recommendations.....	87
	References.....	89
Appendix A	Regression coefficients.....	96
Appendix B	Steady state test parameters	100
Appendix C	Matrices for the thermal electrical network.....	102
Appendix D	Matrices for the energy balance equations model.....	106
Appendix E	Dynamic test conditions.....	108

Appendix F	Dynamic regression results	112
Appendix G	Thermal electrical network results	117
Appendix H	Dynamic energy balance equations results	121

List of Symbols

Nomenclature

a_w	Activity factor	[–]
c_p	Heat capacity	[J/kgK]
c_m	Calibration factor	[–]
d_f	Diameter filament spacer	[m]
d_h	Hydraulic diameter	[m]
e	Residual	[–]
h	Heat transfer rate	[W/m ² K]
h_f	Specific latent heat of evaporation	[J/kg]
k	Thermal conductivity	[W/mK]
l_m	Filament length	[m]
l_d	Discretization length	[m]
m	Mass	[kg]
\dot{m}	Mass flow rate	[kg/s]
m_{NaCl}	Molality of NaCl	[mol/kg]
q_{in}	Specific heat input	[J/kg]
r_{pore}	Membrane pore radius	[m]
t	Thickness	[m]
t_d	Discretization time	[s]
\bar{v}	Mean molecular speed	[m/s]
v_a	Solute molal volume	[m ³ /kmol]
v_{eff}	Effective crossflow velocity	[m/s]
x_l	Water fraction in the air gap	[–]
y	Relative pressure coefficient	[–]
A_m	Membrane area	[m ²]
C	Mass transfer coefficient	[kg/m ² s Pa]
C_a	Heat content of the air gap	[J/K]
C_m	Heat content of the membrane	[J/K]
D	Diffusion	[m ² /s]
D_e^k	Knudson diffusion	[m ² /s]
F_{tot}	Distillate output flow	[kg/m ²]

H_v	Latent heat of evaporation	$[J/kg]$
J	Flux	$[kg/m^2 h]$
K	Solute mass transfer coefficient	$[m/s]$
K_n	Knudsen number	$[-]$
L	Inductance	$[H]$
L_{MD}	Envelope length	$[m]$
M_w	Molecular weight of water	$[kg/mol]$
P	Pressure	$[Pa]$
P^*	Vapour pressure without vapour pressure reduction	$[Pa]$
Q	Energy	$[J]$
$Q_{heating}$	Thermal energy input of the module	$[kW]$
$Q_{cooling}$	Thermal energy output of the module	$[kW]$
R_g	Universal gas constant	$[J/mol K]$
R	Resistance	$[\Omega]$
S	Salinity	$[g/kg]$
T	Temperature	$[K]$
W	Width	$[m]$
Z	Impedance	$[\Omega]$

Greek letters

δ	Thickness	$[m]$
β	Intermediate factor	$[-]$
ε	Porosity	$[-]$
τ	Tortuosity	$[-]$
λ	Thermal conductivity	$[W/mK]$
η	Dynamic viscosity	$[Pas]$
ρ	Density	$[m^3/kg]$
θ	Spacer angle	$[^\circ]$
σ_w	Collision diameter (2.641 Å for water)	$[\text{Å}]$
ϕ	Association factor for solvent	$[-]$

Subscripts

$a, airgap$	Air gap
av	Average
aw	Water in the air gap
bf	Bulk of hot feed

<i>bp</i>	Bulk of cold feed
<i>c</i>	Condenser
<i>ca</i>	Condenser-air gap interface
<i>ch</i>	Channel
<i>cond</i>	Condensation layer
<i>cp</i>	Condenser-cold feed interface
<i>g</i>	Gas
<i>h</i>	Hot feed channel
<i>k</i>	Knudsen
<i>m</i>	Membrane
<i>ma</i>	Membrane-air gap interface
<i>m + a</i>	Membrane + air gap
<i>md</i>	Module
<i>mf</i>	Membrane-hot feed interface
<i>p</i>	Cold feed channel
<i>pore</i>	Pore
<i>s</i>	Solid
<i>sp</i>	Spacer
<i>sw</i>	Seawater
<i>tot</i>	Total
<i>w</i>	Water
<i>wa</i>	Molecular

Antoine coefficients

A	Antoine coefficient	[-]
B	Antoine coefficient	[K]
C	Antoine coefficient	[K]

Dimensionless groups

<i>Nu</i>	Nusselt's number	[-]
<i>Re</i>	Reynolds number	[-]
<i>Sh</i>	Sherwood number	[-]
<i>Sc</i>	Schmidt number	[-]

List of Acronyms

AGMD	Air Gap Membrane Distillation
DAE	Differential algebraic equation
DCMD	Direct Contact Membrane Distillation
EBE	Energy balance equations model
GOR	Gained output ratio
MD	Membrane Distillation
RO	Reverse Osmosis
RSM	Response Surface Methodology
TEN	Thermal electrical network model
V-AGMD	Vacuum assisted Air Gap Membrane Distillation

General

This thesis has two distinct parts that require the same general information. Therefore, it was chosen to divide the thesis in to two parts. More about the two parts will be explained at the end of the first chapter. Then an introduction is given to the construction and modelling of membrane distillation. The thesis ends with an overall conclusion in chapter 10.

Table of contents of general part:

1	Introduction	19
1.1	<i>Desalination by reverse osmosis.....</i>	19
1.2	<i>Desalination by membrane distillation</i>	20
1.3	<i>Applications of membrane distillation</i>	22
1.3.1	Low grade heat	22
1.3.2	Green energy	22
1.4	<i>Thesis goals.....</i>	23
1.5	<i>Overview of the thesis.....</i>	23
2	Introduction to membrane distillation	25
2.1	<i>Construction of a membrane distillation module</i>	25
2.1.1	Construction of a plate and frame module.....	25
2.1.2	Spiral wound modules.....	25
2.2	<i>Modelling of membrane distillation</i>	27
2.2.1	Introduction to the modelling of membrane distillation	28
2.2.2	Heat transfer	29
2.2.3	Mass transfer	32
10	Overall conclusion and recommendations.....	87

1 INTRODUCTION

Water is used in many different domains. Everyone uses water in their household for various tasks such as preparing food, washing and sanitation. Furthermore, the industry uses water to produce various products. For example, water is used in the production of steel, tires and computers [1]. Not only the industry uses large quantities of water, the agricultural sector is the biggest consumer of water in the world [1]. Because the current world population will grow by at least 30% in the next 30 years, this will stress the current freshwater supply [2].

The earth surface consists for 70% out of water but only a fraction of this water is potable. A possible solution to water scarcity is seawater desalination. There are a lot of techniques to desalinate seawater [3]–[6]. Reverse osmosis (RO) is the most widely used desalination technology. 300 million people worldwide received their clean water from desalination plants and more than 60% of the desalinated water is produced using RO in 2015 [7]. The subject of this thesis and a concurrent technology, membrane distillation (MD), is an upcoming technology to desalinate water. The authors of this thesis worked together with Aqua|still. Aqua|still is the leading manufacturer of spiral wound air gap membrane distillation units. RO and MD will be shortly discussed in the following paragraphs. More information about other desalination techniques can be found in [8].

1.1 Desalination by reverse osmosis

The natural phenomenon where a solution flows from the low concentration to the high concentration side through a semi-permeable membrane is called osmosis [9]. This process continues until the solution reaches a concentration equilibrium and when the osmotic pressure of the solution is equal to the pressure difference at both side of the semi-permeable membrane [9]. A schematic representation of this process can be seen in Figure 1-1.

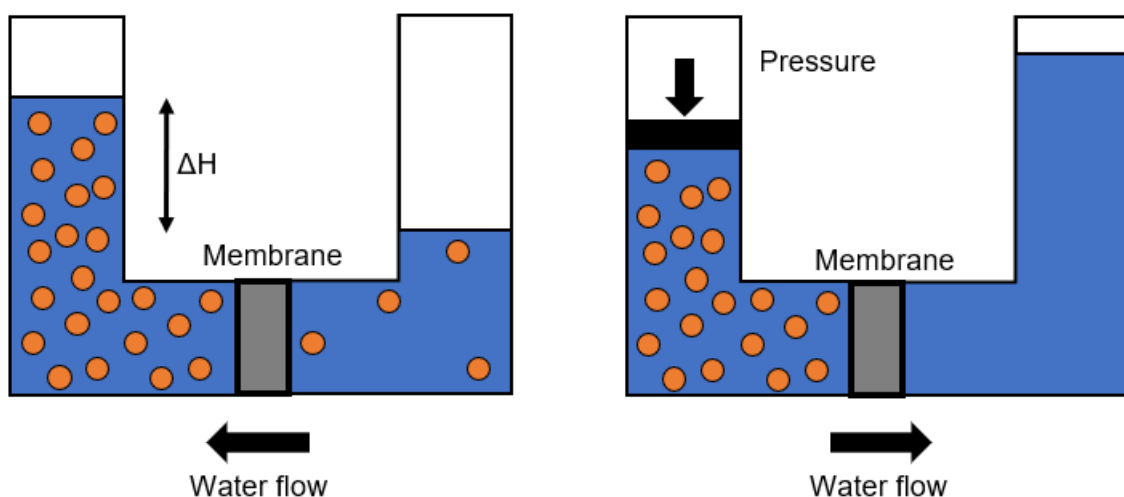


Figure 1-1 Left: Osmosis principle, Right: Reverse Osmosis principle

If the pressure on the high concentration side is higher than a certain value, the water will flow from the high concentration to the low concentration side [10]. The required pressure to reverse

the osmosis process is called the osmotic pressure, which varies between 15 to 80 bar [10]. RO can separate salt from water with a rejection rate from 98 to 99,5% [11].

Advantages of the Reverse Osmosis process [9]:

- Flexible operation mode, low operating cost, low energy consumption.
- Small area is required for high production capacity.
- Less chemicals required than other technologies.
- Environment friendly process.
- Easy to operate and low maintenance is required.

Disadvantages of the Reverse Osmosis process:

- The applied pressure needs to be in the pressure range that the membrane can resist [12].
- Single stage constant pressure reverse osmosis is energetically inefficient [13].
- High pressures [10].

1.2 Desalination by membrane distillation

MD is defined as ‘distillation process in which the liquid and gas phases are separated by a porous membrane, the pores of which are not wetted by the liquid phase’ by the International Union of Pure and Applied Chemistry in 1996 [14].

In contrast to RO, the solution goes through a phase change in the MD process [6]. Therefore, the reverse osmosis separation principle is completely different from MD methods [15]. The simplest configuration consist of a hot liquid feed solution and a cold permeate solution that are separated by a hydrophobic semipermeable membrane [16]. This method is called direct contact membrane distillation (DCMD). A schematic representation of this setup can be seen in Figure 1-2. As can be seen in Figure 1-3, there exist a vapour pressure difference due to the temperature difference over the membrane. This in turn, results in mass transport of the water vapour [16]. The vapour comes from the evaporation of the feed liquid at the boundary of the membrane. Due to the hydrophobic nature of the membrane only water vapour can go through the membrane. When the vapour has moved through the membrane it condenses at the permeate-membrane interface.

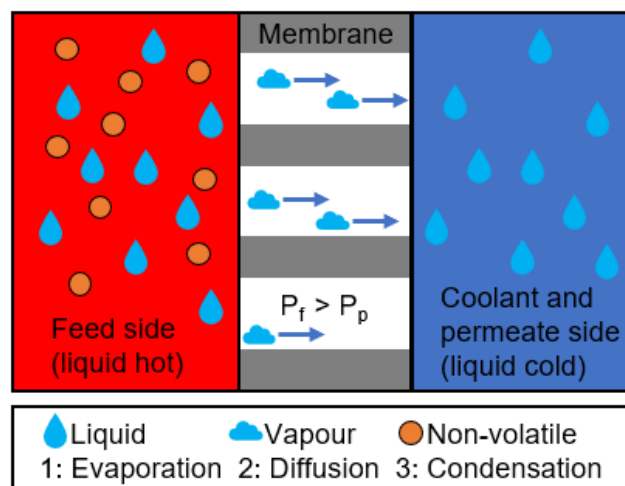


Figure 1-2 Schematic representation of the MD process

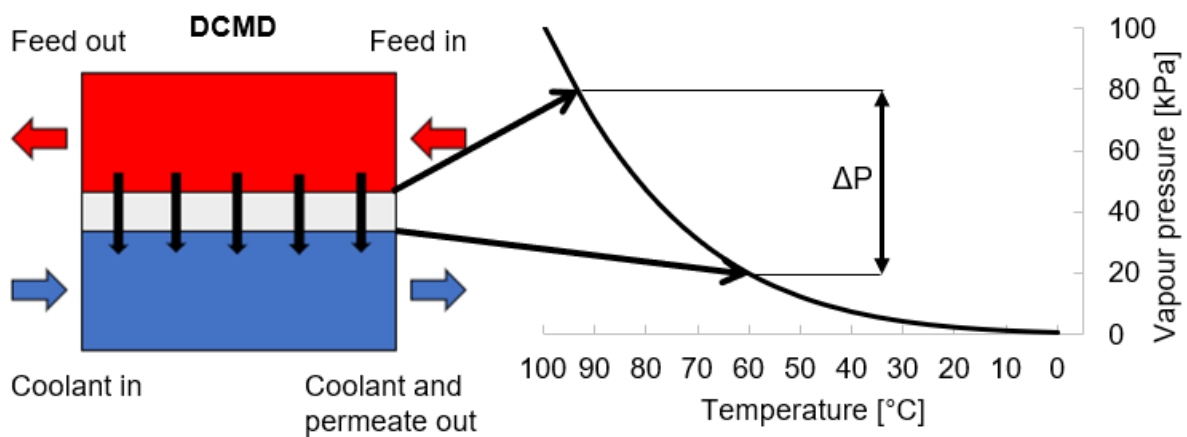


Figure 1-3 Schematic representation of the MD process with Antoine equation

A few MD configurations and setups have been invented. Only the three most used configurations are described. For more information about the other configurations the following work is recommended [17]. The three membrane distillation configurations that are described in the following sections are DCMD, Air Gap Membrane Distillation (AGMD) and Vacuum assisted Air Gap Membrane Distillation (V-AGMD). An illustration of the three processes can be seen in Figure 1-4.

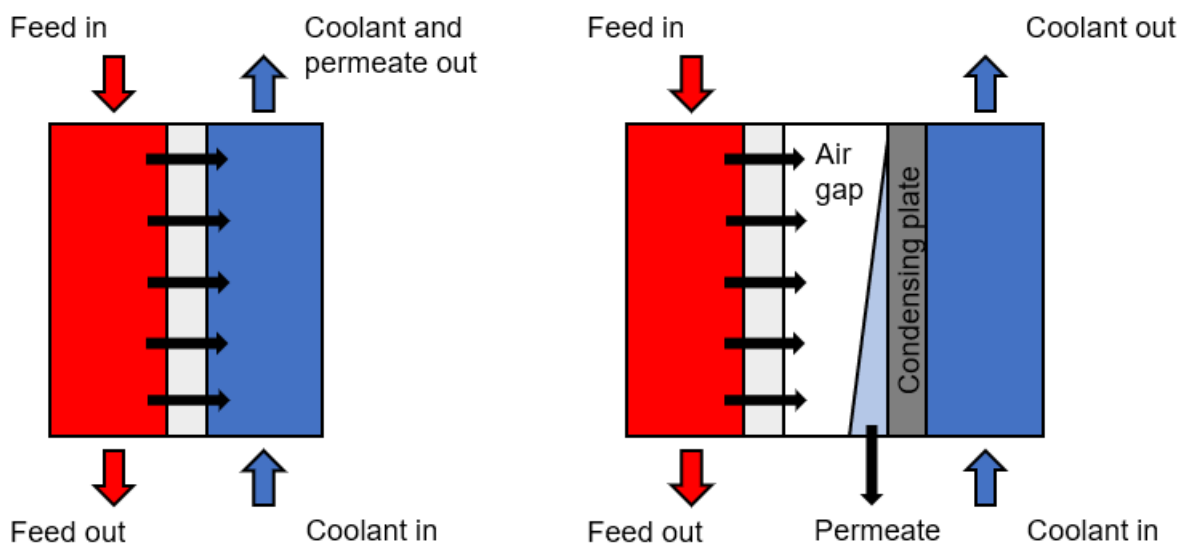


Figure 1-4 DCMD on the right and (V)-AGMD on the left

In DCMD, both fluid streams are in direct contact with the membrane surface. The evaporation takes place at the feed-membrane interface. The vapour moves through the membrane due to the vapour pressure difference between the feed and permeate side. When the vapour is through the membrane it condenses in the colder permeate stream. Because of the hydrophobic characteristic only the water vapour is allowed through the membrane. Therefore, the feed stream cannot penetrate the membrane. The main drawback of DCMD is the large heat loss by conduction [18].

With AGMD, an air gap between the membrane and the coolant is introduced to limit the heat loss by conduction. A downside of this setup is the extra mass resistance due to the static air barrier. However, AGMD has been proven to be more efficient than DCMD [19].

A method that reduces the mass resistance by using a light vacuum in the air gap is called V-AGMD. This results in less mass resistance and results in a higher efficiency and more production of distillate [20]. This configuration is invented and used by Aqua|still.

1.3 Applications of membrane distillation

MD can be used in a wide spectrum of applications. For example, it can be used in the treatment of radioactive wastewater [21], [22] or to concentrate fruit juice [23], [24]. However, the application of green energy, like solar applications, and the use of waste heat are interesting fields that offer its own challenges. In this section those challenges will be explained.

1.3.1 Low grade heat

When using fossil fuelled power production, the water that exist the turbine has a temperature of around 80 degrees Celsius. This low-quality energy is called low grade heat and is not used in the production of electricity due to the low Carnot efficiency. However, the temperature of this wastewater has a high enough temperature to desalinate water. Moreover, the water that is produced can be used as intake water for the boiler [25]. This in turn results in a lower water footprint of the powerplant.

Electricity production is not the only industry that produces low grade waste heat. For example, produced water [26] and mines [27] are two examples of industries that can be used with low grade heat to make water. To use this waste heat wisely, the process conditions and the materials needs to be as best as possible. In order to know what the perfect process conditions and materials are, research needs to be conducted. One goal of this thesis is to determine the optimum process conditions and material properties for V-AGMD.

1.3.2 Green energy

MD can be used with a wide variety of green energy sources. For example, MD can be used in combination with solar [20], [28]–[33], solar ponds [34]–[36], wind energy [37] and geothermal energy [38]. However, the prior mentioned energy sources do not have a constant energy production. This results in a dynamic behaviour of the hot feed side. Which can be seen in Figure 1-5 from [39]. This dynamic behaviour results in a dynamic distillate output. However, there are only a few models concerning the dynamic calculation of the distillate output [33], [40]–[43]. Moreover, to the authors knowledge there exist no fully validated AGMD dynamic model. Another goal of this thesis is to develop a dynamic model because Aqua|still does not possess such a model.

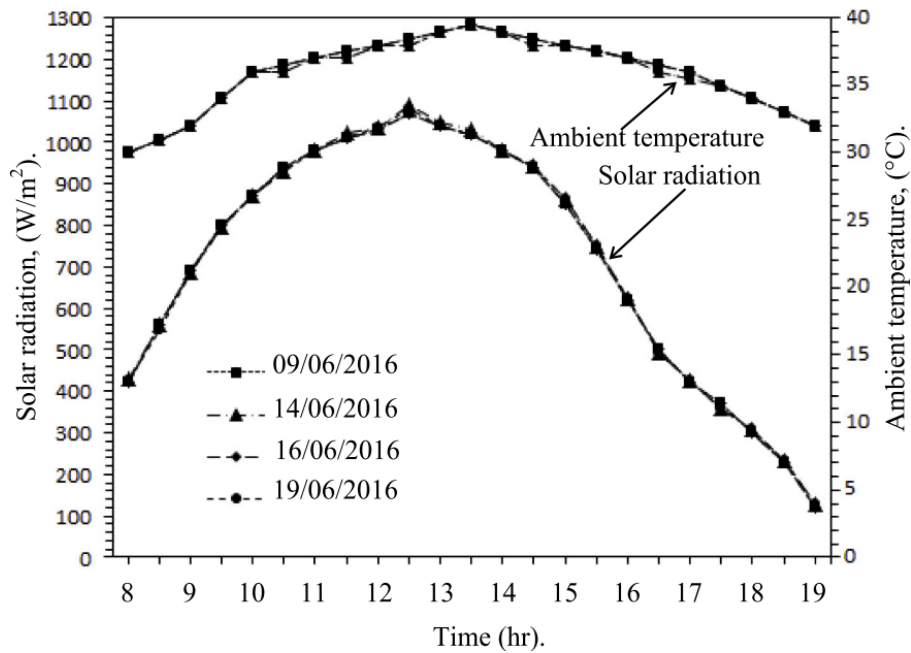


Figure 1-5 Average solar radiation and ambient temperatures, adopted from [20, p. 196]

1.4 Thesis goals

This thesis has two objectives. The first objective is to identify the optimum process conditions and material properties, in order to have the highest production of distillate.

The second objective is the development of a dynamic model to predict the amount of distillate that is produced with changing process conditions.

1.5 Overview of the thesis

The thesis has been divided in to two parts. Part A will consider the optimization work. In part B the dynamic modelling will be explained. Before presenting part A and part B, an introduction is given which is necessary to understand both parts. This will be done in the next chapter.

2 INTRODUCTION TO MEMBRANE DISTILLATION

In the first part of this chapter, the construction of a plate and frame module and an AGMD module are explained. In the second part the equations relating to the mass and heat transfer of an AGMD module are shown.

2.1 Construction of a membrane distillation module

2.1.1 Construction of a plate and frame module

The first and simplest way to build a membrane distillation module is plate and frame. This setup is more simplistic in design but also experience frequent production failures. A schematic representation and a real plate and frame module can be seen in Figure 2-1. This production method is inferior to the spiral wound production method that will be discussed in the next section.

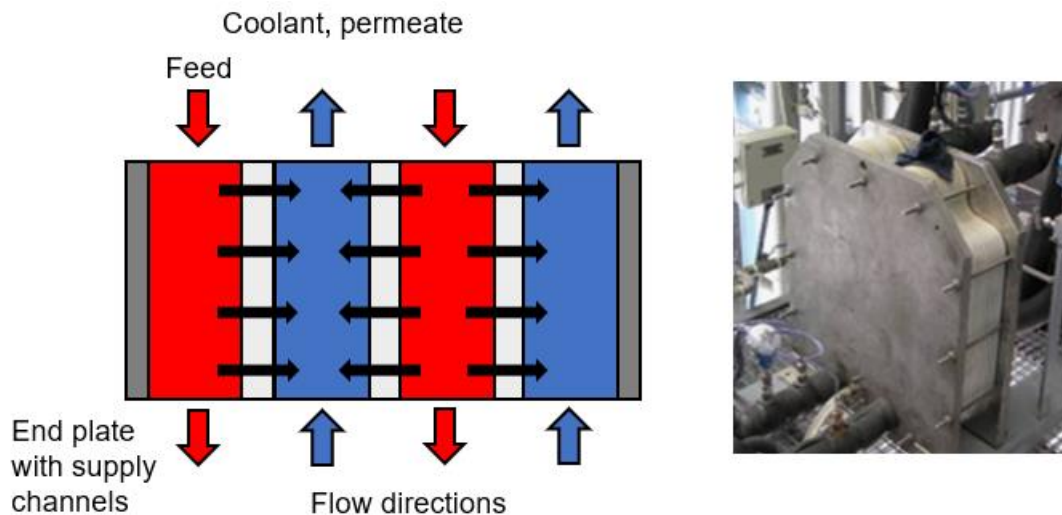


Figure 2-1 Left: Schematic representation of plate and frame, Right: Plate and frame module from Scarab [21, p. 361.]

2.1.2 Spiral wound modules

Another option for membrane distillation is to make a spiral wound membrane distillation module. Aqua|still is the producer of spiral wound AGMD modules. As can be seen in Figure 2-2, such a module consists of five major components. The first component is the hot feed channel in the module. Which is created with a spacer and a membrane. The spacer provides the volume so that water can flow along the membrane. The second component is the coolant channel. This is created in the same way as the hot feed channel but with a highly conductive condenser foil. To create an air gap between the membrane and the condenser foil another spacer is used. One feed channel, one condenser channel and the air gaps between the membrane and condenser is called an envelope. When more envelopes are used, a star shape is created. The "star" looking formation is then coiled so that the MD module is formed into a

round shape. This type of module that uses this process is called a spiral wound MD module. Which can be seen on the right side of Figure 2-2.

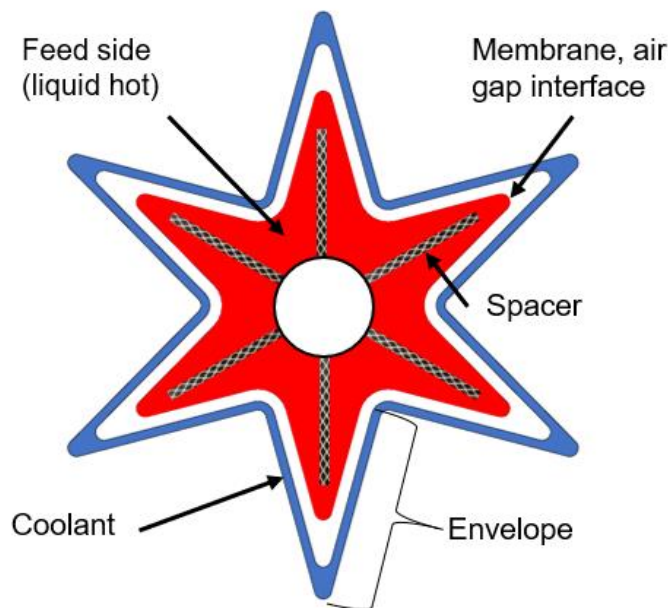


Figure 2-2 Left: Schematic representation of an AGMD module, Right: Two AGMD modules from Aqualstill

As indicated previously a spiral wound air gap membrane distillation unit consists of several envelopes. The length of an envelope is chosen depending on the application. Theoretically every length can be produced. In practice three envelope lengths are used, these are 1.5, 2.7 and 5 meters. A long envelope length will be chosen when high efficiency is required. As can be seen in Figure 2-3, a longer envelope results in a lower temperature difference between the hot and the cold side. This results in a high efficiency. However, the vapour pressure difference will be small. This will result in a low distillate output. A shorter envelope is chosen when a lot of distillate production is needed. The shorter envelope results in a higher temperature difference between the hot and the cold side. This will result in a higher vapour pressure difference and a lower efficiency.

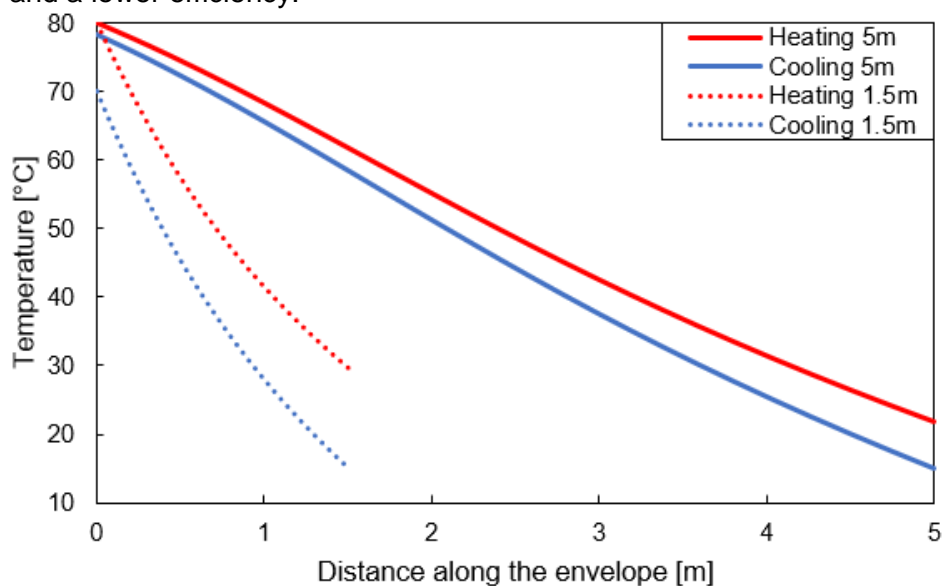


Figure 2-3 Temperature profile of a one point five meter and a five-meter-long envelope

One way to calculate the performance is the gained output ratio (GOR). When the GOR is used to calculate the performance, it is easier to compare a spiral wound air gap membrane distillation module with a plate and frame module. The GOR is the ratio between the latent heat of evaporation h_f and the specific heat input q_{in} [45]. Another common output parameter is the flux of the module J which can be calculated with equation (2-2) where F_{tot} and A_m are the total distillate output flow and the membrane area.

$$GOR = \frac{h_f}{q_{in}} \quad (2-1)$$

$$J = \frac{F_{tot}}{A_m} \quad (2-2)$$

Further improvements to spiral wound modules

Normally, ambient air can enter the air gap which has a lower temperature than the air in the air gap. Therefore, a syphon can be placed by Aqua|still at the distillate exit for higher efficiency. Despite that, this effect has not been proven in literature. The syphon and its effect are visualized in Figure 2-4.

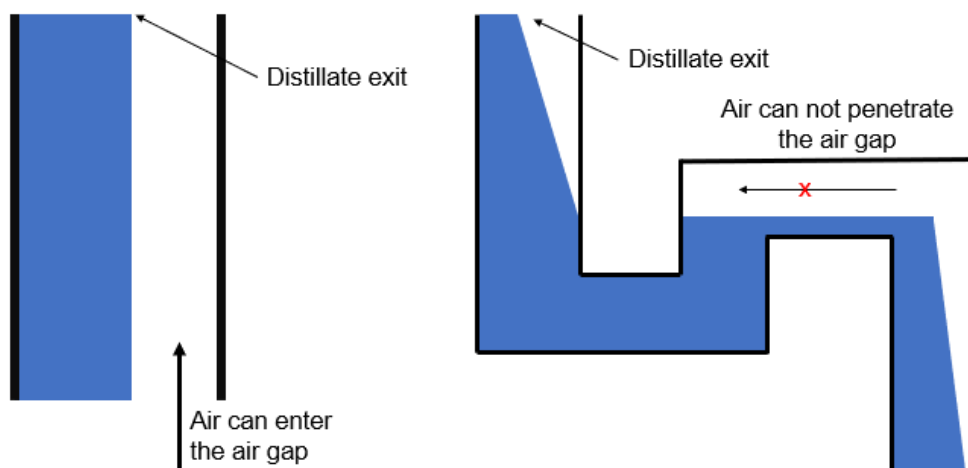


Figure 2-4 Visualized effect of the syphon. On the left: distillate exit with no syphon. On the right: distillate exit with a syphon.

2.2 Modelling of membrane distillation

MD is modelled to predict the amount of distillate production and the energy consumption of a module. This information is needed to design a setup and to make sure that enough water is produced by the system. In this section the methods for calculating membrane distillation are shown. Firstly, an overview is given to provide the simplifications and effects that are neglected in the modelling of AGMD. Secondly, the formula about heat and mass transfer are shown. Modelling of MD requires several thermophysical properties. The equations regarding the thermophysical properties of water can be found in [46], [47].

2.2.1 Introduction to the modelling of membrane distillation

Usually lab scale setups are used to model MD. However, spiral wound modules have certain implications in the way that mass and heat transfer takes place. These implications will be described in this section.

First effect

Normally, only one side of the membrane is modelled. However, with a spiral wound module the feed channel has two sides. This results in twice the heat loss due to conduction and evaporation. As a result, a spiral wound MD unit is equivalent to modelling a one-sided feed channel with twice the heat loss or gain in the feed channels. In Figure 2-5 a schematic representation is shown of a spiral wound and the equivalent scheme.

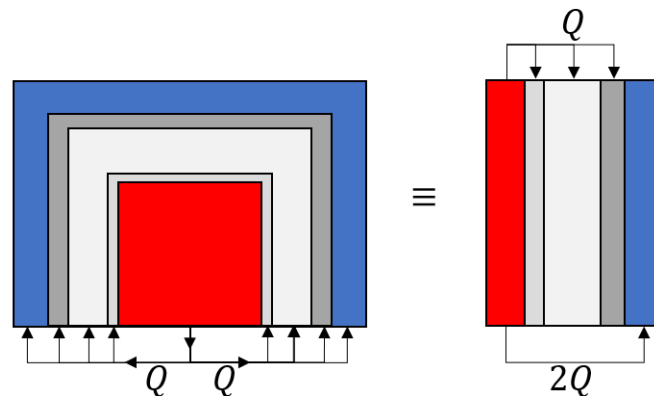


Figure 2-5 Equivalent scheme of air gap membrane distillation

Second effect

The second implication of using a spiral wound module is the effect that the spacer has on the flow of the distillate in the air gap. There are several ways that the distillate can flow down [48]. However, in a spacer filled air gap there are only two ways. The first is one is film wise where the distillate develops as a film on the condenser foil. The second way is wicking, where the distillate is trapped between the spacer and the condenser foil. When there is enough trapped water in neighbouring holes of the spacer the water flows down simultaneously. Both ways have previously been described by Hitshov et al. [19]. A better view of the condensation film can be seen at [49] and wicking at [50]. The trapped water in the spacer has both influence on the heat and the mass transfer, this will be explained in the following two paragraphs.

Third effect

The third effect has not a lot to do about the spiral wound nature but more about the large length of the module compared to a lab scale setup. Due to this large length the distillate has to travel half the length of the envelope before reaching the exit. This results in extra heat loss by conduction. Usually the feed flow rate is significantly larger than the distillate output flow. As a result, this effect can be neglected.

Fourth effect

Another effect is the compaction of the membrane due to the hydraulic pressure in the hot feed channel. This results in a thinner membrane that is more conductive and has slightly less mass resistance [51]. However, membrane compaction effect has only been studied for DCMD. Moreover, modelling of AGMD has been done without taking this effect into account while still providing good results [19], [52]. Therefore, this effect is neglected.

Fifth effect

The fifth effect is only valid for dynamic modelling and happens only when a shock is applied to the module. The air gap can act as a reservoir for distillate due to the wicking of water in the spacer. When a shock is applied to the module, this trapped water can flow down in a short time frame which causes a high distillate flow. Two examples of such a shock are air that moves from the feed side to the air gap or a hydraulic pressure difference in the hot feed side. Moreover, this effect can also occur randomly. Directly after the high distillate flow has ended, the 'reservoir' has to be filled again which causes a lower distillate output. However, in bigger installations with several modules, the depletion and filling of the air gap will be averaged out. Therefore, the filling and emptying of the air gap will be neglected in the dynamic modelling.

Sixth effect

The sixth and last effect concerns scaling and biofouling. Scaling happens when salt particles fall down on the membrane. A schematic representation can be seen in Figure 2-6. For example, scaling due to $CaCO_3$ can happen at high temperatures. $CaCO_3$ is found to be one of the most common scales [53]. However, in Aqua|still pilots, the heat exchanger is placed in front of the module. Therefore, most of the scales will fall down in the heat exchanger. For this reason, scaling will not be considered in this thesis.

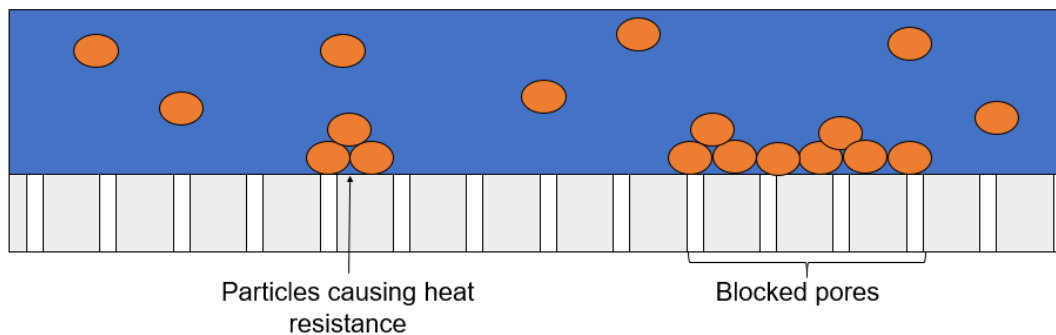


Figure 2-6 Visualization of scaling

Biofouling happens when a biofilm of bacteria is formed on the membrane [53]. As biofouling can be easily solved with water treatment this will not be taken into account.

2.2.2 Heat transfer

The following equations are all based on a steady state operation. However, these equations will be used to model the dynamic behaviour as will be explained in chapter 6.

Energy balance

The following energy balances were found in [33] and were simplified and slightly adjusted to take the previously mentioned second effect into account. x_l is the amount of water that is trapped in pores of the spacer. In Figure 2-7 the heat transfer, Q , and the temperatures, T , are shown where the subscripts h, m, a, c and p stand for the hot bulk fluid, membrane, air gap, condenser and cold bulk fluid respectively. The interfaces between the membrane-hot feed, membrane-air gap, condenser-air gap and condenser-cold feed are noted as mf, ma, ca and cp respectively. The latent heat of evaporation, H_v , can be found with the equation from Alsaadi et al. [54].

$$Q_h - H_v = Q_m \quad (2-3)$$

$$Q_m + x_l H_v = Q_a \quad (2-4)$$

$$Q_a + (1 - x_l) H_v = Q_c \quad (2-5)$$

$$Q_c = Q_p \quad (2-6)$$

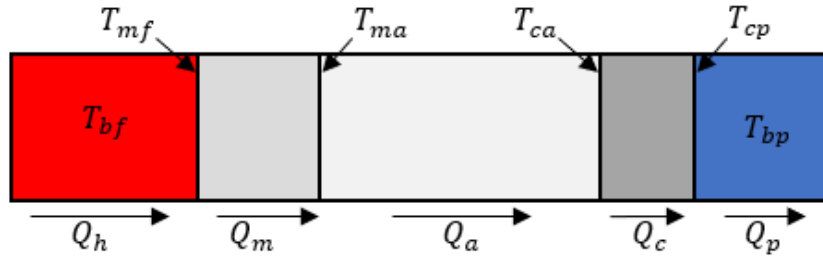


Figure 2-7 Heat transfer and temperatures that are used in the modelling

Heat transfer through the hot feed channel and the coolant channel

The heat transfer through the channel is dependent on the type of spacer in the channel. The heat transfer rate of the channel h_{ch} that can be calculated with equation (2-10) uses an empirical equation for the Nusselt number [55]. This equation can only be used for the current spacer. The hydraulic diameter $d_{h,sp}$ and the porosity of the spacer ϵ_{sp} can be calculated with equation (2-13) and (2-14) respectively [56]. The parameters of the spacer can be seen in Figure 2-8. W_{md} , t_{ch} and v_{eff} are the height of the module, thickness of the channel and the effective speed in the channel respectively. The thermophysical properties are noted as λ , η , ρ for the thermal conductivity, dynamic viscosity and density respectively. \dot{m} is the mass flow in the channel.

$$Q_h = h_{ch} A_m (T_{bf} - T_{mf}) \quad (2-7)$$

$$Q_p = h_{ch} A_m (T_{cp} - T_{bp}) \quad (2-8)$$

$$h_{ch} = \frac{Nu \lambda}{d_{h,sp}} \quad (2-9)$$

$$Nu = 0.19 \cdot Re^{0.68} \quad (2-10)$$

$$Re = \frac{\rho v_{eff} d_{h,sp}}{\eta} \quad (2-11)$$

$$v_{eff} = \frac{\dot{m}}{\rho t_{ch} W_{md} \epsilon_{sp}} \quad (2-12)$$

$$d_{h,sp} = \frac{4 \epsilon_{sp} d_f t_{ch}}{2d_f + 4(1 - \epsilon_{sp} t_{ch})} \quad (2-13)$$

$$\epsilon_{sp} = 1 - \frac{\pi d_f^2}{2l_m h_{ch} \sin(\theta)} \quad (2-14)$$

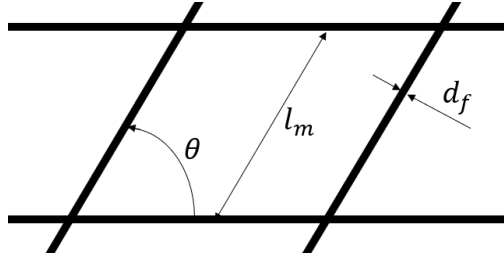


Figure 2-8 Parameters for determination of the spacer porosity and the hydraulic diameter

Heat transfer through the membrane

There exist a few equation to calculate the thermal conductivity of a microporous membrane [57]. However, according to [58] a stretched membrane can be predicted by using the Maxwell's lower bound, equation (2-17). As Aqua|still uses a stretched membrane, this equation could be used. However, it was found that the conductivity could not be predicted exactly [19]. Since the polymer orientation and manufacturing process influences the thermal conductivity, it is not known with great certainty. The authors of [58] used Monte Carlo filtering to find the equation that could predict the membrane k_m exactly. Which resulted in de calibration factor $c_m = 0.93$. The thermal conductivity of air k_g can be calculated by equation (2-19) [59]. The heat transfer rate of the membrane h_m can be calculated with equation (2-16) where t_m is the thickness of the membrane. β and ϵ_m are an intermediate factor and the porosity of the membrane.

$$Q_m = h_m A_m (T_{mf} - T_{ma}) \quad (2-15)$$

$$h_m = \frac{k_m}{t_m} \quad (2-16)$$

$$k_m = c_m \frac{k_g (1 + 2\beta(1 - \epsilon_m))}{1 - \beta(1 - \epsilon_m)} \quad (2-17)$$

$$\beta = \frac{k_s - k_g}{k_s + 2k_g} \quad (2-18)$$

$$k_g = 2.72 \times 10^{-3} + 7.77 \times 10^{-5} T \quad (2-19)$$

Heat transfer through the air gap

The heat transfer through the air gap can be calculated with equation (2-20). The conductivity through the air gap can be determined by equation (2-22) [52]. This equation takes the second effect of the previous section into account. t_a and t_{cond} are the thickness of the air gap and the thickness of the layer of condense on the condenser respectively. k_{sp} , k_g and k_w are the thermal conductivity of the spacer material, air and water respectively. The porosity of the spacer is ϵ_m and x_l is the amount of water that is trapped in pores of the spacer.

$$Q_a = h_a A_m (T_{ma} - T_{ca}) \quad (2-20)$$

$$h_a = \frac{k_a}{t_a - t_{cond}} \quad (2-21)$$

$$k_a = (1 - \epsilon_{sp})k_{sp} + \epsilon_{sp}x_l k_g + \epsilon x_l k_w \quad (2-22)$$

Heat transfer through the condenser

The heat transfer of the condenser and through the condensate film can be calculated with equation (2-23).

$$Q_c = \left(h_c^{-1} + \left(\frac{k_w}{t_{cond}} \right)^{-1} \right)^{-1} A_m (T_{ca} - T_{cp}) \quad (2-23)$$

2.2.3 Mass transfer

Overall equation

The distillate flux can be calculated by equation (2-24) [19]. This equation is a result from the previously mentioned second effect. The first part of the equation regards the water vapour that condenses on the trapped water in the air gap spacer. The second part of the equation regards the water vapour that has to move to the condenser to condense. This will have more resistance as the water vapour has to move through the air gap. The resistance in series approach can be used to calculate the combined permeability C_{m+a} of the membrane C_m and the air gap C_a [60]. P indicates the vapour pressure on both sides of the membrane.

$$J = x_l C_m (P_{mf} - P_{ma}) + (1 - x_l) C_{m+a} (P_{mf} - P_{ca}) \quad (2-24)$$

$$C_{m+a} = (C_m^{-1} + C_a^{-1})^{-1} \quad (2-25)$$

Vapour pressure

The pressure difference can be calculated with the vapour pressure given by equation (2-26), where A, B and C are the Antoine constants that can be found in literature [61]. However, due to salt that is present in the solution the vapour pressure will be lower. The vapour pressure reduction can be calculated with equation (2-27) [62]. Where the activity factor of water is a_w and m_{NaCl} is the molality of $NaCl$.

$$P^* = \exp \left(A - \frac{B}{T - C} \right) \quad (2-26)$$

$$P = P^* a_w = P^*(1 - 0.3112 m_{NaCl} - 0.001482 m_{NaCl}^2) \quad (2-27)$$

Mass transfer in the hot feed channel

Concentration polarization exist due to the water that moves from the feed-membrane interface. This can be calculated with equation (2-28) [18], [63]. The mass transfer coefficient K can be calculated using equation (2-29) [19], [51], [63]. The molecular diffusion coefficient D can be calculated with the empirical correlation of Wilke and Chang (2-32) [64], [65]. The solute molal volume v_a of NaCl can be calculated with the data found in [64], [66]. The association factor ϕ for water is 2.26 [64] and m_w is the mass flow rate of the water. S_{mf} and S_{bf} are the salinity at the membrane-hot feed interface and the bulk of the feed water respectively. Sh, Sc are the Sherwood and the Schmidt number respectively.

$$S_{mf} = S_{bf} e^{\frac{J}{\rho K}} \quad (2-28)$$

$$K = \frac{ShD}{d_h} \quad (2-29)$$

$$Sh = Nu Sc_b^{0.13} \left(\frac{Sc_{bf}}{Sc_{mf}} \right)^{0.25} \quad (2-30)$$

$$Sc = \frac{\eta}{D} \quad (2-31)$$

$$D = \frac{117.3 \times 10^{-18} (\phi m_w)^{0.5} T}{\eta v_a^{0.6}} \quad (2-32)$$

Permeability of membrane

The permeability is governed by the diffusion processes that takes place inside the membrane. There are in total four modes that take place. These are molecular diffusion, Knudsen diffusion, Poiseuille flow and surface diffusion. Molecular diffusion comes from the interaction of molecules with other molecules. Knudsen diffusion comes from the interaction of the molecules with the walls of the pores [18]. Surface diffusion can be neglected due to low molecule-membrane interaction [67] . All modes of transport are shown schematically in Figure 2-9.

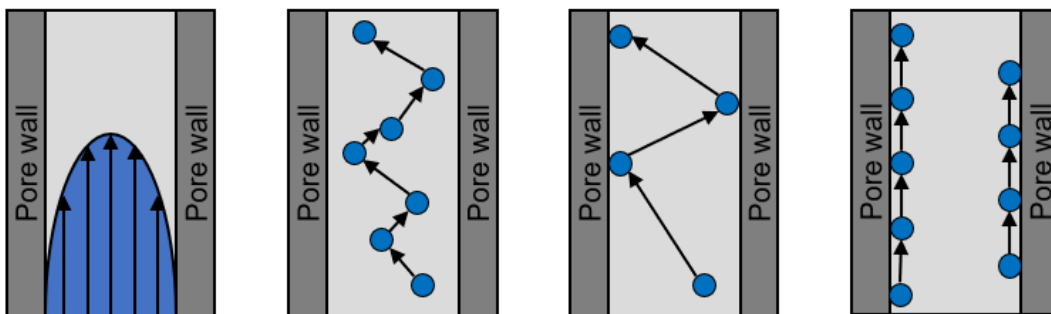


Figure 2-9 Poiseuille flow, Molecular diffusion, Knudsen diffusion and Surface diffusion

Not all three possible modes can happen simultaneously [67]. Hence, the Knudsen number can be used as a guideline for which mode is dominant. The Knudsen number K_n can be calculated by equation (2-33) [68] and the mean free path of the gas with (2-34) [69]. r_{pore} and σ_w are the pore radius of the membrane and the collision diameter of water respectively.

$$K_n = \frac{\lambda}{2r_{pore}} \quad (2-33)$$

$$\lambda = \frac{k_{bf}T}{\sqrt{2}\pi P\sigma_w^2} \quad (2-34)$$

When K_n is very small then Poiseuille flow can be neglected [67]. When $K_n > 1$ than Knudsen diffusion is dominant [18]. For $0.05 < K_n < 1$ a mix between Knudsen and molecular diffusion happens. When $K_n < 0.05$ than molecular diffusion is dominant [68].

The dusty gas model is a common method to calculate the permeability of porous materials. More information about the dusty gas model can be found in [70]. When the dusty gas model is used, equation (2-35) can be found to calculate the permeability of the membrane [19]. The average molecular speed and the diffusion coefficient can be found with equation (2-38) and (2-40) respectively. D_{aw} , δ_m , τ , R_g , D_e^K are the molecular diffusion, thickness of the membrane, tortuosity, universal gas constant and the Knudsen diffusion respectively. y is the partial air pressure of both side of the membrane.

$$C_m = \frac{\epsilon_m D_{aw}(1 + K_n)}{\tau \delta_m R_g T_m} \ln \left(\frac{D_e^K y_{ma} + D_{aw}(1 + K_n)}{D_e^K y_{mf} + D_{aw}(1 + K_n)} \right) \quad (2-35)$$

$$y_{ma} = \frac{P - P_{ma}}{P} \quad (2-36)$$

$$y_{mf} = \frac{P - P_{mf}}{P} \quad (2-37)$$

$$\bar{v} = \sqrt{\frac{8R_g T}{\pi m_w}} \quad (2-38)$$

$$D_e^K = \frac{2\epsilon_m r_{pore}}{3\tau} \bar{v} \quad (2-39)$$

$$D_{aw} = 1.896 \cdot 10^{-5} T_m^{2.072} \quad (2-40)$$

The porosity is defined as the void volume fraction of the membrane. The tortuosity is the deviation from the cylindrical shape, as can be seen in Figure 2-10. The tortuosity can be calculated with equation (2-41) [71].

$$\tau = \frac{(2 - \epsilon)^2}{\epsilon} \quad (2-41)$$



Figure 2-10 Cylindrical pore on the left and tortuous pore on the right

Permeability of air gap

The permeability of the air gap is mostly governed by molecular diffusion. This can be calculated with formula (2-43) [19].

$$D = 4.46 \cdot 10^{-6} T_{airgap}^{2.334} \quad (2-42)$$

$$C_a = \frac{D}{\delta_a R_g T_a} \ln \left(\frac{P - P_c}{P - P_{ma}} \right) \frac{1}{P_{ma} - P_c} \quad (2-43)$$

Water fraction in air gap

The fraction of the trapped water in the pores of the spacer should be empirically determined. However, the empirically defined equation (2-44) from [19] is used which might result in an error. The reason for this decision is that a special setup is needed that is quite complex and can become time intensive.

$$x_l = 0.1676 \ln(J)^{0.571} + 0.02811 \quad (2-44)$$

Part A

Introduction to part A

In this part of this thesis, research is conducted in order to find the perfect process conditions and materials for a V-AGMD module. There are two possible methodologies which can be used for finding the optimum of a process. The first methodology that can be used is response surface methodology (RSM). The second method that is explained in section 3.2 is a methodology designed for finding the optimum of several variables. The second method consist of several steps. These steps are explained in section 3.2. At the end of section 3.2 a conclusion about the methodologies that can be used to find the optimum is given. In section 4 the best methods that were found in section 3 are executed and the results are discussed. The last section of part A is the conclusion on the optimization of membrane distillation.

Table of contents part A:

3	Optimum seeking methods	39
3.1	<i>Response surface methodology</i>	39
3.1.1	Literature.....	39
3.2	<i>Methodology for finding the optimum.....</i>	40
3.2.1	Space filling designs	40
3.2.2	Data acquisition	43
3.2.3	Multiple second order regression model.....	43
3.2.4	Heuristics methods for finding the optimum.....	46
3.2.5	Conclusion	49
4	Optimum parameters of membrane distillation.....	51
4.1	<i>Space filling design</i>	51
4.2	<i>Regression model</i>	52
4.3	<i>Simulated annealing.....</i>	55
4.4	<i>Conclusions</i>	57
5	Conclusions part A	59

3 OPTIMUM SEEKING METHODS

3.1 Response surface methodology

3.1.1 Literature

In general, in most of the designed experiments one parameter is changed while others are kept constant. Consequently, this type of experiment takes a lot of time due to the amount of tests that need to be performed to find an optimum. To prevent that many tests have to be performed that are time consuming, the response surface methodology RSM was designed. In RSM the input parameters are changed simultaneously. Additionally, when RSM is used for an experiment the interaction effects between the different parameters are revealed [7], [72]. According to Khayet et al., the RSM leads to a higher efficiency when it is used in an optimization experiment [72]. In [32], [72]–[74] the optimum process conditions for MD were found by using RSM. In most of the research only four different parameters are changed in the experiments. However, there are 12 process and module parameters that can be changed for reaching an optimum. All the parameters are listed in Table 3-1.

Table 3-1 Process conditions and module parameters

Process conditions	Module parameters
Condenser in temperature [°C]	Heat transfer membrane channel [W]
Membrane in temperature [°C]	Heat transfer membrane [W]
Salinity [g/kg]	Heat transfer air gap [W]
Air gap pressure [kPa]	Heat transfer condenser [W]
Cross flow velocity [m/s]	Heat transfer condenser channel [W]
	Mass transfer rate membrane [kg/s]
	Mass transfer rate air gap [kg/s]

Despite the promising characteristics of RSM there is a downside to this method. The response of the RSM can be graphically represented as a 3D plot or as a contour plot. Every parameter has to be plotted in function of the other parameter, as can be seen in Figure 3-1. In the case of 12 variables, this results in 24 3D plots or contour plots. In this case, the 3D and contour plots are made by keeping the other 10 parameters constant. This way a local optimum can be found. The problem with RSM is that when it is used with a lot of parameters it is hard to know where the global optimum is. Therefore, another methodology is needed for finding the optimum, this will be discussed in section 3.2.

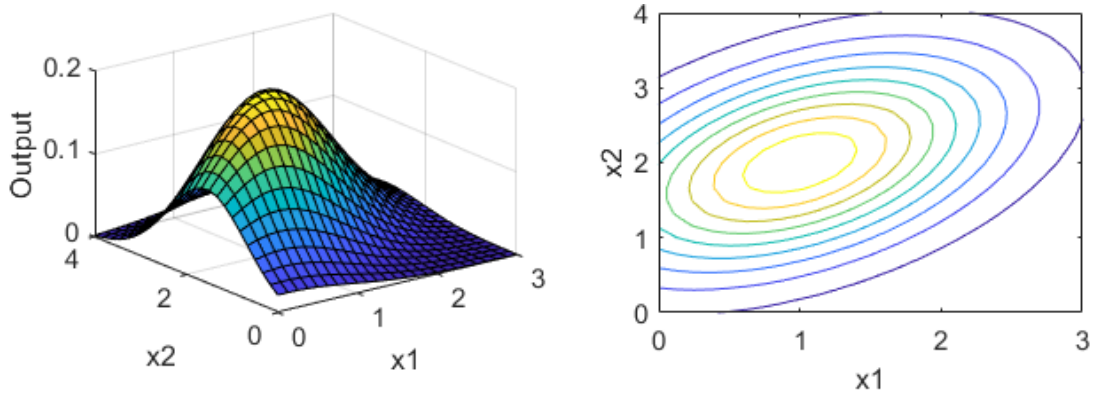


Figure 3-1 3D plot and contour plot of a RSM solution

3.2 Methodology for finding the optimum

In this section the methodology to find the optimum is explained. Firstly, a short introduction is given on the methodology. In the next sections more detailed information is given.

In Figure 3-2 a flowchart of the methodology can be seen. In the first step the design space is created by using a space filling design method. This design space is used as an input for the existing Aqua|still model. Which has been described and validated in [52]. In the next step the obtained flux, GOR, $Q_{heating}$ and $Q_{cooling}$ are used to create regression formula. Every output has its own formula. Therefore, four regression formula are created. In the last step the regression formula are used in an optimum seeking method.

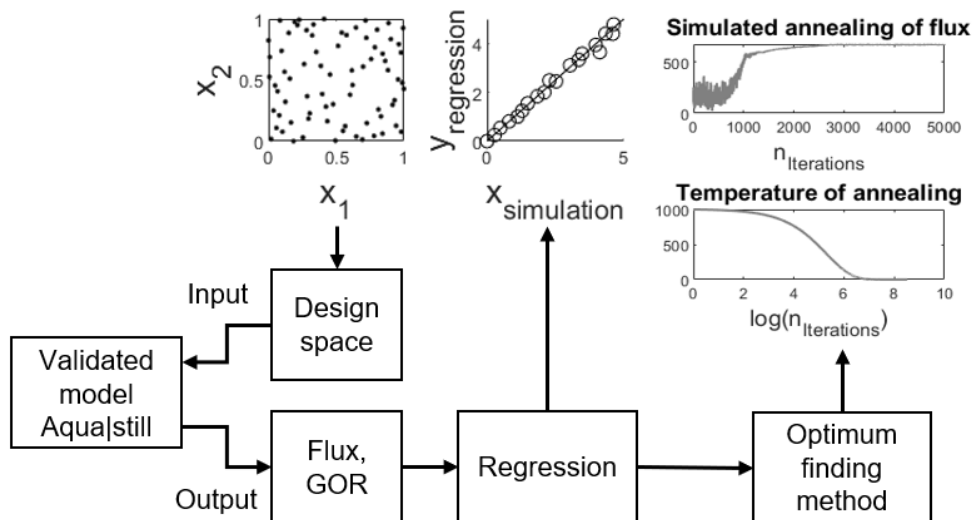


Figure 3-2 Flowchart of the optimum finding methodology

3.2.1 Space filling designs

Two general methods can be used to gather the data needed for creating a regression formula. The first one is by doing physical experiments and the second one is by running computer simulation. Computer simulations are often used when the physical experiments are time or resource intensive. However, a computer model should be available to acquire the necessary

test results. In addition, the computer simulation should represent the real system accurately. Otherwise, it is possible that the results are inaccurate [75], [76].

In this thesis the choice was made to use computer simulations. The main advantage is that simulations are less time consuming. As can be seen in Figure 3-3 the number of measuring points increases when the number of parameters increases. For optimizing the MD process 12 parameters of the module need to be optimized. These parameters are listed in Table 3-2. As one test takes around one hour to perform, this will in total take 2^{12} or 4096 hours to complete when using two-level factorial design. However, a computer simulation will take around five minutes to complete.

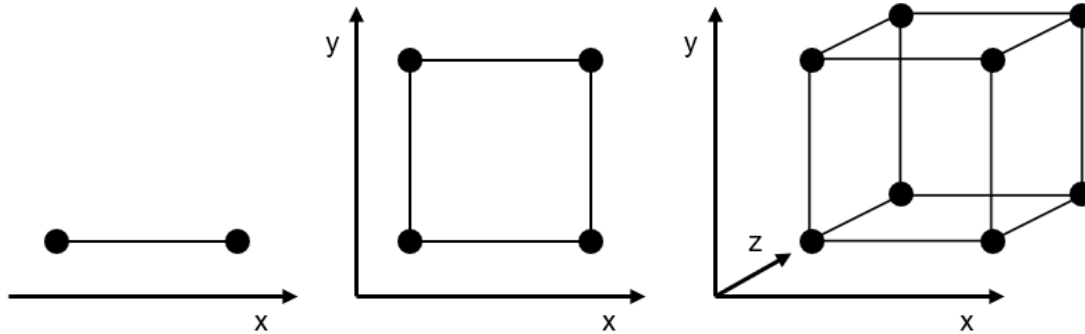


Figure 3-3 Two-level factorial design for $k = 1$, $k = 2$ and $k = 3$

The experiments that are calculated in computer simulation are often based on a design space. This design space is created to make sure there is a design point close for any point in the experimental region [76]. Space filling designs are commonly used methods for creating a design space. In the next paragraphs the most common design spaces are explained briefly.

Minimax distance design

In this method the smallest distance will be maximized between any two points in the design space [77]. An example of this method for seven points is shown in Figure 3-4. Important to notice is that the design space is an unit hypercube [75]. In other words, the values of the x- and y-axis are scaled from zero to one. The downside of this method is the possibility of good space-fillingness for a single dimension while projections in other dimensions may not be sufficient [76].

Maximin distance design

In this design the largest distance will be minimized between any two points in the design space [77]. In Figure 3-4 an example with seven points can be seen. This design method has the same downside as the minimax method. A sufficient projection may exist in one dimension but not in the other dimensions [76].

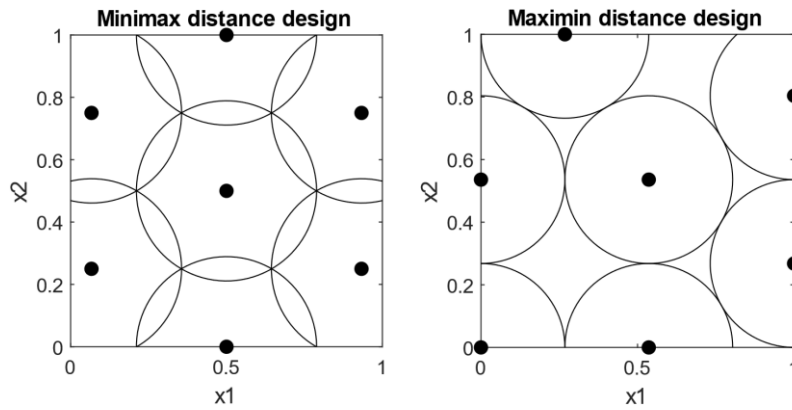


Figure 3-4 Minimax and Maximin distance design for $n = 7$ points

Latin hypercube design

In this method the design space is divided into n^2 squares, where n is the number of points. Afterwards, the points are randomly placed in one of the squares. The only constrain is that only one point can be placed in every row and column. The benefit of this method is better projecting for two dimensions. However, in higher dimensions poor projection is still possible. The second problem is the possibility that the points align diagonally [76]. This can be seen on the right side of Figure 3-5. On the left side of Figure 3-5 a Latin hypercube with sufficient projection is shown.

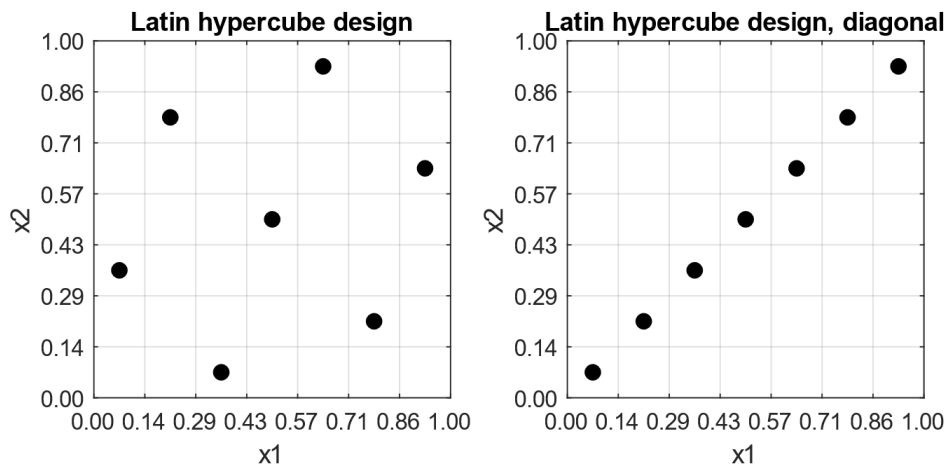


Figure 3-5 Latin hypercube design for $n = 7$ points

To overcome that the points align diagonally the maximin Latin hypercube design was developed. This method works with the same principle as the normal Latin hypercube design expect an extra constrain is added. The extra constrain forces the points to be as far from other points as possible. As a result, there is only a poor projection in high dimensions [76].

Maximum projection method

In the maximum projection method, the poor projection in higher dimension is solved. In this method a weighted Euclidean distance function is used so that the projection is sufficient in every dimension. The maximum projection method is the best overall method [78]. The statistical program R [79] with the Maxpro package [80] will be used to create the design space in this thesis.

3.2.2 Data acquisition

The data was acquired by using the model that was developed by Aqua|still [52]. This numerical model divides the envelopes in several sections. The temperature difference is then calculated based on the inputs of the model. The model gives the length of the envelope needed to exchange the amount of heat as result. If the calculated length is not same as the length of the envelope, a new guess for the temperatures will be made. After a few iterations the calculated length is equal to the length of the envelope. The resulting flux, GOR, $Q_{heating}$, $Q_{cooling}$ will be collected and processed in MATLAB.

3.2.3 Multiple second order regression model

Multiple second order regression is based on several statistical methods. In this section, information about the techniques that will be used in the next chapter will be explained.

Second order multiple regression model

In equation (3-1) the standard second-order multiple regression model can be seen. Since a first-order model won't be able to fit perfect for quadratic relationships between different variables, the second-order model was chosen for designing the regression model. In equation (3-1) β_i with $i = 0, 1, \dots, k$ are the regression coefficients and x_i with $i = 0, 1, \dots, k$ are the variables who are called the predictor variables or regressors [81].

$$y = \beta_0 + \beta_1 x_1 + \beta_2 x_2 + \dots + \beta_k x_k + \beta_{11} x_1^2 + \beta_{22} x_2^2 + \dots + \beta_{kk} x_k^2 + \beta_{12} x_1 x_2 + \beta_{13} x_1 x_3 + \dots + \beta_{1k} x_1 x_k + \beta_{23} x_2 x_3 + \beta_{24} x_2 x_4 + \dots + \beta_{2k} x_2 x_k + \dots + \beta_{k-1,k} x_{k-1} x_k \quad (3-1)$$

In Table 3-2 the predictor variables are listed. In total there are 12 variables that need to be optimized. The first five variables are dependent on the process conditions and the other variables are dependent on the material properties of the module. As can be seen in Table 3-2, the range of the variables are specified. To gain insight on how a module could be optimized some limits were extended beyond their practical range.

The hot feed inlet temperature and the air gap pressure are the two process parameters that were chosen outside their practical range. These two parameters are depended on the technical limitations of the module. The first limitation is the maximum temperature of the resin, 80 °C. At higher temperatures, the resin might not be strong enough. To overcome this problem a new resin could be chosen. However, this is outside the scope of this thesis. A maximum of 90 °C was chosen because this is requires changing the pipes of the installation to stainless steel instead of using plastics.

The minimum air gap pressure is limited by the vapour pressure in the air gap which is on in turn limited by the distillate temperature at the exit of the module. A lower vapour pressure can be reached if the water distillate will be colder. This can be done by moving the distillate exit to the cold feed inlet. This is a major change in module design. Therefore, this problem is omitted in this thesis.

Table 3-2 Predictor variables and the chosen limits

Predictor variables	Minimum value	Maximum value	Symbol
Condenser inlet temperature [$^{\circ}C$]	15	35	$T_{cond,in}$
Membrane inlet temperature [$^{\circ}C$]	65	90	$T_{mem,in}$
Salinity [g/kg]	0	200	S
Air gap pressure [kPa]	10	100	P_{airgap}
Cross flow velocity [m/s]	0.03	0.15	v_{eff}
Heat transfer membrane channel [-]	0.5	2	$C_{Q_{hot}}$
Heat transfer membrane [-]	0.5	2	$C_{Q_{membrane}}$
Heat transfer air gap [-]	0.5	2	$C_{Q_{airgap}}$
Heat transfer condenser [-]	0.5	2	$C_{Q_{condenser}}$
Heat transfer condenser channel [-]	0.5	2	$C_{Q_{cold}}$
Mass transfer rate membrane [-]	0.5	2	$C_{m_{membrane}}$
Mass transfer rate air gap [-]	0.5	2	$C_{m_{airgap}}$

Seawater has a salinity of around 30 g/kg . Because there is no real limit on the salinity a maximum salinity of 200 g/kg was used. This is the maximum salinity Aqua|still uses in their applications.

There are parameters who were limited by the design of the installation or by the quality of the feed water. For example, the maximum cross flow velocity is limited by the pressure drop of the whole installation. Furthermore, the pressure drop is dependent on the pipes, heat exchanger and module. However, the pressure drop of the module is insignificant.

In contrast to the process conditions no exact limitation exist for the module parameters. Therefore, it is difficult to define a minimum and maximum value. To overcome this problem the minimum value of a certain module parameter will be defined as how many times the module parameter is different than the actual value used today by Aqua|still. As can be seen in Table 3-2 the module parameters have a minimum value of 0.5. Thus, the heat transfer is the half of the actual value nowadays.

The same can be done for the maximum values of the module parameters. The maximum value will be defined by how many times the module parameter is higher than the actual value used today by Aqua|still. As can be seen in Table 3-2, the module parameters have a maximum value of two. Thus, the heat transfer is twice as high than the actual value nowadays.

Regression coefficients

For finding the regression coefficients the least squares method will be used. According to Myers et al. [81], this is the most used method for finding the regression coefficients. In equation (3-2) the formula for finding the different regression coefficients can be found. More information on the derivation of the formula can be found in [81]. The matrix b represents all the regression coefficients. The matrix X is called the model matrix, this matrix consists the created experimental points from the design space. The matrix y contains the results that were obtained out of the Aqua|still model.

$$\mathbf{b} = (\mathbf{X}'\mathbf{X})^{-1}\mathbf{X}'\mathbf{y} \quad (3-2)$$

Model adequacy checking

Adequacy checking should be done to make sure that the regression formula corresponds with the real physical system. There are several methods for checking the model adequacy. Some common methods are actual versus prediction plot, residual analysis, scaling residuals, influence diagnostics and testing for lack of fit. More information about these methods can be found in [81]. In this thesis checking model adequacy will be done with an actual versus prediction plot and residual analysis because this is an effective way [82].

In Figure 3-6 the actual versus prediction plot is shown. In this plot the results of regression formula are plotted in function of the simulated response. The straight line in the plot represents the point where the regression formula gives the same result as the simulated values. In other words when all the points align then the regression formula represent the simulation results perfectly [81]. The actual versus prediction plot will only give a good indication if the regression formula represents the simulation results. Therefore, a more advanced method like the residual analysis is needed.

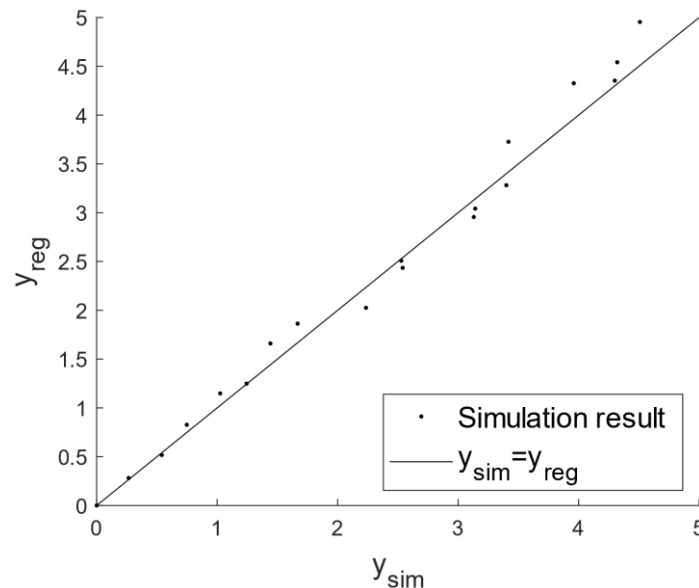


Figure 3-6 Actual versus prediction plot

The residual analysis consists of two parts. In the first part a normal probability plot of the residuals is constructed. The normal probability plot is capable of checking the normality assumption in a simple way [82]. In this plot the residuals are plotted against the normal probability. An example of a normal probability plot can be seen in Figure 3-7. The residuals can be calculated with equation (3-3) where $i = 1, 2, 3, \dots, n$. In the second part a residual plot of will be constructed. In Figure 3-7 the residuals in function of the predicted response can be seen. The residual plot gives more information about the variance of the response.

$$e_i = y_i - \hat{y}_i \quad (3-3)$$

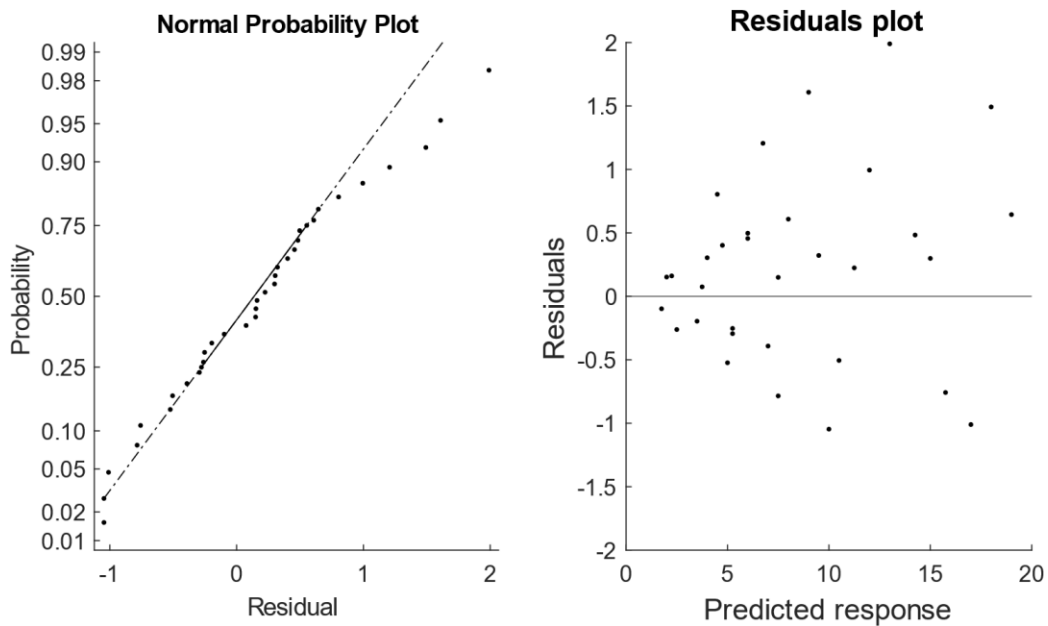


Figure 3-7 Normal probability plot and Residual plot

3.2.4 Heuristics methods for finding the optimum

As told in the conclusion of section 3.1 it is hard to find a global optimum when there are a lot of parameters. However, the problems that may pop up with RSM can be solved by using heuristic methods. A heuristic is defined by Pearl et al. [83] as a criteria, method or principle for deciding which among several alternative courses of action promises to be the most effective in order to achieve some goal. In other words, heuristics methods are designed for solving complex problems when classic methods are insufficient. The three heuristic methods that will be discussed are Monte Carlo, Hill Climbing and Simulated Annealing (SA).

Monte Carlo

Monte Carlo is the easiest to understand and implement. This method takes a user defined number of guesses from a sampling distribution. The final value is the maximum value from the output. This method is dependent on the number of guesses that are made. However, this method uses a lot of computer memory as the amount of parameters and the optimum must be saved [84]. The algorithm is as follows [84]:

1. Generate a vector of parameters X_1, \dots, X_k according to the chosen the sampling distribution.
2. Calculate the value according to the regression.
3. Put the vector and the result in a matrix.
4. When the predefined numbers of runs are finished the maximum value from the results with the parameters can be found.

Hill Climbing

A method that uses less memory is hill climbing [85]. This method only accepts values that are better than the previous value. The iterations stop when the maximum value doesn't change anymore. A possible problem with this model is that it can get stuck at local maximum and will not find the global maximum. A visualization of this problem is shown in Figure 3-8 [86]. The algorithm is as follows:

1. Generate a random vector of initial parameters X_1, \dots, X_k .
2. Generate a vector of parameters Y_1, \dots, Y_k according to chosen sampling distribution.
3. Calculate the value $sol(X)$ and $sol(Y)$ according to the regression.
4. If $sol(Y) > sol(X)$ the new state Y_1, \dots, Y_k is chosen.
5. If $sol(Y) < sol(X)$ state X_1, \dots, X_k stays the same.
6. Reiterate till the value does not change anymore or when a maximum amount of iterations is reached [86].

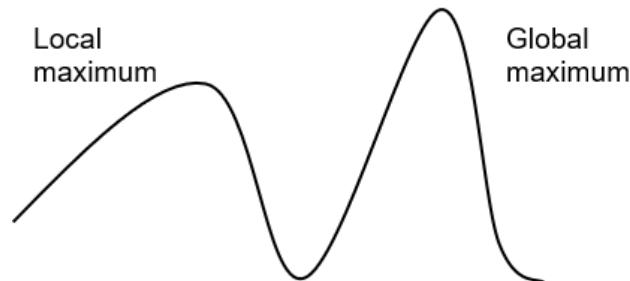


Figure 3-8 Hill climbing, Local and global maximum

Simulated Annealing

The SA method is a good way for the optimization of large-scale problems. In addition, it may be the best method for optimization when the global optimum is hidden in the many local optimums. SA is based on the thermodynamics analogy of a metal that cools down and anneals. The molecules of a metal at high temperatures can move freely between each other. This thermal mobility will be lost when the metal is than cooled down slowly. As a result, the metal molecules align themselves to form a pure crystal. This crystal is then in a minimum energy state. In other words, the slow cooling process gives the atoms time to rearrange while they lose their thermal mobility. Despite the slow cooling it is still possible to get stuck in a local maximum. The Boltzmann distribution describes the chance that the crystal has a low temperature with a high energy state. As a result, the chance that the crystal gets out of the local energy state to find the global energy state is calculated with the Boltzmann distribution, which can be found in equation (3-4) [87].

$$p(x) = e^{\frac{-\Delta E}{kT}} \quad (3-4)$$

This natural phenomenon of annealing is translated into a heuristic algorithm. This algorithm is called simulated annealing and uses the following steps to find a global optimum. One iteration from 3 to 6 is called an epoch. The total amount of iterations is called the epoch length [88].

1. Generate a random vector of initial parameters X_1, \dots, X_k .
2. Generate a starting temperature. This value has nothing to do with the membrane distillation process and is only used as a factor in SA.
3. Select a new vector of parameters.
4. Calculate the new solution.
5. Evaluate the difference of the new solution versus the old solution. If the solution rises, the new solution is accepted. If the solution decreases, it can get accepted with a probability that is based on equation (3-4).

6. Decrease the temperature. Again, this value has nothing to do with the membrane distillation process and is only used as a factor in SA.
7. Repeat step 3 to 6 till the stopping criteria is reached [84].

The initial temperature is important in SA because if it is too high it will take more reduction time to converge [89]. On the other hand, if the initial temperature is too low then there is a chance that this method will get stuck in a local optimum. In Figure 3-9 the effect of the temperature is visualized. There is a high chance that the value will go down the slope when the temperature is high. When the temperature is low there is a higher chance that the value will rise. Therefore, SA is similar to hill climbing for low temperatures.

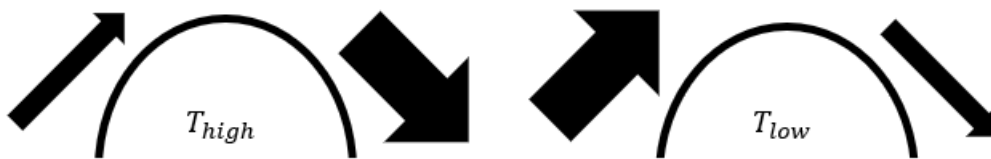


Figure 3-9 Change or rising or lowering at a high or low temperature

SA is chosen as the method to find the optimum of membrane distillation since SA takes less memory capacity Monte Carlo. Furthermore, SA does not get stuck in a local optimum like hill climbing.

In Figure 3-10 the flux and GOR are plotted in function of each other. As can be seen the flux and GOR are correlated. When the flux increases, the GOR will be lower and when the flux decrease the GOR will be higher. To improve both the flux and GOR it is necessary to shift the curved line upwards and to the right. In Figure 3-10 this correspond with shifting from the continues line to the dashed line. However, the membrane distillation process can not be higher than the thermodynamic limit. Because of the movement to the thermodynamic limit the surface under the line will increase. In other words when the surface under the line is maximized then the optimum is found. Therefore, it is necessary to adapt the SA algorithm in order to search for the maximum surface under the Flux-GOR line. Important to notice here is that the surface under the lines will be maximized. This is because the created regression formula have a higher uncertainty when the flux and GOR are high. Because the surface underneath the curve is used, the obtained result is more likely to be better.

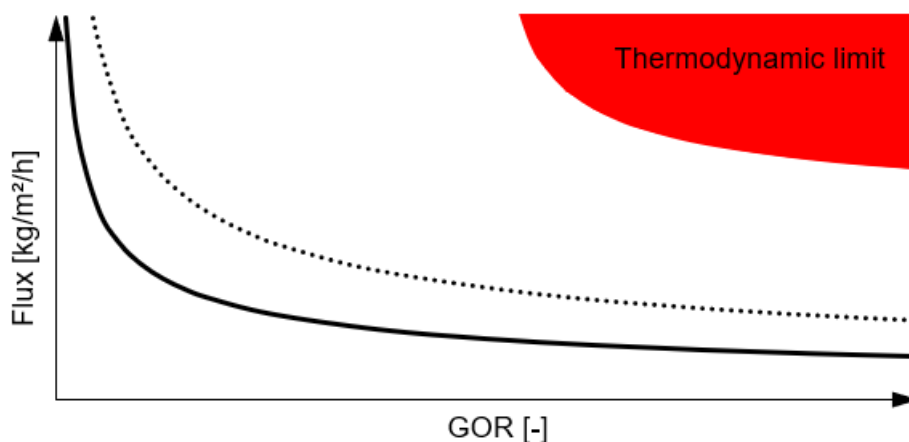


Figure 3-10 Flux versus GOR and the thermodynamic limit

3.2.5 Conclusion

The methods listed in Table 3-3 will be used as they were found to be the best. The methods are listed in order of use.

Table 3-3 Methods that will be used in this thesis

Use	Method
Space filling design	Maximum projection method
Regression	Second order multiple regression
Model adequacy	Residual versus actual, normal probability plot and residual plot
Optimum seeking	Simulated annealing

4 OPTIMUM PARAMETERS OF MEMBRANE DISTILLATION

4.1 Space filling design

In section 3.2.1 the different possible space filling design are described. The maximum projection method was found to be the best method for creating the design space. The design space is created using the statistical program R [79]. The R code that is used can be seen below where n is the number of points and p is the number of dimensions. 400 points was found to be sufficient.

```
library(MaxPro)  
InitialDesign<-MaxProLHD(n = 400, p = 12)$Design  
DOX<-MaxPro(InitialDesign)  
DOX$Design
```

This design space is used as an input for the existing Aqua|still model in excel. Secondly, the existing Aqua|still model was converted to MATLAB. In the next step the obtained flux, GOR, $Q_{heating}$, $Q_{cooling}$ are used to create regression formula.

4.2 Regression model

In this paragraph second order multiple regression models are created for the flux, GOR, $Q_{heating}$ and $Q_{cooling}$. Every regression model will undergo a model adequacy checking as described in section 3.2.3. All the regression coefficients can be found in Appendix A.

Actual versus residual of the regression formula

The actual versus residual plots are shown in Figure 4-1 and Figure 4-2. The points in this plot represent the simulated results in function of the predicted results of the regression model. Almost all points align perfectly on the line. Therefore, it is possible that the regression formula are a good representation of the simulation results. However, some points deviate from the line. Therefore, a residual analysis is needed to make sure that the formula are acceptable.

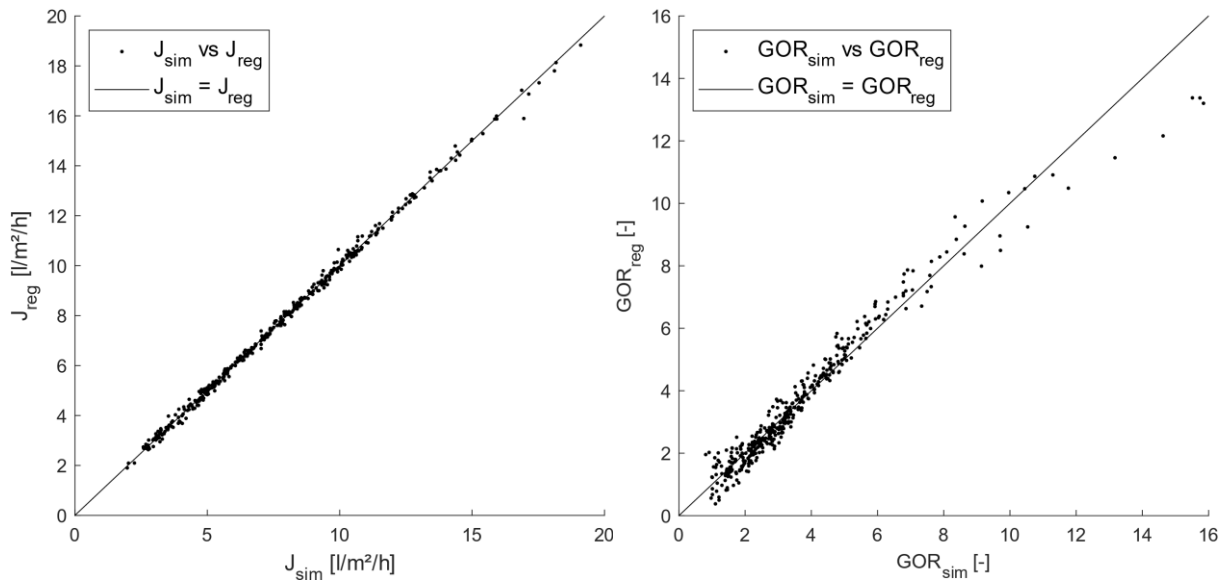


Figure 4-1 Actual versus prediction plot of the flux on the left and GOR on the right

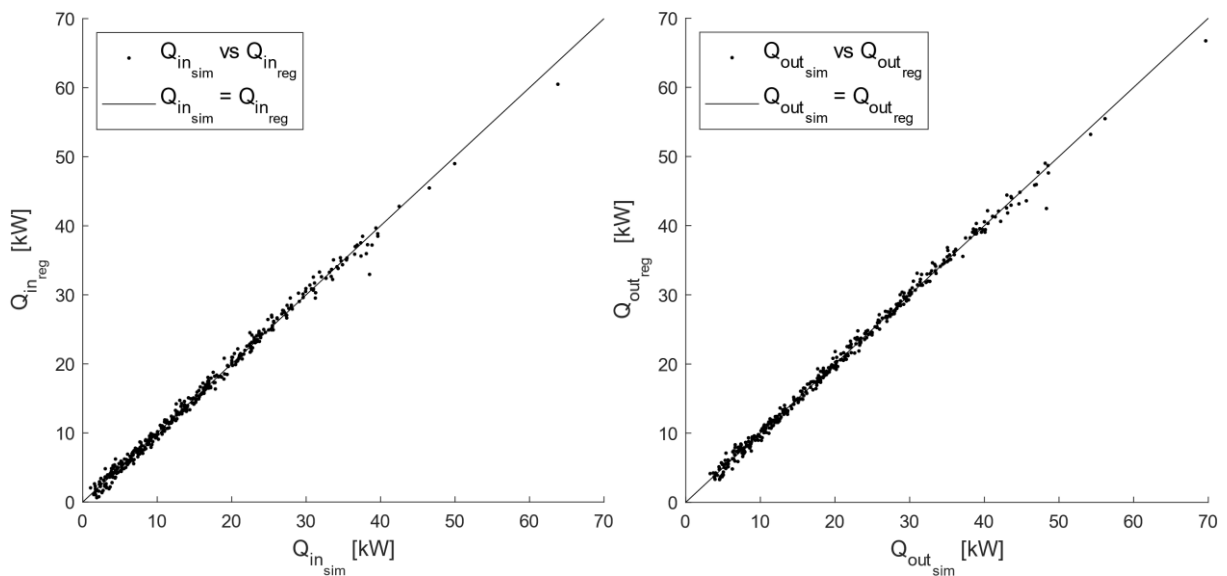


Figure 4-2 Actual versus prediction plot of $Q_{heating}$ on the left and $Q_{cooling}$ on the right

Normal probability of the regression formula

The normal probability plots are shown in Figure 4-3 and Figure 4-4. Most points for the flux are close to the line. However, some points are further away from the line. According to Montgomery et al. [82] these can be outliers. Therefore, the regression formula for the flux is acceptable.

Most points are close to the line for the GOR, $Q_{heating}$ and $Q_{cooling}$. However, some points are further away. This result suggests that there is flattening at the extremes. According to Montgomery et al. [82] this is the result of a distribution that has heavier tails than the normal distribution. Nevertheless, this may not be a problem because the deviation is less than two percent from the normal distribution. Therefore, the regression formula for the GOR, $Q_{heating}$ and $Q_{cooling}$ are acceptable.

However, before concluding that the regression formula is valid it is necessary to look at the residuals of all the regression formula.

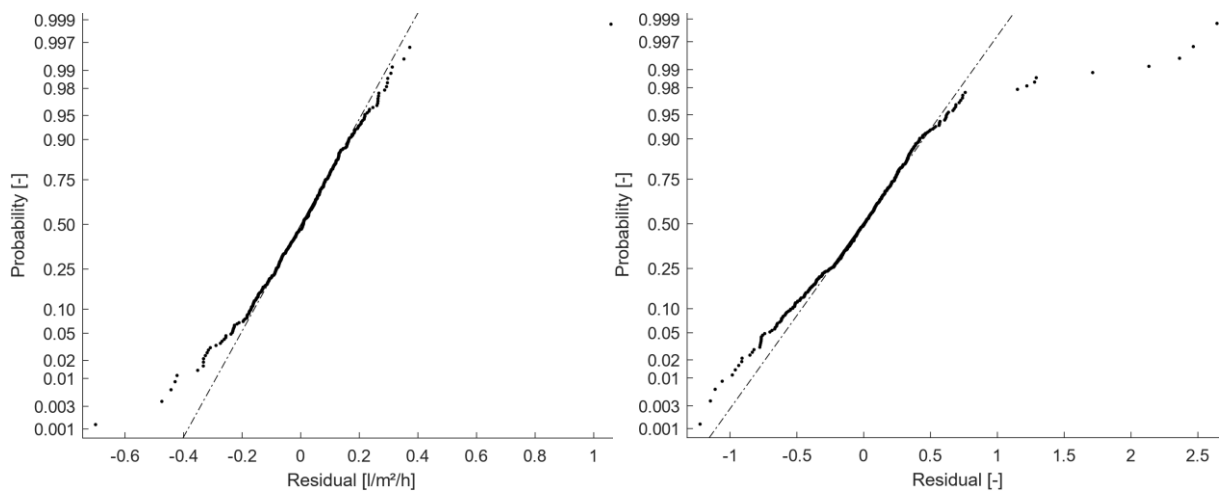


Figure 4-3 Normal probability of the flux on the left and the GOR on the right

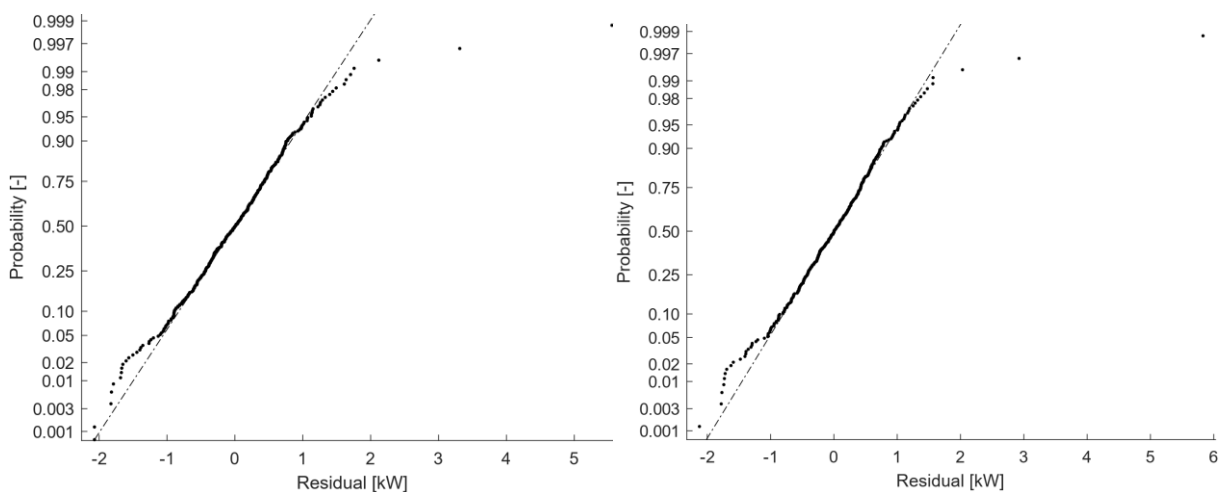


Figure 4-4 Normal probability of $Q_{heating}$ on the left and $Q_{cooling}$ on the right

Residual plots of the regression formula

The residual plots are shown in Figure 4-5 and Figure 4-6. Montgomery et al. [82] state that when there is a horizontal band in the residual plot then there are no model defects most of the times. Therefore, the regression for the flux are correct. However, there are two points who are further away from the band. These two points are the same outliers as discussed in previous section. Therefore, it can be concluded that the regression model for the flux is valid and represents the flux accurately.

For the GOR, $Q_{heating}$ and $Q_{cooling}$ more points are outside the horizontal band. These points are the same deviating points as in the previous section. As these points are less than two percent of the total population the regression formula are valid and accurate.

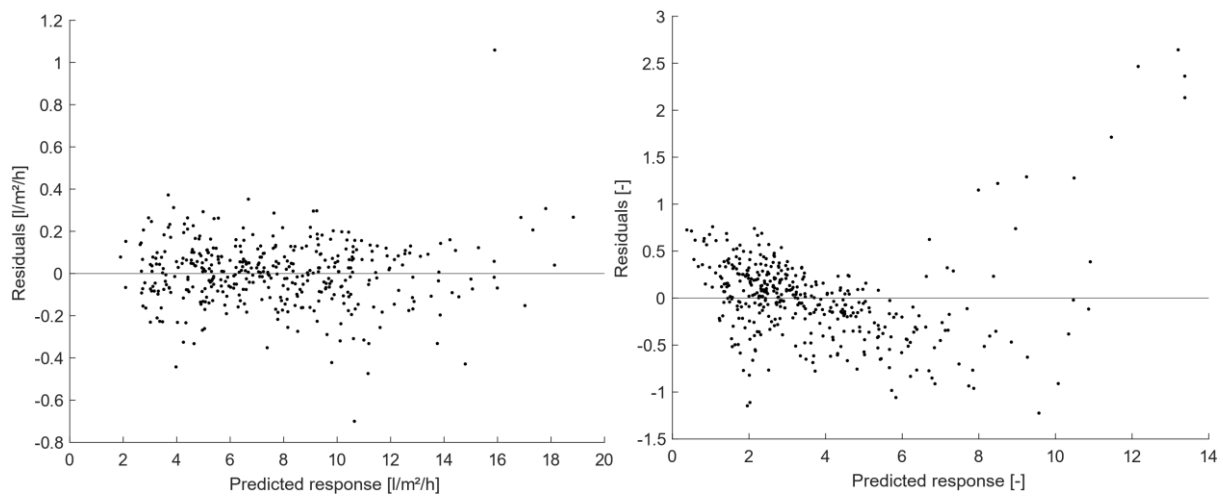


Figure 4-5 Residual plots of the flux on the left and the GOR on the right

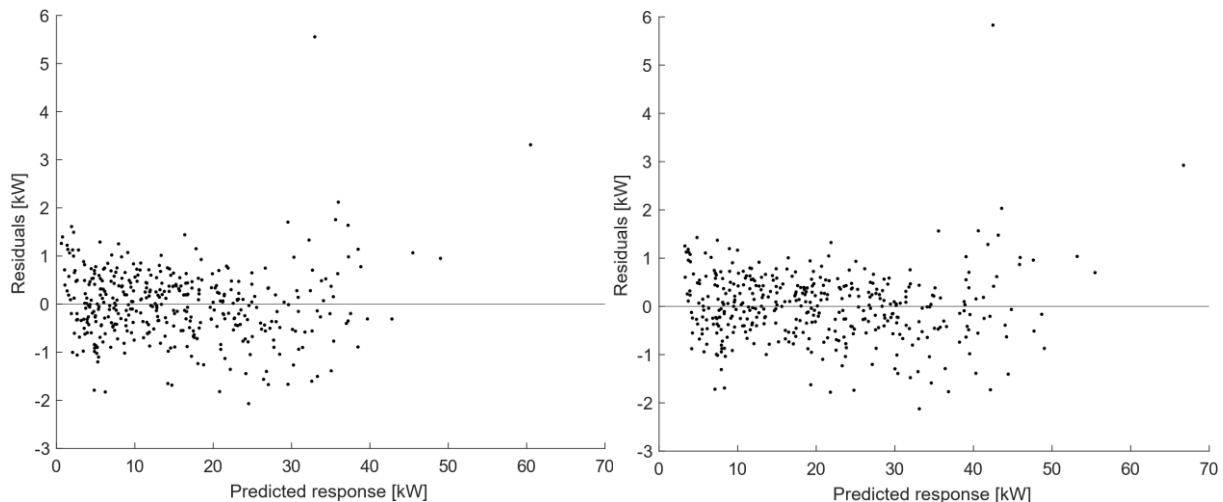


Figure 4-6 Residual plots of $Q_{heating}$ on the left and $Q_{cooling}$ on the right

4.3 Simulated annealing

As told in section 3.2.4 the surface under the dashed line needs to be increased in order to maximize the flux and GOR. The MATLAB algorithm that was created in order to find the optimum can be found [90].

The result of simulated annealing can be seen in Figure 4-7. On the top of the figure the surface is plotted in function of the number of iterations. In the bottom side of the figure the annealing temperature is plotted in function the amount of iterations. Only around 4000 points are shown in order to keep the memory requirement low.

The surface is changing fast in the first subplot because the method is searching for the global optimum. Around 0.5 million iterations the surface starts to converge to the global optimum. Therefore, the temperature is not decreasing as fast anymore, as can be seen in the second subplot. When the SA is around one million iterations, the line that represents the surface becomes flat. This indicates that the solution converged, and a global optimum may be found. This is the point where SA starts to behave like the hill climbing method. After 2.7 million iterations the global optimum was found. It seems like SA could have been stopped around 1.5 million iterations. However, it was found that the solution not always converges at 1.5 million. For example, in one run the solution converged at 2 million iterations. Therefore, the SA was run with 2.7 million iterations.

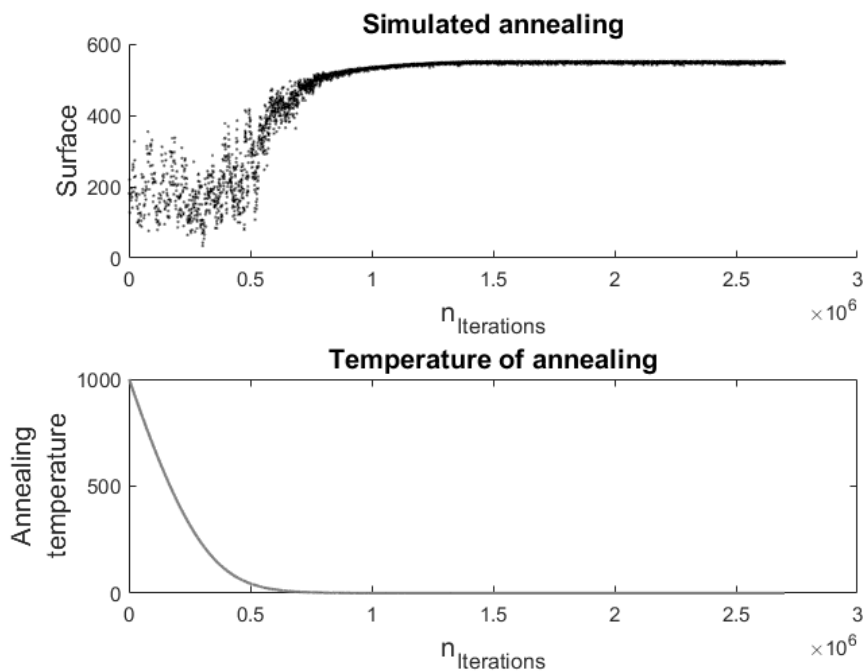


Figure 4-7 Surface optimization with simulated annealing

The different process and module parameters from Table 3-2, can now be calculated because the largest surface under the flux-GOR curve is known. The result of SA can be found in Table 4-1.

The optimum condenser inlet temperature is 30.28 °C. Which is not the minimum of 15 °C. The second parameter is the membrane inlet temperature. The optimum membrane inlet temperature is 90 °C which is logical because a higher the temperature difference between the condenser and the membrane results in a higher flux.

Table 4-1 Optimum values of the different process conditions and module parameters

Predictor variables	Optimum
Condenser inlet temperature [$^{\circ}C$]	30.28
Membrane inlet temperature [$^{\circ}C$]	90
Salinity [g/kg]	0
Air gap pressure [kPa]	10
Heat transfer membrane channel [-]	2
Heat transfer membrane [-]	2
Heat transfer air gap [-]	2
Heat transfer condenser [-]	2
Heat transfer condenser channel [-]	2
Mass transfer rate membrane [-]	2
Mass transfer rate air gap [-]	0.5

The third parameter is the salinity. The lower the salinity the higher the water activity of the feed water. Therefore, it is logical that the flux and GOR are optimal when there is no salt in the water.

The optimal air gap pressure is found at 10 kPa. This is the minimum value that was defined in the design space. When the pressure is low then the vapour pressure difference will be bigger than the atmospheric pressure. This results in a higher mass transfer through the membrane. However, when the pressure is too low then the water will not condense because the vapour pressure of the vapour is higher than the pressure in the air gap.

The following parameters are the heat transfer of the membrane channel, membrane, air gap, condenser and the condenser channel. All these parameters are set at the maximum defined value of two. This is logical since the system transfers heat better when the heat transfer of the module is higher.

The last two parameters are mass transfer rate of the membrane and the air gap. The optimum of the mass transfer rate of the membrane was found to be two. This is logical because when the membrane transfers more mass then the net flux will increase. The mass transfer rate air gap is be found at zero point five. It is likely that the model wants to decrease the mass transfer because than there is less heat of evaporation that needs to be transferred to the condenser channel. In Figure 4-8 the optimum flux in function of GOR can be found.

A benefit of the methods that were used in this thesis is that the optimum can be found when some of the parameters are fixed.

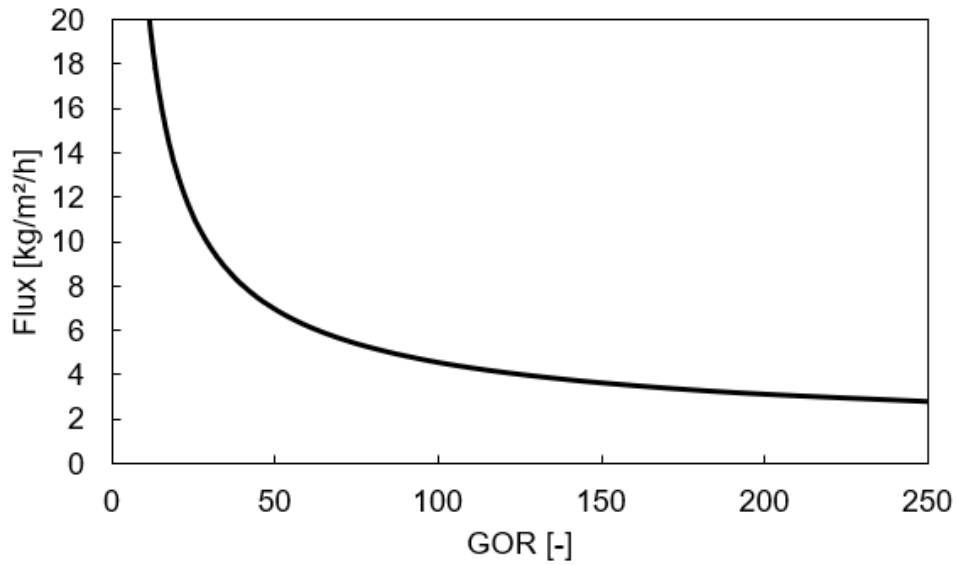


Figure 4-8 Optimum flux versus GOR

4.4 Conclusions

The following conclusions were found:

- 400 points are sufficient to find an adequate regression formula for the flux, GOR, $Q_{heating}$ and $Q_{cooling}$.
- The solution of simulated annealing always converged at 2.7 million iterations and can in some cases converge sooner.
- The method can also find optima when some parameters are kept fixed.
- The optimum was found at the values as listed in Table 4-1.

5 CONCLUSIONS PART A

When using conventional power sources there is low grade heat that is not be used for the production of electricity due to the low Carnot efficiency. However, this waste heat still has a high enough temperature to produce water with membrane distillation. To use this waste heat wisely, the process conditions and the materials need to be as best as possible. In this part of this thesis, research was conducted in order to find the perfect process conditions and materials parameters for V-AGMD.

The following methodology was found to give the best correct results. In the first step the design space is created by using the maximum projection method, which is a space filling design method. This created design space has 400 points in twelve dimensions. Each dimension represents a parameter and has their own range. This design space is then used as an input for the existing Aqua|still model. In the next step the obtained flux, GOR, $Q_{heating}$, $Q_{cooling}$ are used to create four standard second-order multiple regression formula. After the creation of the regression formula, residual analysis was used to check the model adequacy. Therefore, it can be concluded that 400 points for the creation of the design space is enough. In the last step simulated annealing was used to find the optimum of membrane distillation. 2.7 million iterations was found to give correct results where the solution of SA always converges to the global optimum. Furthermore, the chosen methodology can be used to find an optimum when some of the parameters are fixed.

The optimum process conditions were found to be 30.28°C, 90°C, 0 g/kg and 10 kPa for the condenser inlet temperate, membrane inlet temperature, salinity and air gap pressure respectively. All of the mass and heat transfer parameters should increase two times to find the optimum. However, the mass transfer of the air gap should be halved to reach the optimum.

Part B

Introduction to part B

In chapter 6 the models for the dynamic calculation of air gap membrane distillation will be explained and developed. In chapter 7 and 8 the validation will be explained, and the results will be presented. In the last chapter of this part the conclusion will be made for Part B. In chapter 10, the overall conclusion will be made. To fully understand Part B, it is recommended to read chapter 2 from the general part first.

Table of contents Part B

6	Dynamic modelling of air gap membrane distillation	63
6.1	<i>Regression-based model</i>	63
6.2	<i>Thermal electrical networks.....</i>	64
6.3	<i>Energy balance model.....</i>	69
7	Validation of dynamic models	71
7.1	<i>Steady state data</i>	71
7.2	<i>Transient data</i>	72
	7.2.1 Materials and methods.....	72
8	Results and discussion	75
8.1	<i>Steady state validation</i>	75
	8.1.1 Regression model	75
	8.1.2 Thermal electrical network	76
	8.1.3 Energy balance equations model	77
8.2	<i>Dynamic validation</i>	78
	8.2.1 Regression model	78
	8.2.2 Thermal electrical network	80
	8.2.3 Energy balance model	81
8.3	<i>Benchmarking of the models.....</i>	83
8.4	<i>Conclusion</i>	83
9	Conclusion part B	85

6 DYNAMIC MODELLING OF AIR GAP MEMBRANE DISTILLATION

In recent years there has been some efforts to understand and model membrane distillation. Most models concerning membrane distillation are steady state models [19], [51]–[53], [59], [91]–[94]. However, when dealing with temporal variation of the process conditions, dynamic models should be made. There exist some dynamic models for MD, but they have their own drawbacks. The main drawback is that most transient models are not build for AGMD. For example, in [33], [40]–[42] DCMD was modelled. Moreover, there also exist a model that can not be used for different module parameters and only for different process conditions [43].

Three ways of modelling were chosen. The reason for this decision is that it is academically interesting. The other reason is that the best of the three models can be chosen. This will be done in chapter 8.

The first way of modelling is very simplistic by ignoring the transient effect. This model is based on the regression formula that was found in Part A. The second way of modelling is by using a thermal electrical network. This method was first developed by Karam et al. [42] for DCMD. This model will be converted to AGMD. The third method uses energy balance that are translated to partial differential and algebraic equations. This was first done by [33] for AGMD although no sufficient validation was done. In the next following sections, the three chosen models will be developed. The validation of the models will be shown in the next chapter.

6.1 Regression-based model

When assuming that the transient effects are neglectable, which will be further discussed in chapter 8, then the regression formula can be used to model the system. The regression formula from chapter 4.2 can be shortened to (6-1). Where Q_{hot} , Q_{mem} , Q_{airgap} , $Q_{condenser}$, Q_{cold} , m_{mem} and m_{air} are the material parameters of the module.

$$J = f(T_{pin}, T_{hin}, S_{in}, v_{eff}, P_{airgap}, C_{Q_{hot}}, C_{Q_{membrane}}, C_{Q_{airgap}}, C_{Q_{condensor}}, C_{Q_{cold}}, C_{m_{membrane}}, C_{m_{airgap}}) \quad (6-1)$$

In the case of dynamic modelling the last 7 parameters are module dependent and will not deviate over time and are therefore 1. Thus, the equation can be simplified to equation (6-2) where the input parameters are as a function of time. When the input parameters are discretized, the function can be translated to (6-3). The total flux can be calculated with equation (6-4) where l_d is the discretization length.

$$J(t) = f(T_{pin}(t), T_{hin}(t), S_{in}(t), v_{eff}(t), P_{airgap}(t)) \quad (6-2)$$

$$J[k] = f(T_{pin}[k], T_{hin}[k], v_{eff}[k], S_{in}[k], P_{airgap}[k]) \quad (6-3)$$

$$D_{tot} = A_m l_d \sum_1^n J_i \quad (6-4)$$

This model will be further discussed in chapter 8.

6.2 Thermal electrical networks

By using the laws of thermal and electrical systems a dynamic model can be derived. A dynamic model based on the electrical analogy of thermal systems has already been thoroughly described by Karam for DCMD [95]. However, this model can not be used for AGMD. In this section the electrical analogy for AGMD will be developed and described. The electrical analogue for thermal units is shown in Table 6-1.

Table 6-1 Thermal to electrical units

Thermal		Electrical	
Element	Unit	Unit	Element
Temperature	$^{\circ}C$ or K	V	Voltage
Heat transfer	W	A	Current
Resistor	$^{\circ}C/W$	Ω	Resistor
Capacitor	$J/^{\circ}C$	F	Capacitor

The module will be discretised along the channel. The electrical analogue for the n^{th} channel is shown in Figure 6-1. The temperatures of the bulk can be represented as a voltage source. The heat capacity of the hot and cold feed bulk can be modelled as an electric capacitor. The thermal heat resistance can be modelled as an electrical resistor as they both denote the resistance to transfer. The current source Q is the heat transfer due to mass transfer. Which are, the latent heat of evaporation of the water and the heat released due to the thermal capacity reduction of the distillate. The values for each electrical element can be calculated with equations (6-5) to (6-14).

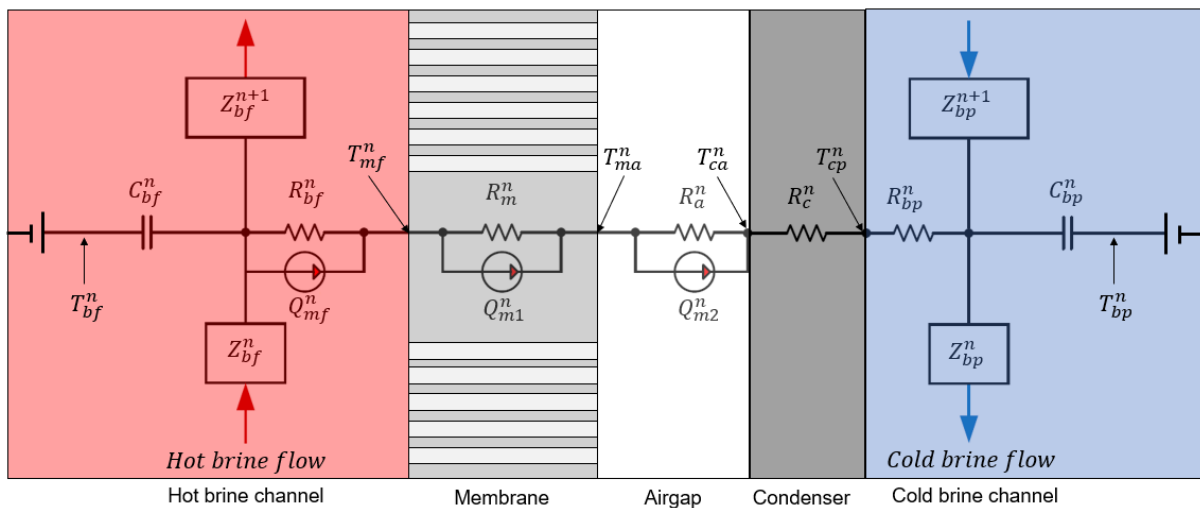


Figure 6-1 Electrical analogue for the n^{th} channel

$$R_{bf}^N = \frac{1}{A_m h_{bf}^N} \quad (6-5)$$

$$R_m^N = \frac{1}{A_m h_m^N} \quad (6-6)$$

$$R_a^N = \frac{1}{A_m h_a^n} \quad (6-7)$$

$$R_c = \frac{1}{A_m h_c} \quad (6-8)$$

$$R_{bp}^N = \frac{1}{A_m h_{bp}^N} \quad (6-9)$$

$$Q_{mf}^N = A_m J c_p T_{bf}^N \quad (6-10)$$

$$Q_{m1} = A_m J c_p H_v \quad (6-11)$$

$$Q_{m2} = (1 - x_l) A_m J c_p T_{ca} + x_l A_m J c_p H_v \quad (6-12)$$

$$C_{bf}^N = \rho c_p v_{bf} \epsilon_{sp} + (1 - \epsilon_{sp}) A_m t_{ch} \rho_{sp} c_{p,sp} \quad (6-13)$$

$$C_{bp}^N = \rho c_p v_{bp} \epsilon_{sp} + (1 - \epsilon_{sp}) A_m t_{ch} \rho_{sp} c_{p,sp} \quad (6-14)$$

The cells are interconnected via the series impedance of Z_f^n and Z_p^n . These are used to simulate the temperature gradient along the channel. The series impedance cannot be determined by direct analogy [96]. However, the impedance should be a function of the mass flow rate and the energy received or given through the membrane [95]. Furthermore, Z_f and Z_p should be verified against experimental data [95]. The value for R_{feq} and R_{peq} are defined by using the steady state model from [52]. This is done by determining which form of equation (6-21) and (6-22) corresponded to the same outlet temperatures.

$$Z_{bf}^n = R_{bfz}^n + j\omega L_{bf}^n \quad (6-15)$$

$$R_{bfz}^n = \frac{1}{\dot{m}_{bf}^n{}^2 c_p^2 R_{bfreq}} \quad (6-16)$$

$$L_{bf}^n = \frac{R_{bfz}^n{}^2 C_{bf}}{4} \quad (6-17)$$

$$Z_{bp}^n = R_{bpz}^n + j\omega L_{bp}^n \quad (6-18)$$

$$R_{pzs} = \frac{1}{\dot{m}_{bp}^n{}^2 c_p^2 R_{bppeq}} \quad (6-19)$$

$$L_{bp}^n = \frac{R_{bpzs}^n{}^2 C_{bp}}{4} \quad (6-20)$$

$$R_{bfreq} = \frac{R_{bf}}{2} + \frac{R_m}{1.5} + \frac{R_a}{1.75} + 1.5R_c + 3R_{bp} \quad (6-21)$$

$$R_{bppeq} = 1.5R_{bf} + \frac{R_m}{1.1} + R_a + R_c + R_{bp} \quad (6-22)$$

The inductors account for the dynamic response and the resistance for the steady state response. The electrical network can now be completed. The complete electrical equivalent thermal network analogue for AGMD can be seen in Figure 6-2.

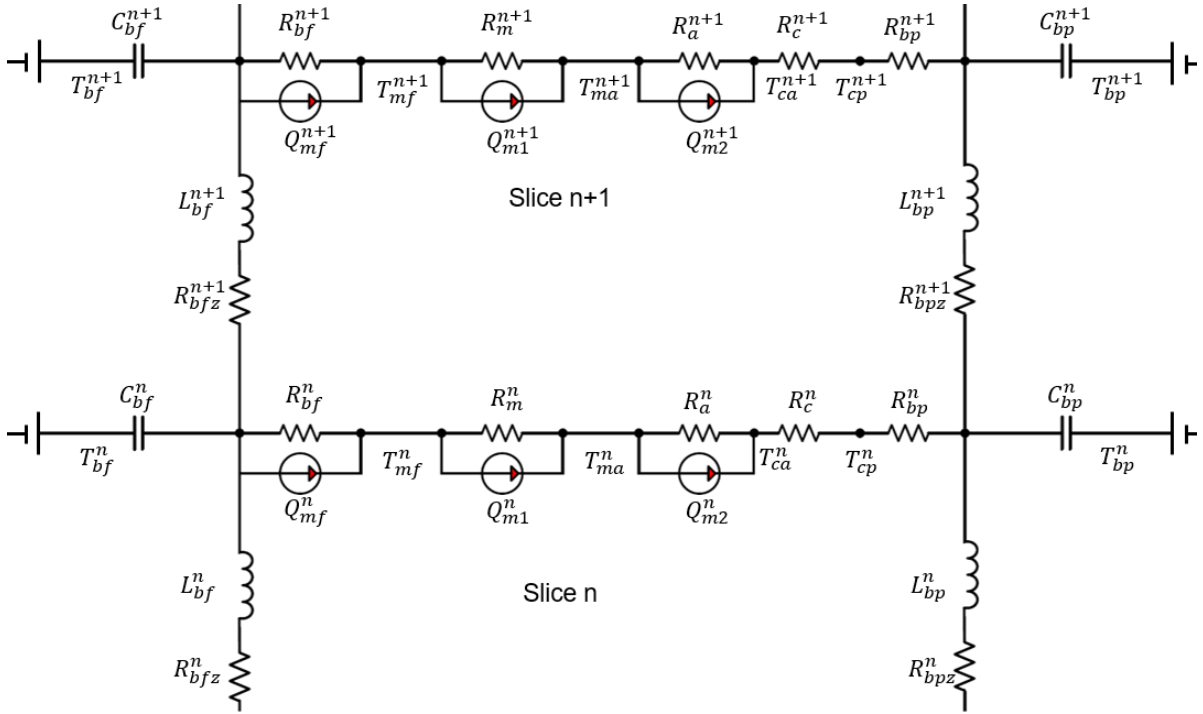


Figure 6-2 Complete electrical equivalent thermal network for AGMD

The feeding and termination of the network should be done by changing the voltage source T_f^{in} and T_p^{in} . The heat supply of the hot feed inlet and outlet can be found calculation with equation (6-23) and (6-24). The heat leaving the module from the cold feed side can be found with formula (6-25). It is clear from equation (6-23) that the input impedance should be $1/M_f^{in} c_p$ so that a voltage can be developed at the feed input terminal.

$$Q_{bf}^{in} = Q_{bf}^1 = \dot{m}_{bf}^{in} c_p T_{bf}^{in} \quad (6-23)$$

$$Q_{bf}^{out} = \dot{m}_{bf}^N c_p T_{bf}^{out} \quad (6-24)$$

$$Q_{bp}^{out} = Q_{bp}^1 = \dot{m}_{bp}^1 c_p T_{bp}^{out} \quad (6-25)$$

By using the conservation of energy, the following two equations can be found to terminate the electrical network [95]. According to the conservation of energy the temperature of the cold feed can not exceed the hot feed temperature.

$$0 = T_{bf}^{out} - T_{bp}^{in} - \frac{Q_{bf}^{N+1}}{\dot{m}_{bf}^N c_p} \quad (6-26)$$

$$0 = T_{bp}^{out} - T_{bf}^{in} + \frac{Q_{bp}^1}{\dot{m}_{bp}^1 c_p} \quad (6-27)$$

Now all the electrical parameters have been identified the electrical laws can be applied to the network. However, the thermal equations will be shown first to fully understand the electrical equations.

The change of energy in the n^{th} slice of the hot feed channel can be calculated with equation (6-28). Similarly, the change in energy of the cold feed side can be calculated with equation (6-29). These two equations are adapted from the work of Karam [42] in order to model AGMD.

$$C_{bf} \frac{dT_{bf}^N}{dt} = Q_{bf}^N - Q_{bf}^{N+1} - 2A_m(h_{bf}(T_{bf}^N - T_{mf}^N) + J^N c_p T_{bf}^N) \quad (6-28)$$

$$C_{bp} \frac{dT_{bp}^N}{dt} = Q_{bp}^N - Q_{bp}^{N+1} + 2A_m h_p (T_{cp} - T_{bp}) \quad (6-29)$$

Now that the thermal equations are developed, the electrical corresponded equation can be assessed. By applying the Kirchhoff's current law at the n^{th} node of the electrical network equation (6-30) and (6-31) can be found.

$$\frac{dT_{bf}^N}{dt} = \frac{1}{C_{bp}^N} Q_{bf}^N - \frac{1}{C_{bf}} Q_{bf}^{N+1} - \frac{2}{C_{bf}^N} \left(\frac{1}{R_{bf}^N} + J^N A_m c_p \right) + \frac{2}{C_{bf}^N R_{bf}^N} T_{mf}^N \quad (6-30)$$

$$\frac{dT_{bp}^N}{dt} = \frac{1}{C_{bp}^N} Q_{bp}^N - \frac{1}{C_{bp}^N} Q_{bp}^{N+1} - \frac{2}{C_{bp}^N R_{bp}^N} T_{bp}^N + \frac{2}{C_{bp}^N R_{bp}^N} T_{cp}^N \quad (6-31)$$

The rate of change of heat transfer rate between the cells can be calculated with equation (6-32) and (6-33). These equations take the series impedance Z_f^n and Z_p^n into account.

$$\frac{dQ_{bf}^N}{dt} = \frac{1}{L_{bf}^N} T_{bf}^{N-1} - \frac{R_{bfz}^N}{L_{bf}^N} Q_{bf}^N - \frac{1}{L_{bf}^N} T_{bf}^N \quad (6-32)$$

$$\frac{dQ_{bp}^N}{dt} = \frac{1}{L_{bp}^N} T_{bp}^{N-1} - \frac{R_{pzz}^N}{L_{bp}^N} Q_{bp}^N - \frac{1}{L_{bp}^N} T_{bp}^N \quad (6-33)$$

The coupling between the hot feed and the cold feed channel can be written as algebraic constraints (6-34) to (6-37). The constraints are based on the energy balance that were established in section 2.2.2 and translated to the electrical components.

$$T_{bf}^n \left(\frac{1}{R_{bf}^n} + A_m^n J^n c_p \right) + T_{ma}^n \left(\frac{1}{R_m^n} + A_m^n J^n c_p \right) - T_{mf}^n \left(\frac{1}{R_{bf}^n} + \frac{1}{R_m^n} + 2A_m^n J^n c_p \right) - J A_m H_v = 0 \quad (6-34)$$

$$T_{mf}^n \left(\frac{1}{R_m^n} + A_m^n J c_p \right) + x_l J A_m H_v + T_{ca}^n \left(\frac{1}{R_a^n} + A_m^n J c_p \right) - T_{ma}^n \left(\frac{1}{R_m^n} + \frac{1}{R_a^n} \right) = 0 \quad (6-35)$$

$$T_{ma}^n \left(\frac{1}{R_a^n} + A_m^n J c_p \right) + T_{cp} \left(\frac{1}{R_c^n} \right) - T_{ca} \left(\frac{1}{R_a^n} + A_m^n J c_p + \frac{1}{R_c^n} \right) + (1 - x_l) J A_m H_v = 0 \quad (6-36)$$

$$T_{ca} \left(\frac{1}{R_c^n} \right) + T_{bp} \left(\frac{1}{R_{bp}^n} \right) - T_{cp} \left(\frac{1}{R_c^n} + \frac{1}{R_{bp}^n} \right) = 0 \quad (6-37)$$

Equations (6-26), (6-27) and (6-30) to (6-37) can be combined to form the differential algebraic equation (DAE) (6-38). x represents all the states of the system, M is the mass matrix, B and B_2 are the input channels and H represents the latent heat.

$$[M][\dot{x}] = [F][x] + [B] + [H] \quad (6-38)$$

All the matrices will be explained and shown in the next section.

6.3 Energy balance model

In the work of Chang et al [33] equation (6-47) and (6-48) were found. However, this model was solved by software that Aqua|still does not have. Therefore, a numerical model was made from the previously mentioned equations.

$$\frac{\partial T_{bf}}{\partial t} = -L_{MD} \left[\frac{\dot{m}_{bf}}{m_{bf}} \frac{\partial T_{bf}}{\partial z} + \frac{W_{MD}}{m_{bf} C_p} (h_{bf} + J C_p) (T_{bf} - T_{mf}) \right] \quad (6-47)$$

$$\frac{\partial T_{bp}}{\partial t} = L_{MD} \left[\frac{\dot{m}_{bp}}{m_{bp}} \frac{\partial T_{bp}}{\partial z} + \frac{W_{MD} h_{bp}}{m_{bp} C_p} (T_{cp} - T_{bp}) \right] \quad (6-48)$$

When taking the first effect from chapter 2.2.1 into account and using backwards difference approximation equation (6-47) can be converted to equation (6-50). The same can be done for equation (6-48) but with forward difference approximation. The backward and forward difference equations are shown in equation (6-49) and (6-51) respectively.

$$\frac{\partial T_{bf}}{\partial z} = \frac{(T_{bf_i}^n - T_{bf_{i-1}}^n)}{\Delta z} \quad (6-49)$$

$$\frac{dT_{bf_i}}{dt} = -L_{MD} \left[\frac{\dot{m}_{bf}}{m_{bf}} \frac{(T_{bf_i}^n - T_{bf_{i-1}}^n)}{\Delta z} + 2 \frac{W_{MD}}{m_{bf} C_p} (h_{bf} + J C_p) (T_{bf} - T_{mf}) \right] \quad (6-50)$$

$$\frac{\partial T_{bp}}{\partial z} = \frac{(T_{bp_{i+1}}^n - T_{bp_i}^n)}{\Delta z} \quad (6-51)$$

$$\frac{dT_{bp_i}}{dt} = L_{MD} \left[\frac{\dot{m}_{bp}}{m_{bp}} \frac{(T_{bp_{i+1}}^n - T_{bp_i}^n)}{\Delta z} + 2 \frac{W_{MD} h_{bp}}{m_{bp} C_p} (T_{cp} - T_{bp}) \right] \quad (6-52)$$

When these equations are written out equation (6-53) and (6-54) are found.

$$\begin{aligned} \frac{dT_{bf_i}}{dt} = & T_{bf_i}^n \left(-L_{MD} \frac{\dot{m}_{bf}}{m_{bf} \Delta z} - L_{MD} \frac{2W_{MD}}{m_{bf} C_p} (h_{bf} + J C_p) \right) + T_{bf_{i-1}}^n \left(L_{MD} \frac{\dot{m}_{bf}}{m_{bf} \Delta z} \right) \\ & + T_{mf} \left(L_{MD} \frac{2W_{MD}}{m_{bf} C_p} (h_{bf} + J C_p) \right) \end{aligned} \quad (6-53)$$

$$\begin{aligned} \frac{dT_{bp_i}}{dt} = & T_{bp_{i+1}}^n \left(L_{MD} \frac{\dot{m}_{bp}}{m_{bp} \Delta z} \right) + T_{cp} \left(\frac{2W_{MD} L_{MD} h_{bp}}{m_{bp} C_p} \right) \\ & + T_{bp} \left(-\frac{2L_{MD} W_{MD} h_{bp}}{m_{bp} C_p} - L_{MD} \frac{\dot{m}_{bp}}{m_{bp} \Delta z} \right) \end{aligned} \quad (6-54)$$

7 VALIDATION OF DYNAMIC MODELS

According to [97] there is no single approach for checking if a mathematical model is correct in comparison with reality. However, in case of dynamic modelling, steady state validation is just as important as transient validation. Two sources will be used for the steady state validation. These will be explained in section 7.1.

To have a dynamic output a test setup was needed to perform step input responses. Therefore, a setup was designed in this thesis. This will be explained in section 7.2.

7.1 Steady state data

The first source of the steady state data is a dataset provided by Aqua|still. This dataset contains several envelope lengths and a wide range of salinity and air gap pressures. The dataset is listed in Table B- 1 in the appendix. This data comes from an installation that uses a syphon as explained in section 2.1.2.

The second and final source for the steady state data comes from [52] where a module with 1.5 meter long envelopes was used to validate the existing Aqua|still model. This data has been listed in Table B- 2. For these tests the air gap pressure, module length and number of envelopes was 101325 Pa, one point five meter and six respectively. In this dataset no syphon was placed at the exit.

A typical setup that was used for the steady state data can be seen in Figure 7-1.

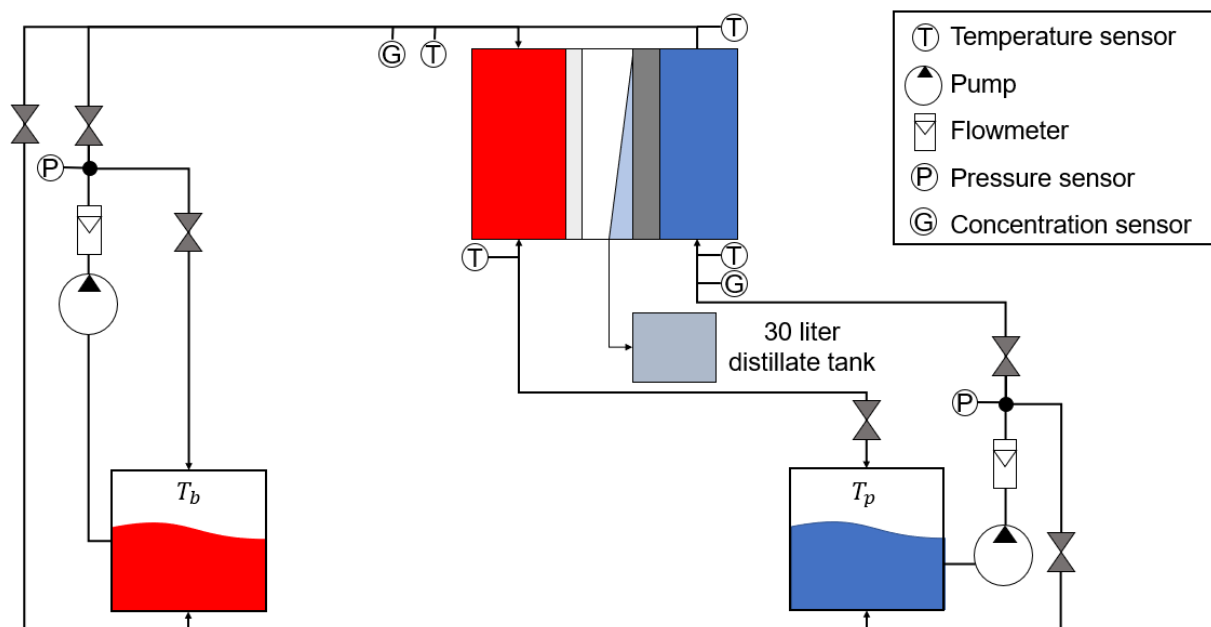


Figure 7-1 Schematic representation of a steady state test setup

7.2 Transient data

A step input can be rather easily applied in most mechanical and electrical systems. However, in thermal/hydraulic systems it is hard to apply a step input like the temperature of water. For example, in normal Aqua|still pilots it is not possible to apply a step input of the temperature of the feedwater. By contrast, it is possible to apply a step input if two pilots are interconnected. So, a test setup with two pilots was designed in this thesis.

7.2.1 Materials and methods

As can be seen in Figure 7-2, the hot feed tanks and cold feed tanks from the two pilots are connected to the AGMD module by using two pumps. Therefore, it is possible to have two hot and two cold feed water temperatures. In order to switch between the two tanks valves are placed in front of the entry of the module. This way, it is possible to switch quickly in order to perform a step input. To make sure that the feed flow from both pilots are the same a bypass valve was used. When the hot feed water has cooled down in the module it is transferred to the cold feed tanks. The cold feed water is heated up by the module and is afterwards transfers to the hot feed tanks. The hot feed water tanks were heated by using electrical heaters. The cold feed tanks were cooled by using a heat exchanger with water cooling. The distillate produced by the module is collected in a 30-litre tank and weighted on a scale. In Table 7-1 all the used measuring equipment are listed. In Figure 7-3 the total setup can be seen.

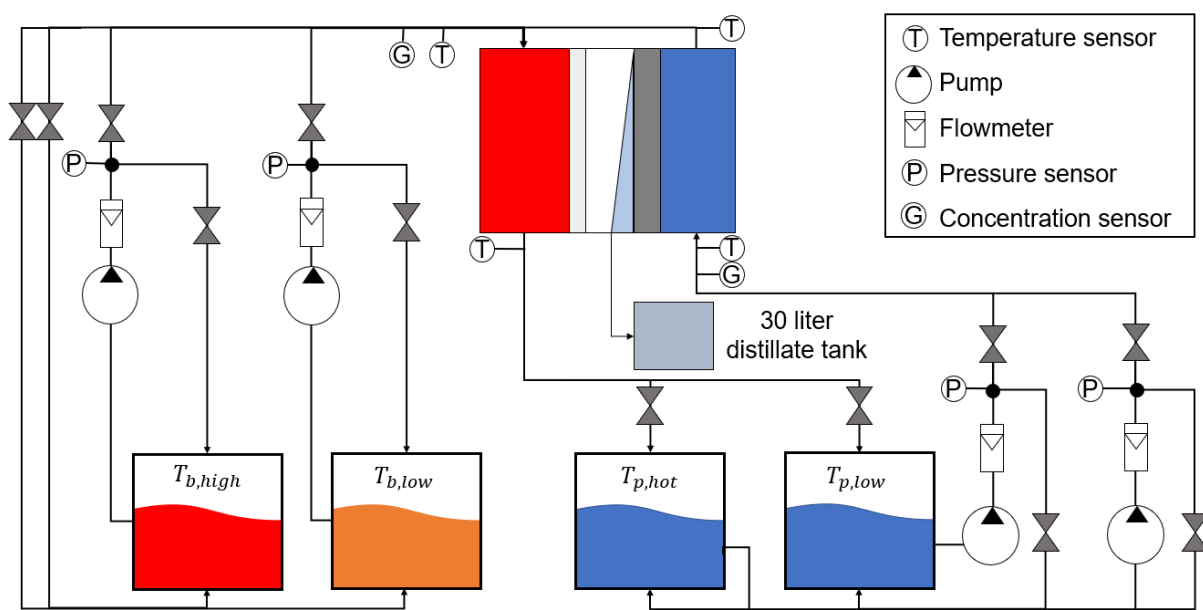


Figure 7-2 Schematic representation of the dynamic test setup



Figure 7-3 Actual setup

In order to have a measurable response, the magnitude of the step input should be significant. However, in order to see the effect of the magnitude several step magnitudes were chosen. All the input charts can be seen in Appendix E. The pressure in the air gap and the cold feed temperature is kept constant as this does not change quickly in real applications. In the first test the water temperature was raised in a slow manner. This is done to replicate the conditions that happen during start up. An extra test was performed to gain insight in the emptying of the air gap. This phenomenon happens when a shock is applied to the module, as described earlier in section 2.2.1.

The salinity could not be measured experimentally because the value was out of range of the sensors. Therefore, the salinity was calculated based on the amount of water in the tank and the amount of salt that was added to the tank.

Table 7-1 Measurement equipment

Measurement	Type
Flow	Burkert 8041 and Burkert 8020
Salinity	Burkert 8228
Temperature	Burkert Pt-100
Balance	Vida xl A4-LCD

8 RESULTS AND DISCUSSION

The models will be evaluated by using a dataset that has been provided by Aqua|still and from the existing steady state model validation [52]. Furthermore, the dynamic result will be used to determine the correctness of the transient effects.

The difference between the dataset provided by Aqua|still and the one from the article is the module. In [52] the envelope length was 1.5 meter. In contrast, the modules used in the dataset are 1.5, 2.7 and 5 meters, have a slightly thinner air gap and vacuum was used in the test. As the regression model was developed for the 1.5-meter module that was used in the dataset, the $Q_{air\ gap}$ term will be slightly adjusted to take this into account.

8.1 Steady state validation

8.1.1 Regression model

As can be seen in Figure 8-1 the regression model and the test result for the flux correspond quite well except for some points for the dataset that was provided by Aqua|still. This could be due to scaling or due to the syphon that was placed at the distillate exit. More information is needed to confirm one of the two possibilities. This will be picked up again in the following sections.

The thermal energy input and output are not as precise as the flux. A reason for this might be that the experimental thermal energy is only calculated on the input and output temperatures whereas the regression model takes the temperature change while heating and cooling into account. This way the changing thermal physical properties are considered. Therefore, the regression might be more accurate than the calculated values from the experimental data.

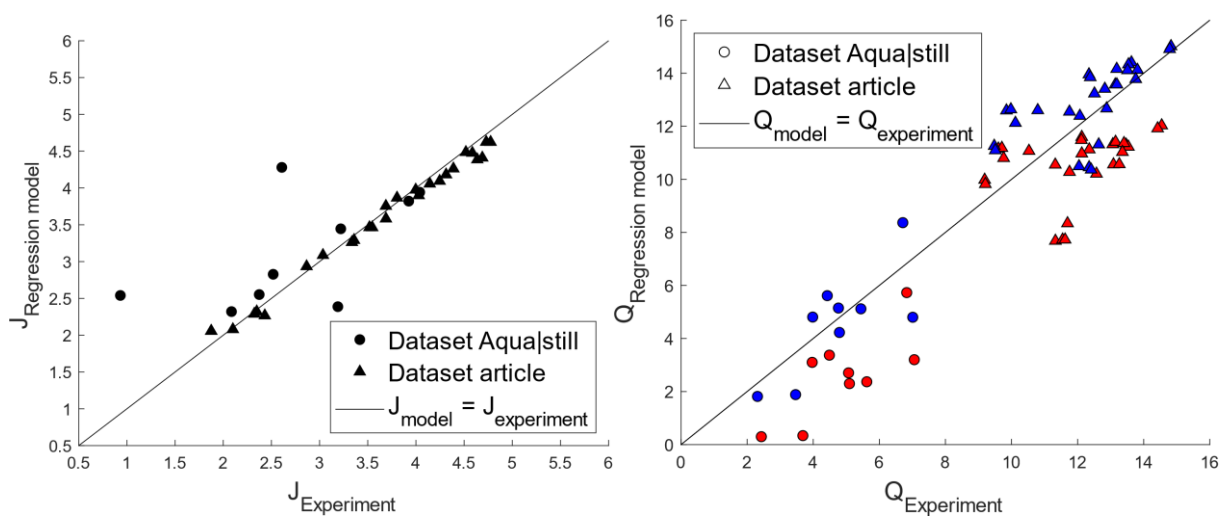


Figure 8-1 Predicted versus measured flux of the regression model on the left. On the right the predicted versus measured output (blue) and input (red) heat flows.

8.1.2 Thermal electrical network

When trying to solve the thermal electrical network (TEN) by using ode15s, the solver gave the error that the step size was lower than the minimum allowed step size. This means that the solver uses very small steps and it will take a long time to complete the calculations. To solve this issue the relative tolerance is increased to 10%. The relative tolerance makes sure that the transient response is within a certain error range. When increasing the relative tolerance, the error range is also increased. This means that the transient response will have a higher error and can be inaccurate. However, this does not influence the steady state response.

On the left side of Figure 8-2 the flux according to the model versus the experimental flux is shown. As can be seen, the model does not provide accurate results. However, to be able to model the air gap pressure was raised from 10 kPa to 40 kPa. This comes from the partial pressure of air that reduces with vacuum. At a certain point, only water vapour exists in the air gap. As there is only water vapour, the molecular diffusion can be neglected in the air gap. This is a good assumption for the membrane because the mass flow will be limited by Knudsen diffusion. However, in the air gap no Knudsen diffusion is taking place. This can be visualized in Figure 8-3 where the air gap pressure is lowered. To summarize, when the air gap pressure is lower than the vapour pressure in the process is more compatible with vacuum membrane distillation. However, it is not known how to incorporate this into V-AGMD.

As can be seen on the right side of Figure 8-2, the predicted temperatures have a slightly offset from the actual values. A possibility for this error is the flux that is not modelled correctly. A second possibility is that other values for R_{feq} and R_{peq} might define the temperatures correctly.

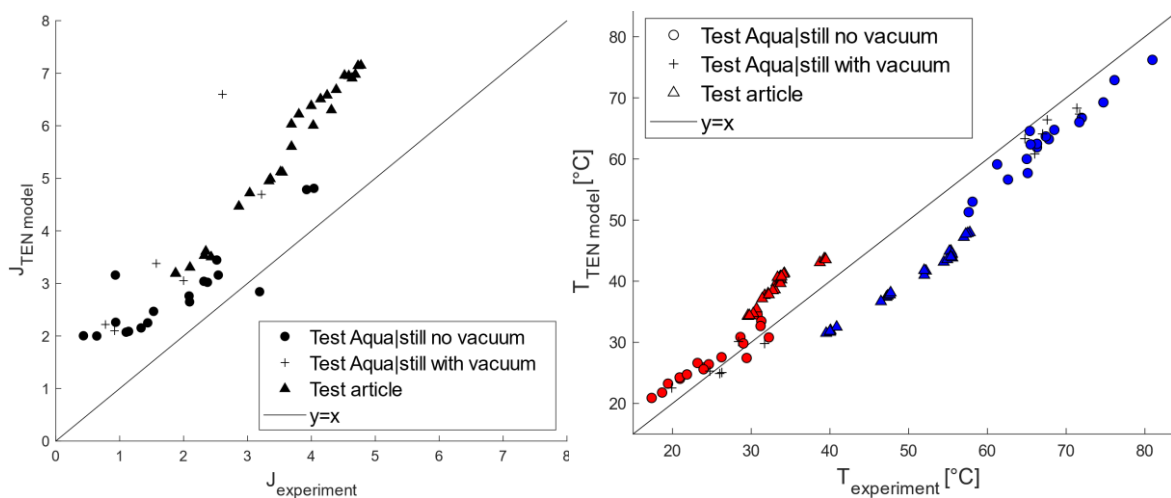


Figure 8-2 Predicted versus measured flux and temperatures of the TEN model

Another reason for the offset of the temperatures and the flux could be the reduction in thickness of the air gap due to the hydraulic pressure in both the hot and cold feed channel. Therefore, the system was remodelled with half the air gap thickness. However, the correlation for the water fraction, x_l , was kept the same. This could lead to an error and should, ideally, be determined theoretically or experimentally. Sadly, this is time consuming and is therefore out of the scope of this thesis.

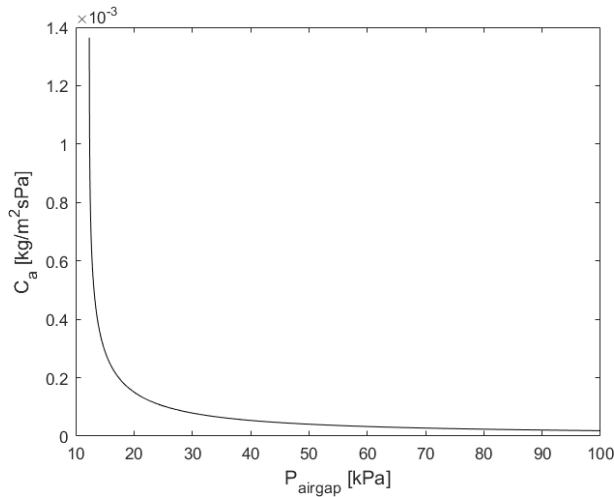


Figure 8-3 Air gap permeability plotted against air gap pressure.

As can be seen in Figure 8-4, when modelling an air gap that is twice as thin, the flux and temperatures are modelled more precisely. This could indicate that the air gap is thinner due to the hydraulic pressures. In contrast, it could be a fault in the model and that the air gap does not change in thickness. However, one can only be sure if it is measured. Again, this is out of scope of this thesis because this is not an easy thing to measure or to model.

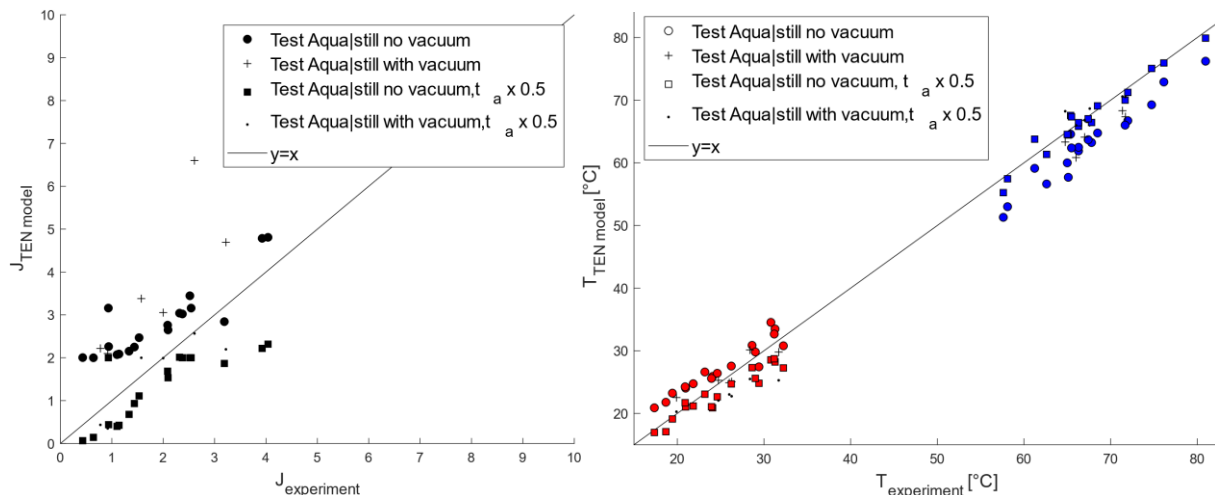


Figure 8-4 Predicted flux and temperatures modelled with $0.5t_a$, TEN model

8.1.3 Energy balance equations model

As can be seen in Figure 8-5, the dataset from [52] show good correlation. However, the dataset provided by Aqua|still shows less good correlation. However, it is suspected that the pressure in the air gap is not the same as the applied pressure. In order to investigate this assumption, the model was run with environmental pressure in the air gap, which are represented as squares in Figure 8-5. As can be seen, the squares are much closer to the actual test data. This could indicate that there is a difference between the applied pressure and the actual pressure in the air gap.

Similar to the flux, the energy balance equations (EBE) model predicts the output temperatures inaccurately for the dataset that was provided by Aqua|still. A reason for this behaviour might be scaling. This would result in less heat and mass transfer which would

result in a lower flux, higher hot feed output temperature and a colder cold feed output temperature. However, only the lower flux is happening. This means that scaling could be happening but minimally. However, this would indicate that the syphon which was placed at the distillate exit improves the module efficiency. Despite that, it is unknown what the effect of the syphon is and how it should be modelled.

As can be seen in Figure 8-5, the model gives slightly better results when calculating the air gap with half its thickness. This could indicate that the membrane and condenser foil are pushed inside of the air gap and decreases the overall air gap thickness.

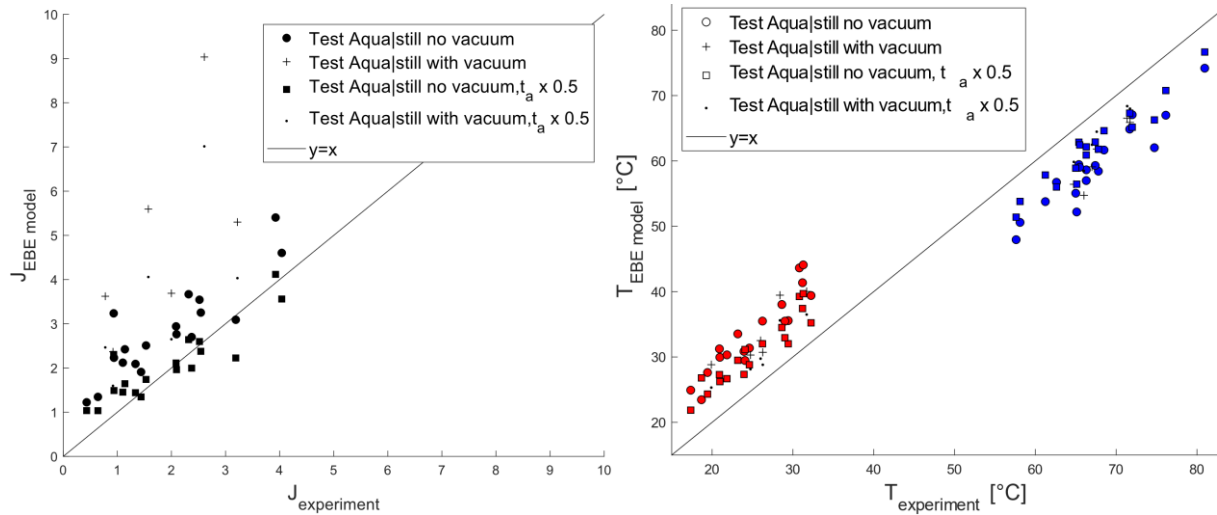


Figure 8-5 Predicted flux and temperatures modelled with $0.5 t_a$, EBE model

8.2 Dynamic validation

In this section the dynamic validation will be done. These will be based on the collected data with the test setup that is described in section 7.2.1.

8.2.1 Regression model

Only two graphs are shown as all graphs are similar to the ones in Appendix F. As can be seen in Figure 8-6 and Figure 8-7, the regression follows the test results closely. However, in the other graphs the regression follows less closely. The reason for this is the water in the air gap. As described earlier, the air gap can act as a water reservoir that can empty suddenly. For example, at the end of test 1 the flux and total production changes quickly. It was at this moment that a suddenly extra increase in production was observed during the test. This also happened in the other direction, where no distillate came out of the module. Furthermore, it was found that the shutdown of the pilot could not be modelled correctly. However, in general the regression model followed the production closely.

The test result with the salt concentration deviate slightly for test number 8 and deviate highly for test number 9. This could mean that the salt concentration was lower in the module than estimated. This means that the salinity should be measured directly instead of estimation.

As can be seen in Figure 8-8, the estimated thermal energy and output energy are not near the measured values. A reason might be that there is more energy loss in the system or that the measured output temperatures are not correct.

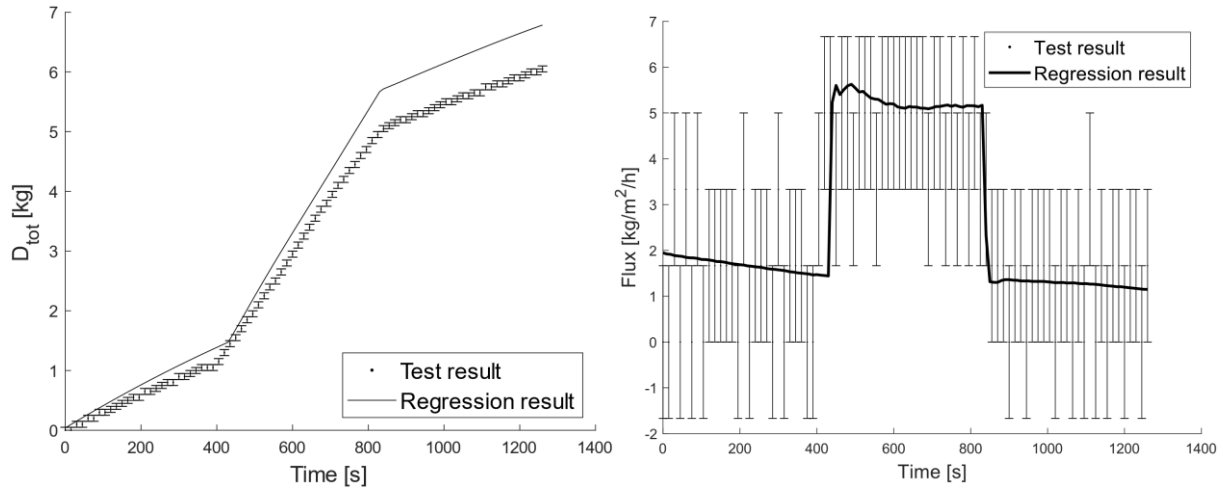


Figure 8-6 Test result of test 2. On the left the total production. On the right the flux.

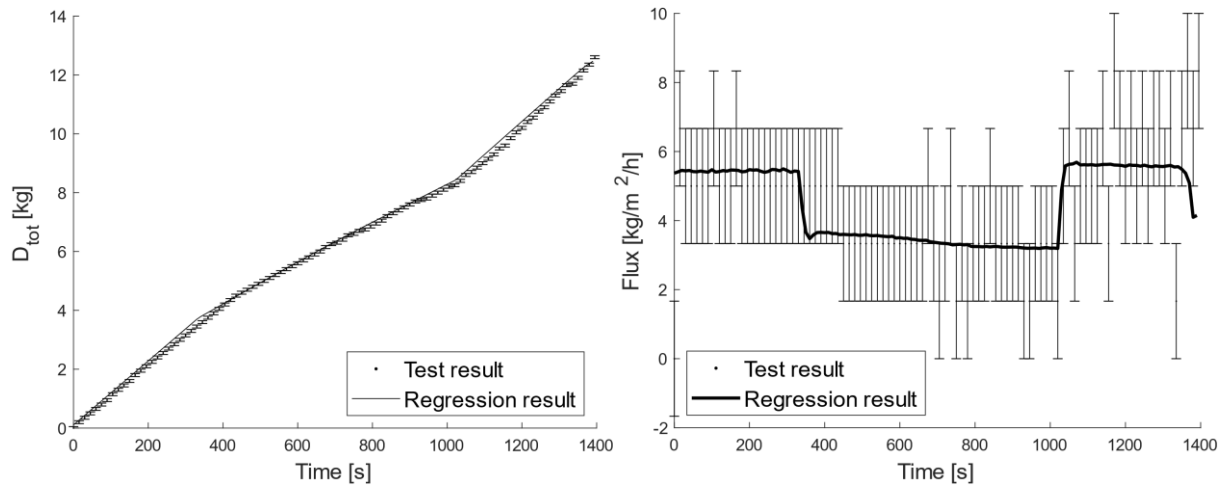


Figure 8-7 Test result of the test 6. On the left the total production. On the right the flux.

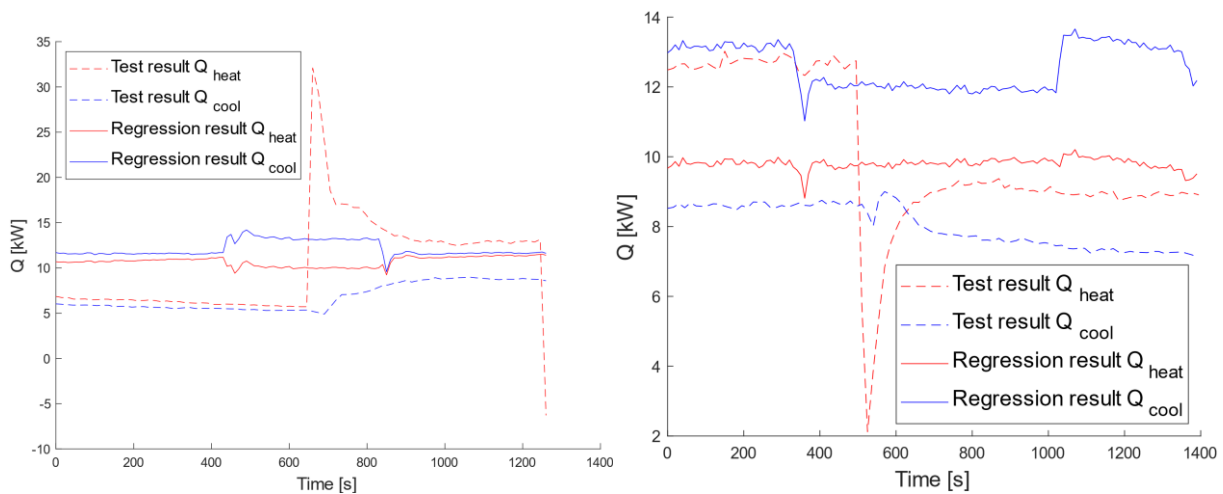


Figure 8-8 Test result of the temperatures of test 2 on the left and test 6 on the right.

8.2.2 Thermal electrical network

As explained in last section, the relative tolerance was increased in order to model the system. This was due to the deviation between the initial values of the test and the model. To solve this, the model was run two times. The first run lasted for five seconds, and the final state values will become the initial values for the second run. Therefore, no transient effect will be seen at the start of the graphs due to the wrong initial values. Moreover, the relative tolerance can now be lowered to 5 percent. Which is still a big increase from 0.01% which is the original relative tolerance.

Furthermore, due to the discontinuous sampling, the provided data to the model is discretized. To solve this issue the function `interp1` in MATLAB is used. This function interpolates between the data in a linear manner.

As can be seen in Figure 8-9 and Figure 8-10, the TEN-model underestimates the flux and the total production. However, the predicted temperatures are close to the tested values. Which can be seen in Figure 8-11. The rest of the results are shown in Appendix G. Test number 7 could not be calculated. A reason for this is that the measured flows might be negative and registered as positive by the sensors. For test number 2 the relative tolerance was increased to 30 percent. This resulted in a big error in the transient behaviour of this test result.

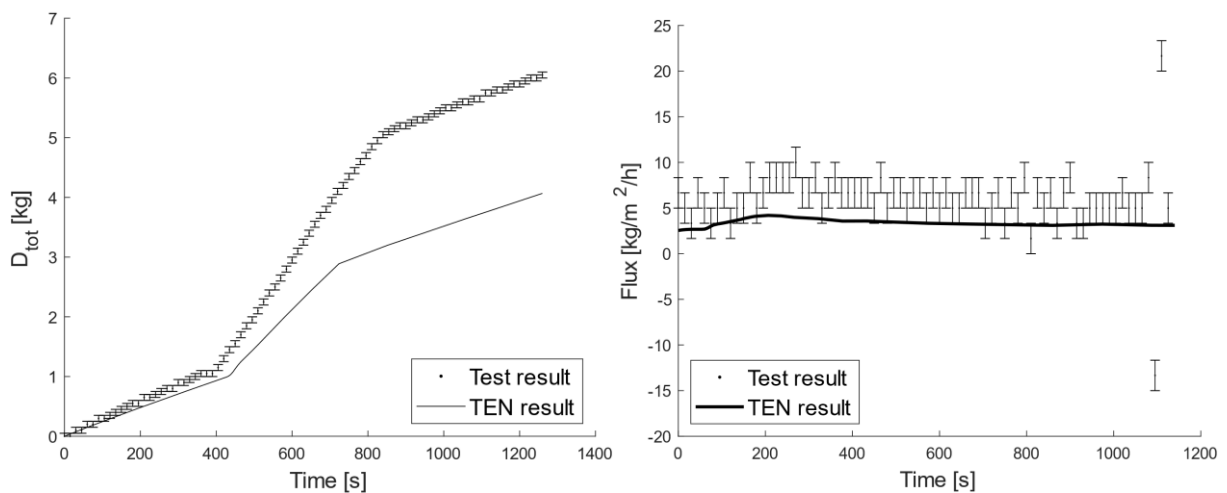


Figure 8-9 Test result of test 2. On the left the total production. On the right the flux.

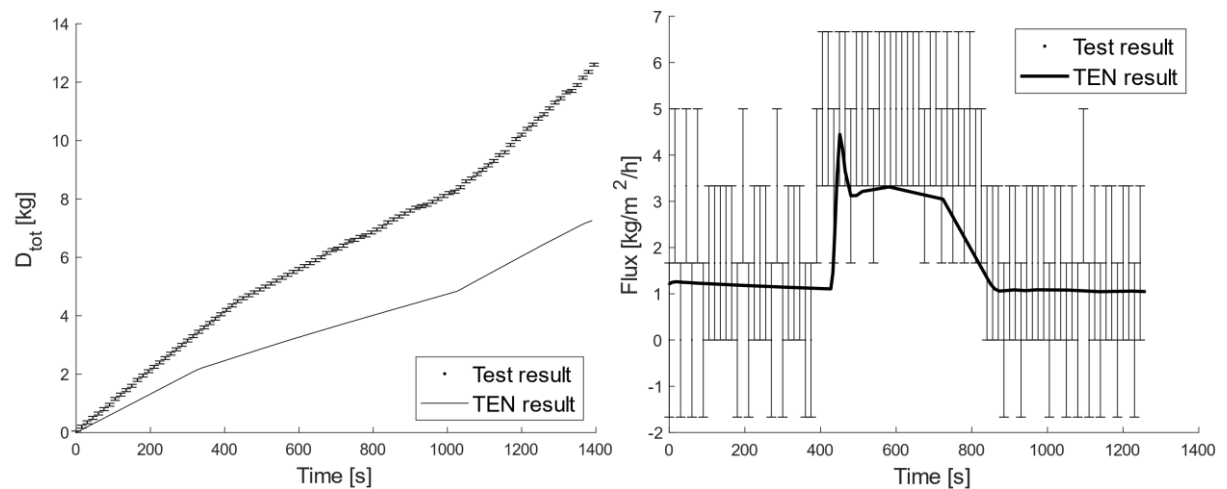


Figure 8-10 Test result of test 6. On the left the total production. On the right the flux.

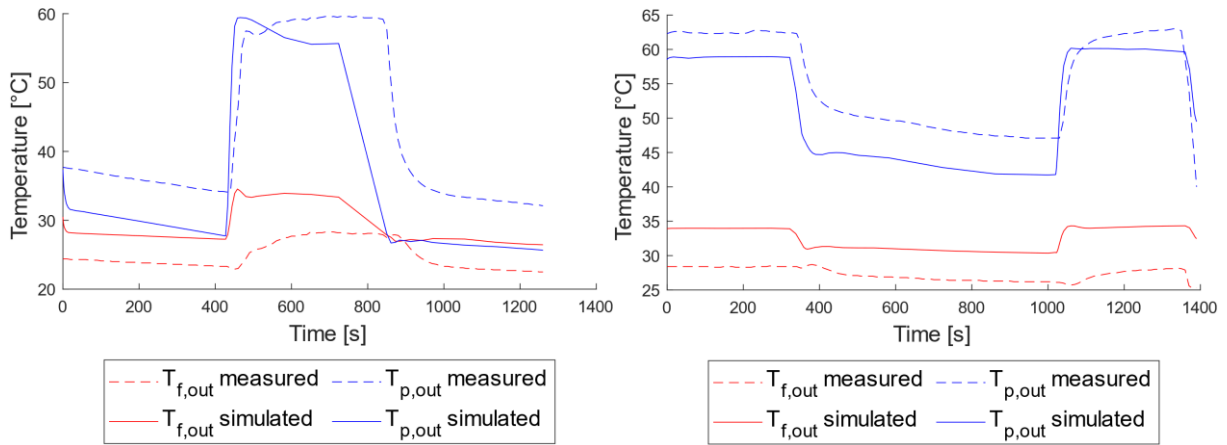


Figure 8-11 Test result of the temperatures of test 2 (left) and test 6 (right).

8.2.3 Energy balance model

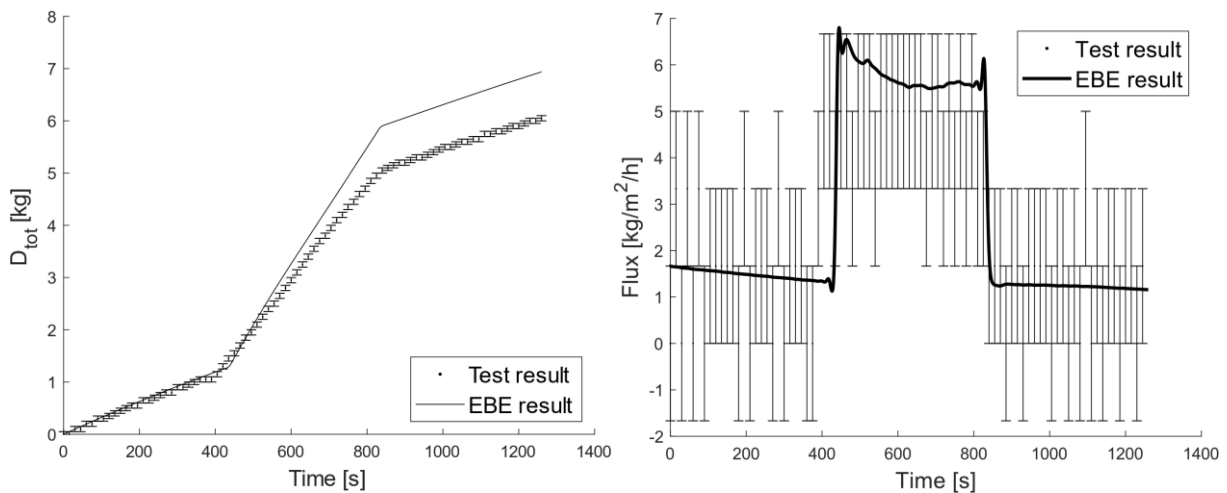


Figure 8-12 to Figure 8-14. The other results can be found in Appendix H. The relative tolerance is 0.01%. The EBE model slightly overestimates the flux and the total production. Moreover, the temperatures change quicker than the test results and deviate highly. Overall this model provides good flux estimation but bad temperature estimation. This means that the model can not be used to estimate the amount of thermal energy input and output needed for a module.

The model underestimates the flux and total production for test number 9. This is a further indication that the salinity of this test was lower than expected. Test number 7 could not be calculated. This is due to the same reason as in section 8.2.2.

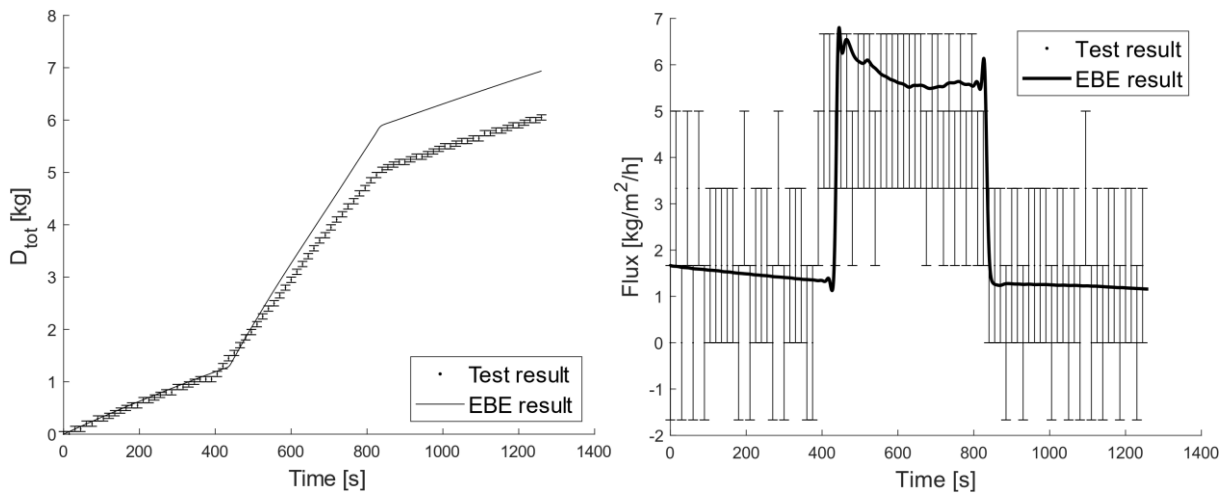


Figure 8-12 Test result of test 2. On the left the total production. On the right the flux.

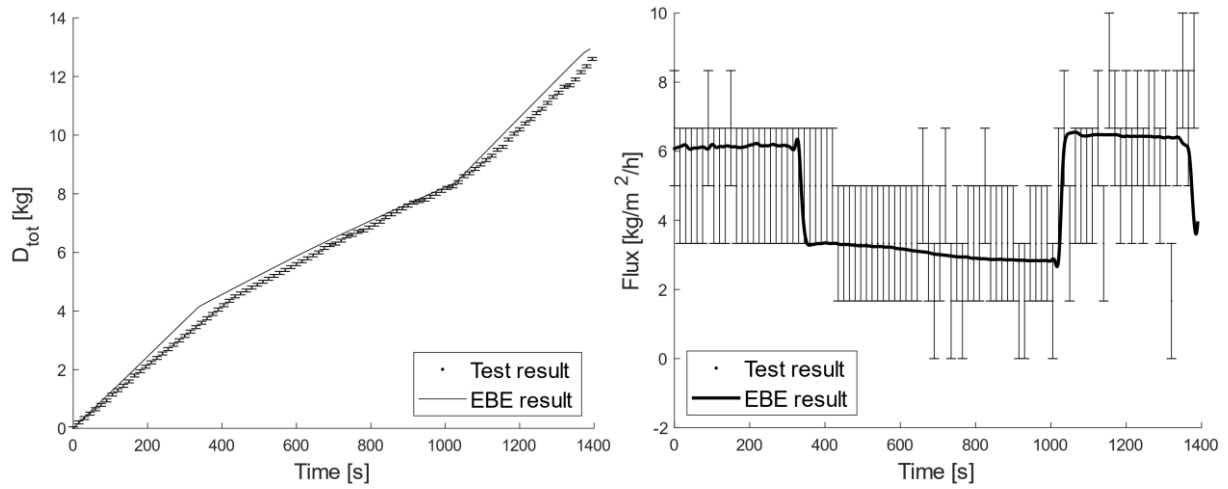


Figure 8-13 Test result of test 6. On the left the total production. On the right the flux.

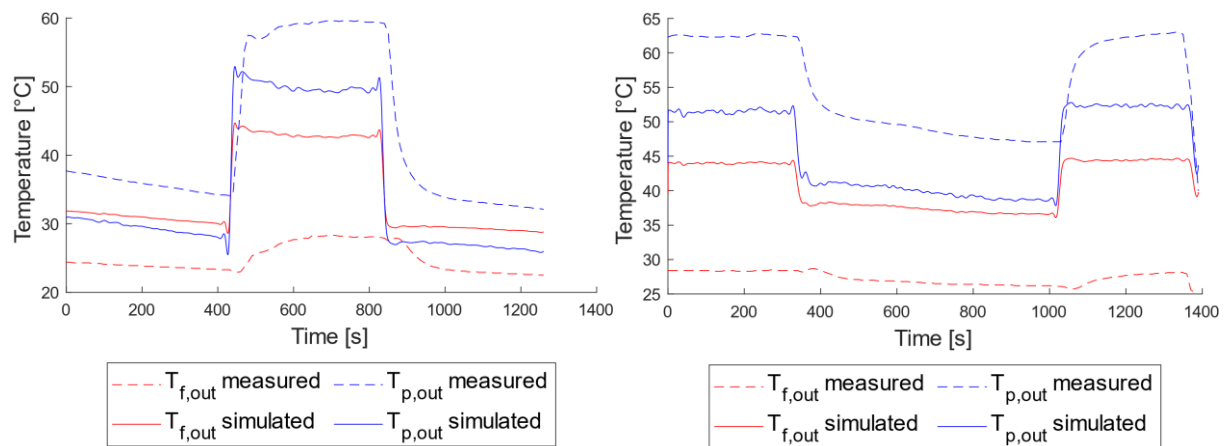


Figure 8-14 Test result of the temperatures of test 2 (left) and test 6 (right).

8.3 Benchmarking of the models

Steady state error

The steady state error is the least for the regression model and the EBE-model. The thermal electrical network has a high deviation. To further improve the models, it is recommended to experimentally or theoretically define the water behaviour in the air gap as this can have a distinct effect on the predicted flux and output temperatures.

Transient response

When modelling transient response, the TEN does not provide accurate solution. However, the value for the condenser can be changed to more accurately represent the system. In contrast, it was found that the TEN model offer some challenges to make ode15s work. Therefore, it is not advised to use the TEN model.

The EBE-model does not take a lot of time to compute and follows the flux and the total production accurately. However, the model was too quickly in following the temperatures which also deviated significantly.

The regression model quit accurately describes the flux. Moreover, the results can be improved when decreasing the time between the calculation points. Furthermore, it is easy to implement in software like Excel or MATLAB and does not offer the challenges to make ode15s work.

The predicted temperatures for the EBE-model and the predicted $Q_{heating}$ and $Q_{cooling}$ from the regression both deviate highly from the test results while still providing accurate results for the flux. This is possibly due faults in the modelling.

Further improvements of the test setup

As was stated earlier the salinity of the water was determined indirectly. This could be improved in further work to measure it accurately. Furthermore, the error on the balance was 50 grams. A better balance could be chosen to decrease the inaccuracy and to provide better results. This would result in a better measurable transient response of the flux.

8.4 Conclusion

The following conclusions were found:

- More research about the behaviour of the air gap is needed to fully model V-AGMD.
- More work is needed to fully model the system including the heat exchangers, pumps tanks and pipelines.
- A better test setup could be used to get more accurate result and to improve the models even more.
- It is not advised to use the thermal electrical network model to simulate membrane distillation.
- The energy balance equations model delivers better results than the thermal electrical network model.
- It is advised to use the regression model as this produced the best results and because it is the simplest model.

9 CONCLUSION PART B

When using green energy to generate the needed heat for membrane distillation the provided water temperatures are not constant. Therefore, a dynamic model is developed in order to simulate the transient behaviour of membrane distillation.

In order to assess dynamic inputs three models were developed. This first model is based on regression formula that calculates the output with small timesteps in between the inputs. The second model is based on the thermal electrical network where the thermal components are translated into electrical components. The laws of electrical networks are then used to make a differential algebraic equation. The third method start from the energy balance who are transformed to a set of differential algebraic equation by using forward and backwards discretization. The DAE is the expended in order to take the heat balances into account.

All three models were tested on the steady state and on the dynamic behaviour. Two sources for the steady state data were used. The first source is a dataset that was provided by Aqua|still. The second set of data came from an article that was performed on an Aqua|still air gap membrane distillation module.

In order to test the dynamic behaviour a new test setup was developed in this thesis. In previous setups the temperatures and flows can not be changed fast enough. Therefore, two test setups were interconnected to form one big test setup.

The regression and the EBE model gave the best overall results on both the steady state and dynamic behaviour. The thermal electrical network did not provide accurate result on the steady state and dynamic behaviour. The overall best method is the regression model as this is the simplest and most accurate model.

During the dynamic test it was found that the test setup should be improve further to deliver more accurate results. For example, the error of the scale was too high to deliver accurate results for the dynamic behaviour of the flux. Moreover, the salinity could not be measured directly and was calculated based on the amount of salt that was added to the tank. This resulted in a greater error when simulating the test where the salinity was changed rapidly. The reason for this was that the calculated value was not the same as the actual water salinity.

Different values of the air gap were used in the modelling and it was clear that more research should be done about the water behaviour in the air gap. Furthermore, the behaviour of the air gap with low pressures is not clearly defined in research.

10 OVERALL CONCLUSION AND RECOMMENDATIONS

When using conventional power sources there is low grade heat that is not be used for the production of electricity due to the low Carnot efficiency. However, this waste heat still has a high enough temperature to produce water with membrane distillation. To use this waste heat wisely, the process conditions and the materials need to be as best as possible. This was the first goal of this thesis.

Simulated annealing was used to find the optimum of membrane distillation. SA used the regression formula that where developed in the first part of this thesis. The data for making the regression formula came from the existing steady state Aqua|still model. This methodology can also be used if one or more of the parameters is fixed. The optimum process conditions were found to be 30.28°C, 90°C, 0g/kg and 10 kPa for the condenser inlet temperate, membrane inlet temperature, salinity and air gap pressure respectively. All of the mass and heat transfer parameters should increase two times to find the optimum. However, the mass transfer of the air gap should be halved to reach the optimum.

When using green energy to generate the needed heat for membrane distillation the provided water temperatures are not constant. Therefore, a dynamic model was developed in order to simulate the transient behaviour of membrane distillation. This was the second goal of this thesis.

In order to assess dynamic inputs three models were developed. This first model is based on regression formula that calculates the output with small timesteps in between the inputs. The second model is based on the thermal electrical network where the thermal components are translated into electrical components. The laws of electrical networks are then used to make differential algebraic equations. The third method start from the energy balance. This model was named energy balance equations model.

All three models were tested on the steady state and dynamic behaviour. The test data for steady state was already available before this thesis. In order to test the dynamic behaviour a new test setup was developed in this thesis. In previous setups the temperatures and flows can not be changed fast enough. Therefore, two test setups were interconnected to form one big test setup.

The regression and the EBE model gave the best overall results on both the steady state and dynamic behaviour. The thermal electrical network did not provide accurate result on the steady state and dynamic behaviour. The overall best method is the regression model as this is the simplest and most accurate model.

During the dynamic test it was found that the test setup should be improver further to deliver more accurate results. For example, further improvements can be made to improve the accuracy of the scale and the salinity sensor.

Different values of the air gap were used in the modelling and it was clear that more research should be done about the water behaviour in the air gap. Furthermore, the behaviour of the air gap with low pressures is not clearly defined in research. Therefore, more research is needed.

Future work:

In future work the models that were developed in this thesis can be used to develop controllers for membrane distillation. Another interesting topic that was left out in this thesis is to reach the optimum in a real module. To do this, the module materials and setup should be improved which is not an easy topic.

The behaviour of the air gap is still uncertain, and more information is needed to model V-AGMD correctly. The syphon, water fraction in the air gap and the behaviour of the vapour at lower air pressure could all be investigated. This could be an interesting and challenging topic.

References

- [1] E. Holbrook, "Water, Water Everywhere . . . But Not Enough for Business," *Risk Manag.*, vol. 56, no. 5, p. 20, 2009.
- [2] P. Fournier, *Potable Water*, vol. 30, no. 10–12. Cham: Springer International Publishing, 2014.
- [3] G. Amy *et al.*, "Membrane-based seawater desalination: Present and future prospects," *Desalination*, vol. 401, pp. 16–21, 2017.
- [4] J. R. Werber, A. Deshmukh, and M. Elimelech, "Can batch or semi-batch processes save energy in reverse-osmosis desalination?," *Desalination*, vol. 402, pp. 109–122, 2017.
- [5] T. Y. Cath, A. E. Childress, and M. Elimelech, "Forward osmosis: Principles, applications, and recent developments," *J. Memb. Sci.*, vol. 281, no. 1–2, pp. 70–87, 2006.
- [6] A. Kumar, A. Rashmi, A. Agarwal, T. Gupta, B. Ram, and G. Editors, *Seawater Desalination*. 2009.
- [7] I. Hitsov, *PhD Dissertation: Model-based analysis and optimization of membrane distillation*. 2017.
- [8] B. K. Pramanik, Y. Gao, L. Fan, F. A. Roddick, and Z. Liu, "Antiscalting effect of polyaspartic acid and its derivative for RO membranes used for saline wastewater and brackish water desalination," *Desalination*, vol. 404, pp. 224–229, 2017.
- [9] B. Vander and B. Advisor, "Optimization of the Membrane Sublayer for Development of Reverse Osmosis Membranes with Improved Fouling Resistance," no. September, 2011.
- [10] W. Li, B. Van der Bruggen, and P. Luis, "Integration of reverse osmosis and membrane crystallization for sodium sulphate recovery," *Chem. Eng. Process. Process Intensif.*, vol. 85, pp. 57–68, 2014.
- [11] M. Wilf, "Fundamentals of RO-NF technology," *Anim. Genet.*, vol. 39, no. 5, pp. 7–8, 2008.
- [12] L. Birnhack, N. Voutchkov, and O. Lahav, "Fundamental chemistry and engineering aspects of post-treatment processes for desalinated water-A review," *Desalination*, vol. 273, no. 1, pp. 6–22, 2011.
- [13] S. Lin and M. Elimelech, "Kinetics and energetics trade-off in reverse osmosis desalination with different configurations," *Desalination*, vol. 401, pp. 42–52, 2017.
- [14] K. T. W. J, Y. MA, and S. H, "Edelight," vol. 120, pp. 1479–1489, 1996.
- [15] B. Van der Bruggen, "Desalination by distillation and by reverse osmosi - trends towards the future," *Membr. Technol.*, no. February, pp. 6–9, 2003.
- [16] L. Eykens, "PhD Dissertation: A comprehensive study of membrane distillation: membrane development, configuration assessment and applications," p. 244, 2017.
- [17] D. Winter, *A Thermodynamic , Technological and Technological and Economic Analysis*. 2014.
- [18] A. Alkhudhiri, N. Darwish, and N. Hilal, "Membrane distillation: A comprehensive review," *Desalination*, vol. 287, pp. 2–18, 2012.
- [19] I. Hitsov, K. De Sitter, C. Dotremont, P. Cauwenberg, and I. Nopens, "Full-scale validated Air Gap Membrane Distillation (AGMD) model without calibration parameters,"

- J. Memb. Sci.*, vol. 533, no. April, pp. 309–320, 2017.
- [20] A. Ruiz-aguirre, D.-C. Alarcón-Padilla, and G. Zaragoza, “Productivity analysis of two spiral-wound membrane distillation prototypes coupled with solar energy,” *Desalin. Water Treat.*, vol. 55, no. 10, pp. 2777–2785, 2015.
- [21] M. Khayet, “Treatment of radioactive wastewater solutions by direct contact membrane distillation using surface modified membranes,” *Desalination*, vol. 321, pp. 60–66, 2013.
- [22] X. Wen, F. Li, B. Jiang, X. Zhang, and X. Zhao, “Effect of surfactants on the treatment of radioactive laundry wastewater by direct contact membrane distillation,” *J. Chem. Technol. Biotechnol.*, vol. 93, no. 8, pp. 2252–2261, 2018.
- [23] S. Nene, S. Kaur, K. Sumod, B. Joshi, and K. S. M. S. Raghavarao, “Membrane distillation for the concentration of raw cane-sugar syrup and membrane clarified sugarcane juice,” *Desalination*, vol. 147, no. 1–3, pp. 157–160, 2002.
- [24] C. A. Quist-Jensen *et al.*, “Direct contact membrane distillation for the concentration of clarified orange juice,” *J. Food Eng.*, vol. 187, pp. 37–43, 2016.
- [25] N. E. Koeman-Stein, R. J. M. Creusen, M. Zijlstra, C. K. Groot, and W. B. P. van den Broek, “Membrane distillation of industrial cooling tower blowdown water,” *Water Resour. Ind.*, vol. 14, pp. 11–17, Jun. 2016.
- [26] A. Venkatesan and P. C. Wankat, “Produced water desalination: An exploratory study,” *Desalination*, vol. 404, pp. 328–340, 2017.
- [27] U. K. Kesime and H. Aral, “Application of membrane distillation and solvent extraction for water and acid recovery from acidic mining waste and process solutions,” *J. Environ. Chem. Eng.*, vol. 3, no. 3, pp. 2050–2056, 2015.
- [28] W. G. Shim, K. He, S. Gray, and I. S. Moon, “Solar energy assisted direct contact membrane distillation (DCMD) process for seawater desalination,” *Sep. Purif. Technol.*, vol. 143, pp. 94–104, 2015.
- [29] M. R. Qtaishat and F. Banat, “Desalination by solar powered membrane distillation systems,” *Desalination*, vol. 308, pp. 186–197, 2013.
- [30] G. Zaragoza, J. A. Andrés-Mañas, and A. Ruiz-Aguirre, “Commercial scale membrane distillation for solar desalination,” *npj Clean Water*, vol. 1, no. 1, pp. 1–6, 2018.
- [31] A. Ruiz-Aguirre, M. I. Polo-López, P. Fernández-Ibáñez, and G. Zaragoza, “Assessing the validity of solar membrane distillation for disinfection of contaminated water,” *Desalin. Water Treat.*, vol. 55, no. 10, pp. 2792–2799, 2015.
- [32] A. Ruiz-Aguirre, J. A. Andrés-Mañas, J. M. Fernández-Sevilla, and G. Zaragoza, “Experimental characterization and optimization of multi-channel spiral wound air gap membrane distillation modules for seawater desalination,” *Sep. Purif. Technol.*, vol. 205, no. May, pp. 212–222, 2018.
- [33] H. Chang, G. B. Wang, Y. H. Chen, C. C. Li, and C. L. Chang, “Modeling and optimization of a solar driven membrane distillation desalination system,” *Renew. Energy*, vol. 35, no. 12, pp. 2714–2722, 2010.
- [34] K. Rahaoui *et al.*, “Sustainable Membrane Distillation Coupled with Solar Pond,” *Energy Procedia*, vol. 110, no. December 2016, pp. 414–419, 2017.
- [35] K. Nakoa, K. Rahaoui, A. Date, and A. Akbarzadeh, “An experimental review on coupling of solar pond with membrane distillation,” *Sol. Energy*, vol. 119, pp. 319–331, 2015.
- [36] F. Suárez, S. W. Tyler, and A. E. Childress, “A theoretical study of a direct contact membrane distillation system coupled to a salt-gradient solar pond for terminal lakes reclamation,” *Water Res.*, vol. 44, no. 15, pp. 4601–4615, 2010.

- [37] H. Chen, Z. Ye, and W. Gao, "A desalination plant with solar and wind energy," in *IOP Conference Series: Materials Science and Engineering*, 2013, vol. 52, no. TOPIC 7.
- [38] M. Gryta, "The concentration of geothermal brines with iodine content by membrane distillation," *Desalination*, vol. 325, pp. 16–24, 2013.
- [39] A. E. Kabeel, M. Abdelgaied, and E. M. S. El-Said, "Study of a solar-driven membrane distillation system: Evaporative cooling effect on performance enhancement," *Renew. Energy*, vol. 106, pp. 192–200, 2017.
- [40] E. Ali, "Dynamic analysis and modeling of direct contact membrane distillation for water desalination during startup using linear system theory," *Chem. Eng. Process. - Process Intensif.*, vol. 136, no. November 2018, pp. 17–27, 2019.
- [41] F. Eleiwi, N. Ghaffour, A. S. Alsaadi, L. Francis, and T. M. Laleg-Kirati, "Dynamic modeling and experimental validation for direct contact membrane distillation (DCMD) process," *Desalination*, vol. 384, pp. 1–11, 2016.
- [42] A. M. Karam, A. S. Alsaadi, N. Ghaffour, and T. M. Laleg-Kirati, "Analysis of direct contact membrane distillation based on a lumped-parameter dynamic predictive model," *Desalination*, vol. 402, pp. 50–61, 2017.
- [43] R. Porrizzo, A. Cipollina, M. Galluzzo, and G. Micale, "A neural network-based optimizing control system for a seawater-desalination solar-powered membrane distillation unit," *Comput. Chem. Eng.*, vol. 54, pp. 79–96, 2013.
- [44] E. Guillen-Burrieza, A. Ruiz-Aguirre, G. Zaragoza, and H. A. Arafat, "Membrane fouling and cleaning in long term plant-scale membrane distillation operations," *J. Memb. Sci.*, vol. 468, pp. 360–372, 2014.
- [45] H. W. Chung, J. Swaminathan, D. M. Warsinger, and J. H. Lienhard V, "Multistage vacuum membrane distillation (MSVMD) systems for high salinity applications," *J. Memb. Sci.*, vol. 497, pp. 128–141, 2016.
- [46] M. H. Sharqawy, J. H. Lienhard, and S. M. Zubair, "Thermophysical properties of seawater: a review of existing correlations and data," *Desalin. Water Treat.*, vol. 16, no. 1–3, pp. 354–380, Apr. 2010.
- [47] K. G. Nayar, M. H. Sharqawy, L. D. Banchik, and J. H. Lienhard, "Thermophysical properties of seawater: A review and new correlations that include pressure dependence," *Desalination*, vol. 390, pp. 1–24, 2016.
- [48] D. M. Warsinger, J. Swaminathan, L. L. Morales, and J. H. Lienhard V, "Comprehensive condensation flow regimes in air gap membrane distillation: Visualization and energy efficiency," *J. Memb. Sci.*, vol. 555, no. February, pp. 517–528, 2018.
- [49] Biomath, "Setup for measurement of the condensate layer thickness," 2016. [Online]. Available: <http://bit.ly/2gppl0A>.
- [50] Biomath, "Air gap condensation in membrane distillation," 2016. [Online]. Available: <http://bit.ly/2glgoDg>.
- [51] I. Hitsov, L. Eykens, W. De Schepper, K. De Sitter, C. Dotremont, and I. Nopens, "Full-scale direct contact membrane distillation (DCMD) model including membrane compaction effects," *J. Memb. Sci.*, vol. 524, no. November 2016, pp. 245–256, 2017.
- [52] M. Bindels, N. Brand, and B. Nelemans, "Modeling of semibatch air gap membrane distillation," *Desalination*, vol. 430, no. December 2017, pp. 98–106, 2018.
- [53] D. M. Warsinger, J. Swaminathan, E. Guillen-Burrieza, H. A. Arafat, and J. H. Lienhard V, "Scaling and fouling in membrane distillation for desalination applications: A review," *Desalination*, vol. 356, pp. 294–313, 2015.
- [54] A. S. Alsaadi *et al.*, "Modeling of air-gap membrane distillation process: A theoretical

- and experimental study," *J. Memb. Sci.*, vol. 445, pp. 53–65, 2013.
- [55] A. Hagedorn, G. Fieg, D. Winter, J. Koschikowski, A. Grabowski, and T. Mann, "Membrane and spacer evaluation with respect to future module design in membrane distillation," *Desalination*, vol. 413, pp. 154–167, 2017.
- [56] A. R. Da Costa, A. G. Fane, and D. E. Wiley, "Spacer characterization and pressure drop modelling in spacer-filled channels for ultrafiltration," *J. Memb. Sci.*, vol. 87, no. 1–2, pp. 79–98, Feb. 1994.
- [57] M. C. García-Payo and M. A. Izquierdo-Gil, "Thermal resistance technique for measuring the thermal conductivity of thin microporous membranes," *J. Phys. D. Appl. Phys.*, vol. 37, no. 21, pp. 3008–3016, 2004.
- [58] I. Hitsov *et al.*, "Calibration and analysis of a direct contact membrane distillation model using Monte Carlo filtering," *J. Memb. Sci.*, vol. 515, pp. 63–78, 2016.
- [59] A. Bahmanyar, M. Asghari, and N. Khoobi, "Numerical simulation and theoretical study on simultaneously effects of operating parameters in direct contact membrane distillation," *Chem. Eng. Process. Process Intensif.*, vol. 61, pp. 42–50, 2012.
- [60] A. Cipollina, M. G. Di Sparti, A. Tamburini, and G. Micale, "Development of a Membrane Distillation module for solar energy seawater desalination," *Chem. Eng. Res. Des.*, vol. 90, no. 12, pp. 2101–2121, 2012.
- [61] M. Qtaishat, T. Matsuura, B. Kruczek, and M. Khayet, "Heat and mass transfer analysis in direct contact membrane distillation," *Desalination*, vol. 219, no. 1–3, pp. 272–292, 2008.
- [62] I. Hitsov, T. Maere, K. De Sitter, C. Dotremont, and I. Nopens, "Modelling approaches in membrane distillation: A critical review," *Sep. Purif. Technol.*, vol. 142, pp. 48–64, 2015.
- [63] L. Martínez-Díez and M. . Vázquez-González, "Temperature and concentration polarization in membrane distillation of aqueous salt solutions," *J. Memb. Sci.*, vol. 156, no. 2, pp. 265–273, 1999.
- [64] R. E. Treybal, *Mass-Transfer Operations, 3rd Edition*. McGraw-Hill Book Co, 1981.
- [65] N. Nagaraj, G. Patil, B. R. Babu, U. H. Hebbar, K. S. M. S. Raghavarao, and S. Nene, "Mass transfer in osmotic membrane distillation," *J. Memb. Sci.*, vol. 268, no. 1, pp. 48–56, 2006.
- [66] C. N. Singman, "Atomic volume and allotropy of the elements," *J. Chem. Educ.*, vol. 61, no. 2, p. 137, 2009.
- [67] R. W. Field, H. Y. Wu, and J. J. Wu, "Multiscale modeling of membrane distillation: Some theoretical considerations," *Ind. Eng. Chem. Res.*, vol. 52, no. 26, pp. 8822–8828, 2013.
- [68] D. U. Lawal and A. E. Khalifa, "Flux Prediction in Direct Contact Membrane Distillation," *Int. J. Mater. Mech. Manuf.*, vol. 2, no. 4, pp. 302–308, 2014.
- [69] M. Khayet, A. Velázquez, and J. I. Mengual, "Modelling mass transport through a porous partition: Effect of pore size distribution," *J. Non-Equilibrium Thermodyn.*, vol. 29, no. 3, pp. 279–299, 2004.
- [70] E. A. Mason and A. P. Malinauskas, *Gas transport in porous media: Dusty-gas model*. Elsevier Science Ltd, 1983.
- [71] S. Srisurichan, R. Jiratananon, and A. G. Fane, "Mass transfer mechanisms and transport resistances in direct contact membrane distillation process," *J. Memb. Sci.*, vol. 277, no. 1–2, pp. 186–194, 2006.
- [72] M. Khayet, C. Cojocar, and C. García-Payo, "Application of response surface

- methodology and experimental design in direct contact membrane distillation,” *Ind. Eng. Chem. Res.*, vol. 46, no. 17, pp. 5673–5685, 2007.
- [73] M. Khayet, C. Cojocaru, and A. Baroudi, “Modeling and optimization of sweeping gas membrane distillation,” *Desalination*, vol. 287, pp. 159–166, 2012.
- [74] A. Boubakri, A. Hafiane, and S. A. T. Bouguecha, “Application of response surface methodology for modeling and optimization of membrane distillation desalination process,” *J. Ind. Eng. Chem.*, vol. 20, no. 5, pp. 3163–3169, 2014.
- [75] S. Burke and D. Ph, “Computer Experiments : Space Filling Design and Gaussian Process Modeling,” no. September, 2018.
- [76] V. R. Joseph, “Space-filling designs for computer experiments: A review,” *Qual. Eng.*, vol. 28, no. 1, pp. 28–35, 2016.
- [77] F. Wahl and F. Wahl, “Measuring the quality of maximin space-filling designs,” 2015.
- [78] V. R. Joseph, E. Gul, and S. Ba, “Maximum projection designs for computer experiments,” *Biometrika*, vol. 102, no. 2, pp. 371–380, 2015.
- [79] The R Foundation, “The R Project for Statistical Computing,” 2019. [Online]. Available: <https://www.r-project.org/>.
- [80] V. R. Joseph, E. Gul, and S. Ba, “MaxPro: Maximum Projection Designs,” 2018. [Online]. Available: <https://cran.r-project.org/web/packages/MaxPro/index.html>. [Accessed: 06-Apr-2019].
- [81] R. H. Myers, D. C. Montgomery, and C. M. Anderson-Cook, *Response surface methodology: Process and product optimization using designed experiments*. 2016.
- [82] D. C. Montgomery, E. A. Peck, and G. G. Vining, *Introduction to Linear Regression Analysis.*, vol. 43, no. 2. 2012.
- [83] J. Pearl, *Heuristics: Intelligent search strategies for computer problem solving*, vol. 21, no. 2. 1984.
- [84] D. P. Kroese, “Monte Carlo methods,” *Wiley Period. Inc.*, p. 11, 2011.
- [85] E. K. Burke and Y. Bykov, “The late acceptance Hill-Climbing heuristic,” *Eur. J. Oper. Res.*, vol. 258, no. 1, pp. 70–78, 2017.
- [86] C. Storey, “Applications of a hill climbing method of optimization,” *Chem. Eng. Sci.*, vol. 17, no. 1, pp. 45–52, 1962.
- [87] W. H. Press, S. A. Teukolsky, W. T. Vetterling, and B. P. Flannery, *Numerical Recipes: The Art of Scientific Computing*, Third Edit. 2007.
- [88] S. Ledesma, J. Ruiz, and G. Garci, “Simulated Annealing Evolution,” *Simulated Annealing - Adv. Appl. Hybridizations*, 2012.
- [89] L. M. R. Rere, M. I. Fanany, and A. M. Arymurthy, “Simulated Annealing Algorithm for Deep Learning,” *Procedia Comput. Sci.*, vol. 72, pp. 137–144, 2015.
- [90] M. Bindels and B. Medaer, “Numerical modelling and optimization of air gap membrane distillation: MATLAB code of simulated annealing, energy balance equations and thermal electrical network.” [Online]. Available: <https://git.io/fjG1b>.
- [91] H. W. Chung, M. David, J. H. Lienhard, V. M. Distillation, C. Applied, and E. December, “Membrane distillation model based on heat exchanger theory and configuration comparison.” 2018.
- [92] J. Zhang, S. Gray, and J. De Li, “Modelling heat and mass transfers in DCMD using compressible membranes,” *J. Memb. Sci.*, vol. 387–388, no. 1, pp. 7–16, 2012.
- [93] A. R. Kurdian, M. Bahreini, G. H. Montazeri, and S. Sadeghi, “Modeling of direct contact

membrane distillation process: Flux prediction of sodium sulfate and sodium chloride solutions," *Desalination*, vol. 323, pp. 75–82, 2013.

- [94] K. Charfi, M. Khayet, and M. J. Safi, "Numerical simulation and experimental studies on heat and mass transfer using sweeping gas membrane distillation," *Desalination*, vol. 259, no. 1–3, pp. 84–96, 2010.
- [95] A. M. Karam, "Reduced-Order Dynamic Modeling , Fouling Detection , and Optimal Control of Solar-Powered Direct Contact Membrane Distillation," 2016.
- [96] R. L. Ford, "Electrical analogues for heat exchangers," *Proc. IEE - Part B Radio Electron. Eng.*, vol. 103, no. 7, pp. 65–82, 2014.
- [97] D. J. Murray-Smith, *Testing and Validation of Computer Simulation Models: Principles, Methods and Applications*. 2015.

Appendices

- Appendix A Regression coefficients
- Appendix B Steady state test parameters
- Appendix C Matrices for the thermal electrical network
- Appendix D Matrices for the energy balance equations model
- Appendix E Dynamic test condition
- Appendix F Dynamic regression results
- Appendix G Thermal electrical network results
- Appendix H Dynamic energy balance equations results

Appendix A REGRESSION COEFFICIENTS

Table A- 1 Regression coefficients for the flux

β_0	5.98E+00	β_{20}	-1.78E-02	β_{39}	1.51E-01	β_{58}	1.37E-06	β_{77}	-2.73E-01
β_2	3.95E-03	β_{21}	-9.88E-02	β_{40}	5.89E-03	β_{59}	3.69E-06	β_{78}	-4.99E-02
β_3	-7.42E-02	β_{22}	-4.26E-02	β_{41}	9.68E-03	β_{60}	-3.95E-09	β_{79}	3.28E-02
β_4	6.84E-03	β_{23}	-2.11E-01	β_{42}	7.95E-03	β_{61}	-6.25E-07	β_{80}	-1.09E-01
β_5	-3.24E-05	β_{24}	-8.96E-01	β_{43}	6.75E-03	β_{62}	8.81E-06	β_{81}	-3.13E-02
β_6	-5.10E+00	β_{25}	6.98E-02	β_{44}	1.09E-02	β_{63}	1.02E-06	β_{82}	2.22E-02
β_7	-1.72E-01	β_{26}	2.25E-04	β_{45}	2.06E-02	β_{64}	2.67E-01	β_{83}	1.75E-01
β_8	-3.28E-01	β_{27}	1.67E-04	β_{46}	-1.25E-03	β_{65}	2.85E-01	β_{84}	-6.10E-02
β_9	-5.36E-01	β_{28}	5.74E-07	β_{47}	3.36E-08	β_{66}	3.18E-01	β_{85}	-6.63E-05
β_{10}	-6.08E-01	β_{29}	-5.58E-02	β_{48}	-7.35E-03	β_{67}	1.81E-01	β_{86}	-9.21E-03
β_{11}	-9.55E-01	β_{30}	-6.03E-03	β_{49}	-1.93E-04	β_{68}	2.97E-01	β_{87}	6.47E-02
β_{12}	7.47E-01	β_{31}	-3.71E-03	β_{50}	8.35E-04	β_{69}	1.57E+00	β_{88}	5.60E-05
β_{13}	-8.10E-01	β_{32}	-1.61E-03	β_{51}	8.19E-04	β_{70}	3.77E-02	β_{89}	1.64E-01
β_{14}	-1.09E-03	β_{33}	2.02E-03	β_{52}	5.71E-04	β_{71}	4.90E-02	β_{90}	1.03E-01
β_{15}	1.98E-04	β_{34}	-7.00E-04	β_{53}	-6.48E-05	β_{72}	1.25E-01	β_{91}	8.23E-02
β_{16}	1.17E-05	β_{35}	-4.50E-02	β_{54}	-1.70E-03	β_{73}	-4.68E-02		
β_{17}	6.34E-11	β_{36}	1.18E-02	β_{55}	1.02E-03	β_{74}	5.13E-02		
β_{18}	-6.62E-01	β_{37}	-2.62E-04	β_{56}	-1.68E-05	β_{75}	1.31E-01		
β_{19}	-2.18E-01	β_{38}	-7.81E-08	β_{57}	-1.03E-06	β_{76}	4.01E-02		

Table A- 2 Regression coefficients for the GOR

β_0	3.59E+00	β_{20}	-7.54E-02	β_{39}	-4.86E-02	β_{58}	8.77E-07	β_{77}	-1.22E-02
β_2	5.51E-02	β_{21}	-9.57E-02	β_{40}	2.32E-02	β_{59}	-1.23E-06	β_{78}	-1.39E-01
β_3	-1.74E-01	β_{22}	-7.83E-02	β_{41}	9.47E-03	β_{60}	-5.59E-06	β_{79}	1.95E-01
β_4	9.65E-03	β_{23}	-6.17E-01	β_{42}	-1.35E-03	β_{61}	-1.26E-05	β_{80}	2.20E-02
β_5	2.09E-05	β_{24}	-8.14E-01	β_{43}	1.35E-02	β_{62}	-7.71E-06	β_{81}	1.46E-01
β_6	-3.90E-01	β_{25}	1.52E-01	β_{44}	2.86E-02	β_{63}	1.63E-06	β_{82}	2.67E-01
β_7	5.78E-01	β_{26}	1.94E-03	β_{45}	2.42E-02	β_{64}	-9.31E-01	β_{83}	-2.44E-01
β_8	-5.36E-01	β_{27}	-5.89E-04	β_{46}	1.30E-03	β_{65}	-1.77E-02	β_{84}	-1.01E-01
β_9	1.11E+00	β_{28}	-2.89E-07	β_{47}	1.25E-07	β_{66}	-4.11E-01	β_{85}	1.28E-01
β_{10}	-7.47E-01	β_{29}	-6.07E-02	β_{48}	1.56E-02	β_{67}	-5.25E-01	β_{86}	3.85E-01
β_{11}	1.24E+00	β_{30}	1.65E-02	β_{49}	-2.87E-03	β_{68}	-1.11E+00	β_{87}	6.67E-02
β_{12}	2.70E+00	β_{31}	-1.81E-02	β_{50}	1.13E-03	β_{69}	-1.12E+00	β_{88}	1.52E-01
β_{13}	-1.01E+00	β_{32}	3.46E-03	β_{51}	-6.12E-04	β_{70}	2.99E-02	β_{89}	7.92E-01
β_{14}	-1.34E-03	β_{33}	1.24E-02	β_{52}	-5.36E-03	β_{71}	1.07E-01	β_{90}	-2.97E-01
β_{15}	1.04E-03	β_{34}	1.56E-02	β_{53}	-4.90E-03	β_{72}	-4.59E-02	β_{91}	-2.41E-01
β_{16}	3.09E-06	β_{35}	2.08E-02	β_{54}	-7.98E-03	β_{73}	3.70E-01		
β_{17}	1.47E-10	β_{36}	1.35E-02	β_{55}	1.56E-03	β_{74}	1.17E-01		
β_{18}	2.33E+00	β_{37}	-1.14E-04	β_{56}	1.61E-05	β_{75}	6.38E-01		
β_{19}	-6.00E-01	β_{38}	-5.54E-07	β_{57}	-1.02E-05	β_{76}	-2.97E-02		

Table A- 3 Regression coefficients for $Q_{heating}$

β_0	5.11E+01	β_{20}	4.38E-01	β_{39}	1.91E-01	β_{58}	9.43E-06	β_{77}	1.48E-01
β_2	-7.07E-01	β_{21}	-1.01E-01	β_{40}	-1.18E-02	β_{59}	4.93E-06	β_{78}	5.14E-01
β_3	-3.73E-01	β_{22}	8.17E-01	β_{41}	2.26E-02	β_{60}	6.10E-06	β_{79}	6.06E-01
β_4	-6.22E-02	β_{23}	2.25E+00	β_{42}	1.72E-02	β_{61}	9.27E-06	β_{80}	1.14E-02
β_5	-3.49E-05	β_{24}	4.06E+00	β_{43}	-1.80E-02	β_{62}	-2.34E-05	β_{81}	3.90E-01
β_6	1.22E+01	β_{25}	3.16E-01	β_{44}	-1.30E-02	β_{63}	1.24E-06	β_{82}	1.29E-01
β_7	-6.31E+00	β_{26}	-8.16E-05	β_{45}	-6.40E-02	β_{64}	-1.31E+00	β_{83}	5.13E-01
β_8	-5.76E+00	β_{27}	3.99E-04	β_{46}	3.69E-02	β_{65}	7.50E-02	β_{84}	-8.12E-02
β_9	-3.91E+00	β_{28}	-1.60E-06	β_{47}	-4.49E-08	β_{66}	7.52E-01	β_{85}	3.71E-01
β_{10}	-2.66E+00	β_{29}	-5.73E-01	β_{48}	5.30E-03	β_{67}	-1.24E+00	β_{86}	1.63E-01
β_{11}	-9.37E+00	β_{30}	4.79E-02	β_{49}	-8.81E-04	β_{68}	-1.36E+00	β_{87}	-3.70E-01
β_{12}	-7.07E+00	β_{31}	1.62E-02	β_{50}	2.51E-03	β_{69}	-6.74E+00	β_{88}	3.74E-01
β_{13}	-7.09E+00	β_{32}	1.34E-02	β_{51}	3.19E-03	β_{70}	2.60E-01	β_{89}	-1.78E-01
β_{14}	9.50E-03	β_{33}	3.69E-02	β_{52}	3.34E-03	β_{71}	-4.95E-03	β_{90}	4.27E-01
β_{15}	1.67E-03	β_{34}	8.00E-02	β_{53}	2.78E-03	β_{72}	9.56E-02	β_{91}	2.92E-01
β_{16}	3.99E-05	β_{35}	2.01E-01	β_{54}	9.53E-03	β_{73}	1.68E-01		
β_{17}	-1.86E-10	β_{36}	9.42E-03	β_{55}	1.92E-03	β_{74}	-1.93E-01		
β_{18}	5.29E+00	β_{37}	2.61E-04	β_{56}	8.64E-05	β_{75}	-8.89E-02		
β_{19}	1.91E+00	β_{38}	4.82E-07	β_{57}	1.32E-05	β_{76}	3.70E-01		

Table A- 4 Regression coefficients for $Q_{cooling}$

β_0	4.91E+01	β_{20}	3.56E-01	β_{39}	2.71E-01	β_{58}	1.01E-05	β_{77}	-7.07E-02
β_2	-7.37E-01	β_{21}	-1.93E-01	β_{40}	-1.03E-02	β_{59}	6.95E-06	β_{78}	4.78E-01
β_3	-3.17E-01	β_{22}	7.67E-01	β_{41}	2.65E-02	β_{60}	5.61E-06	β_{79}	6.00E-01
β_4	-5.43E-02	β_{23}	2.10E+00	β_{42}	2.10E-02	β_{61}	8.59E-06	β_{80}	-7.28E-02
β_5	-5.39E-05	β_{24}	3.42E+00	β_{43}	-1.48E-02	β_{62}	-1.75E-05	β_{81}	3.51E-01
β_6	1.02E+01	β_{25}	3.45E-01	β_{44}	-1.04E-02	β_{63}	1.56E-06	β_{82}	1.33E-01
β_7	-6.16E+00	β_{26}	1.10E-03	β_{45}	-5.47E-02	β_{64}	-1.14E+00	β_{83}	5.80E-01
β_8	-5.36E+00	β_{27}	4.65E-04	β_{46}	3.58E-02	β_{65}	2.68E-01	β_{84}	-1.75E-01
β_9	-3.67E+00	β_{28}	-1.29E-06	β_{47}	-2.88E-08	β_{66}	9.70E-01	β_{85}	3.64E-01
β_{10}	-2.83E+00	β_{29}	-5.96E-01	β_{48}	-2.58E-04	β_{67}	-1.12E+00	β_{86}	1.54E-01
β_{11}	-9.41E+00	β_{30}	4.59E-02	β_{49}	-8.80E-04	β_{68}	-1.19E+00	β_{87}	-3.20E-01
β_{12}	-6.02E+00	β_{31}	1.11E-02	β_{50}	2.94E-03	β_{69}	-5.70E+00	β_{88}	3.56E-01
β_{13}	-7.23E+00	β_{32}	7.72E-03	β_{51}	3.56E-03	β_{70}	2.78E-01	β_{89}	-9.86E-02
β_{14}	8.32E-03	β_{33}	3.82E-02	β_{52}	3.44E-03	β_{71}	1.67E-02	β_{90}	4.41E-01
β_{15}	1.05E-03	β_{34}	7.94E-02	β_{53}	2.66E-03	β_{72}	1.45E-01	β_{91}	3.20E-01
β_{16}	3.45E-05	β_{35}	1.75E-01	β_{54}	8.40E-03	β_{73}	1.33E-01		
β_{17}	-1.43E-10	β_{36}	1.36E-02	β_{55}	2.30E-03	β_{74}	-1.53E-01		
β_{18}	4.85E+00	β_{37}	1.13E-04	β_{56}	7.46E-05	β_{75}	-2.53E-02		
β_{19}	1.75E+00	β_{38}	4.67E-07	β_{57}	1.22E-05	β_{76}	3.81E-01		

Appendix B STEADY STATE TEST PARAMETERS

Table B- 1 Provided steady state test data

Test Number	Hot feed in temperature [$^{\circ}C$]	cold feed in temperature [$^{\circ}C$]	Input flow [m^3/h]	Input salinity [g/kg]	Air gap pressure [kPa]	Envelope length [m]	Number of envelopes [-]	Total membrane area [m^2]
1	76.6	18.9	0.29	56.1	101.3	1.5	6	7.2
2	75.2	19.2	0.29	56.6	101.3	1.5	6	7.2
3	75.3	20.9	0.60	56.8	101.3	1.5	6	7.2
4	65.3	20.9	0.46	56.8	101.3	1.5	6	7.2
5	84.6	22.0	0.46	56.8	101.3	1.5	6	7.2
6	75.7	21.1	0.46	57.4	10.0	1.5	6	7.2
7	74.8	19.8	0.46	57.4	70.0	1.5	6	7.2
8	75.1	21.7	0.46	116.6	101.3	1.5	6	7.2
9	75.6	18.1	0.46	186.1	101.3	1.5	6	7.2
10	74.7	16.3	0.24	56.9	101.3	5.0	6	24.0
11	75.2	25.8	0.60	57.2	101.3	5.0	6	24.0
12	65.4	21.2	0.45	57.7	101.3	5.0	6	24.0
13	85.0	21.5	0.46	57.2	101.3	5.0	6	24.0
14	75.0	23.0	0.45	57.6	10.0	5.0	6	24.0
15	75.1	21.8	0.46	57.0	70.0	5.0	6	24.0
16	75.8	14.0	0.93	73.0	101.3	2.7	12	25.9
17	75.3	11.9	0.61	62.7	101.3	2.7	12	25.9
18	75.2	15.8	1.20	62.0	101.3	2.7	12	25.9
19	64.9	13.6	0.90	62.6	101.3	2.7	12	25.9
20	84.8	14.1	0.91	66.1	101.3	2.7	12	25.9
21	75.0	19.9	0.87	64.9	10.0	2.7	12	25.9
22	75.2	13.3	0.93	72.5	70.0	2.7	12	25.9
23	74.9	14.6	0.93	112.7	101.3	2.7	12	25.9
24	75.2	15.3	0.91	171.1	101.3	2.7	12	25.9

Table B- 2 Steady state test data from [52]

Test Number	Hot feed in temperature [°C]	cold feed in temperature [°C]	Input flow [m^3/h]	Input salinity [g/kg]
25	50.3	19.1	0.83	41.4
26	50.4	19.1	0.83	39.5
27	60.0	18.7	0.84	41.1
28	60.0	19.2	0.85	41.1
29	66.1	19.2	0.83	40.0
30	70.1	19.1	0.79	41.4
31	70.1	19.0	0.79	43.0
32	70.2	18.9	0.82	40.5
33	70.2	19.1	0.82	41.3
34	51.8	19.5	0.87	84.9
35	49.8	19.6	0.86	85.1
36	60.4	19.7	0.87	84.1
37	60.4	19.6	0.86	85.2
38	65.7	19.7	0.87	85.8
39	69.7	18.7	0.86	86.4
40	70.3	18.4	0.85	86.5
41	50.3	19.0	0.82	117.1
42	50.4	19.1	0.81	118.3
43	59.1	18.3	0.82	118.7
44	60.9	18.7	0.82	118.4
45	66.1	19.3	0.82	118.8
46	70.4	18.1	0.83	120.0
47	70.2	18.6	0.82	118.9
48	69.5	25.2	0.83	41.6

Appendix C MATRICES FOR THE THERMAL ELECTRICAL NETWORK

Diagonal and tridiagonal matrices are indicated with $\text{diag}(\text{matrix})$ and $\text{tridiag}(\text{matrix})$ respectively for ease of notation.

$$\mathbf{B} = \begin{matrix} 1 \\ 2 \\ \vdots \\ \vdots \\ 4N+2 \\ 4N+3 \\ 4N+4 \\ 4N+5 \\ \vdots \\ 8N+4 \end{matrix} \begin{bmatrix} 1/L_{bf}^{in} & 0 \\ 0 & 0 \\ \vdots & \vdots \\ 0 & 0 \\ 0 & -1/L_{bp}^{in} \\ 0 & -1 \\ -1 & 0 \\ 0 & 0 \\ \vdots & \vdots \\ 0 & 0 \end{bmatrix} \begin{bmatrix} T_{bf,in} \\ T_{bp,in} \end{bmatrix} \quad (\text{C-1})$$

$$\mathbf{H} = \begin{matrix} 1 \\ \vdots \\ 4N+4 \\ 4N+5 \\ \vdots \\ 5N+4 \\ 5N+5 \\ \vdots \\ 6N+4 \\ 6N+5 \\ \vdots \\ 7N+4 \\ 7N+5 \\ \vdots \\ 8N+4 \end{matrix} \begin{bmatrix} 0 \\ \vdots \\ 0 \\ -A_m J H_v \\ \vdots \\ -A_m J H_v \\ x_l A_m J H_v \\ \vdots \\ x_l A_m J H_v \\ (1-x_l) A_m J H_v \\ \vdots \\ (1-x_l) A_m J H_v \\ 0 \\ \vdots \\ 0 \end{bmatrix} \quad (\text{C-2})$$

$$\text{tridiag}(A_{bf}) = \begin{bmatrix} -\frac{R_{bfz}^{in}}{L_{bf}^{in}} & & -\frac{1}{L_{bf}^{in}} \\ \frac{1}{C_{bf}^1} & -\frac{1}{C_{bf}^1 R_{bf}^1} + \frac{J^1 A_m^1 c_p^1}{C_{bf}^1} & -\frac{1}{C_{bf}^2} \\ \frac{1}{L_{bf}^1} & -\frac{R_{fz}^2}{L_{bf}^2} & -\frac{1}{L_{bf}^2} \\ \vdots & \vdots & \vdots \\ \frac{1}{L_{bf}^{N-2}} & -\frac{R_{fz}^{N-1}}{L_{bfz}^{N-1}} & -\frac{1}{L_{bf}^{N-1}} \\ \frac{1}{C_{bf}^N} & -\frac{1}{C_{bf}^N R_{bf}^N} + \frac{J^N A_m^N c_p^N}{C_{bf}^N} & -\frac{1}{C_{bf}^{N+1}} \\ \frac{1}{L_{bf}^N} & -\frac{R_{fz}^N}{L_{bf}^N} & \end{bmatrix} \quad (\text{C-3})$$

$$Z_{bf1} = \begin{bmatrix} 0 & 0 \\ \vdots & \vdots \\ 0 & 0 \\ -\frac{1}{L_{bf}^N} & 0 \end{bmatrix} \quad (\text{C-4})$$

$$Z_{bf2} = \begin{bmatrix} 0 & 0 & 0 & \cdots & 0 \\ \frac{1}{C_{bf}^1 R_{bf}^1} & 0 & 0 & \cdots & 0 \\ 0 & 0 & 0 & \cdots & 0 \\ 0 & \frac{1}{C_{bf}^2 R_{bf}^2} & 0 & \cdots & 0 \\ 0 & 0 & 0 & \cdots & 0 \\ 0 & 0 & \frac{1}{C_{bf}^n R_{bf}^n} & \cdots & 0 \\ \vdots & \vdots & \vdots & \ddots & \vdots \\ 0 & 0 & 0 & \cdots & 0 \\ 0 & 0 & 0 & \cdots & \frac{1}{C_{bf}^N R_{bf}^N} \\ 0 & 0 & 0 & \cdots & 0 \end{bmatrix} \quad (\text{C-5})$$

$$\text{tridiag}(A_{bp}) = \begin{bmatrix} & -\frac{R_{bpz}^1}{L_{bp}^1} & -\frac{1}{L_{bp}^1} \\ \frac{1}{C_{bp}^1} & \frac{1}{C_{bp}^1 R_{bp}^1} & -\frac{1}{C_{bp}^2} \\ \frac{1}{L_{bp}^1} & -\frac{R_{bpz}^2}{L_{bp}^2} & -\frac{1}{L_{bp}^2} \\ \vdots & \vdots & \vdots \\ \frac{1}{L_{bp}^N} & -\frac{R_{bpz}^N}{L_{bp}^N} & -\frac{1}{L_{bp}^N} \\ \frac{1}{C_{bp}^N} & -\frac{1}{C_{bp}^N R_{bp}^N} & -\frac{1}{C_{bp}^N} \\ \frac{1}{L_{bp}^{in}} & -\frac{R_{bpz}^{in}}{L_{bp}^{in}} & \end{bmatrix} \quad (\text{C-6})$$

$$Z_{bp1} = \begin{bmatrix} 0 & \frac{1}{L_{bp}^1} \\ \vdots & \vdots \\ 0 & 0 \\ 0 & 0 \end{bmatrix} \quad (\text{C-7})$$

$$Z_{bp2} = \begin{bmatrix} 0 & 0 & \cdots & 0 \\ \frac{1}{C_{bp}^1 R_{bp}^1} & 0 & \cdots & 0 \\ 0 & 0 & \cdots & 0 \\ 0 & \frac{1}{C_{bp}^2 R_{bp}^2} & \cdots & 0 \\ \vdots & \vdots & \ddots & \vdots \\ 0 & 0 & \cdots & 0 \\ 0 & 0 & \cdots & \frac{1}{C_{bp}^N R_{bp}^N} \\ 0 & 0 & \cdots & 0 \end{bmatrix} \quad (\text{C-8})$$

$$T_{bf0} = \begin{bmatrix} 0 & \cdots & 0 & -\frac{1}{m_{bf}^N c_p^N} \\ 0 & \cdots & 0 & 0 \end{bmatrix} \quad (\text{C-9})$$

$$T_{bp0} = \begin{bmatrix} 0 & 0 & \cdots & 0 \\ \frac{1}{m_{bp}^1 c_p^1} & 0 & \cdots & 0 \end{bmatrix} \quad (\text{C-10})$$

$$Z_1 = \begin{bmatrix} 0 & \frac{1}{R_{bf}^1} + J^1 A_m^1 c_p^1 [T_{bf}^1] & 0 & \cdots & \cdots & 0 \\ \vdots & \vdots & \frac{1}{R_{bf}^2} + J^2 A_m^2 c_p^2 [T_{bf}^2] & \cdots & \cdots & 0 \\ 0 & \cdots & \cdots & \ddots & 0 & \vdots \\ 0 & \cdots & \cdots & 0 & \frac{1}{R_{bf}^N} + J^N A_m^N c_p^N [T_{bf}^N] & 0 \end{bmatrix} \quad (\text{C-11})$$

$$\text{diag}(Z_2) = \left[-\frac{1}{R_{bf}^1} - \frac{1}{R_m^1}, -\frac{1}{R_{bf}^2} - \frac{1}{R_m^2}, \dots, -\frac{1}{R_{bf}^N} - \frac{1}{R_m^N} \right] \quad (\text{C-12})$$

$$\text{diag}(Z_3) = \left[\frac{1}{R_m^1}, \frac{1}{R_m^2}, \dots, \frac{1}{R_m^N} \right] \quad (\text{C-13})$$

$$\text{diag}(z_4) = \left[\frac{1}{R_m^1}, \frac{1}{R_m^2}, \dots, \frac{1}{R_m^N} \right] \quad (\text{C-14})$$

$$\text{diag}(z_5) = \left[-\frac{1}{R_m^1} - \frac{1}{R_a^1}, -\frac{1}{R_m^2} - \frac{1}{R_a^2}, \dots, -\frac{1}{R_m^N} - \frac{1}{R_a^N} \right] \quad (\text{C-15})$$

$$\text{diag}(Z_6) = \left[\frac{1}{R_a^1}, \frac{1}{R_a^2}, \dots, \frac{1}{R_a^N} \right] \quad (\text{C-16})$$

$$\text{diag}(Z_7) = \left[\frac{1}{R_a^1} + A_m^1 J^1 c_p, \frac{1}{R_a^2} + A_m^2 J^2 c_p, \dots, \frac{1}{R_a^N} + A_m^N J^N c_p \right] \quad (\text{C-17})$$

$$\text{diag}(Z_8) = \left[-\frac{1}{R_a^1} - \frac{1}{R_c}, -\frac{1}{R_a^2} - \frac{1}{R_c}, \dots, -\frac{1}{R_a^N} - \frac{1}{R_c} \right] \quad (\text{C-18})$$

$$\text{diag}(Z_9) = \left[\frac{1}{R_c}, \dots, \frac{1}{R_c} \right] \quad (\text{C-19})$$

$$Z_9 = \begin{bmatrix} 0 & \frac{1}{R_{bp}^1} & 0 & \cdots & \cdots & 0 \\ \vdots & \vdots & \frac{1}{R_{bp}^2} & \cdots & \cdots & 0 \\ 0 & \cdots & \cdots & \ddots & 0 & \vdots \\ 0 & \cdots & \cdots & 0 & \frac{1}{R_{bp}^N} & 0 \end{bmatrix} \quad (\text{C-20})$$

$$\text{diag}(Z_{10}) = \left[\frac{1}{R_c}, \dots, \frac{1}{R_c} \right] \quad (\text{C-21})$$

$$\text{diag}(Z_{11}) = \left[-\frac{1}{R_c} - \frac{1}{R_{bp}^1}, -\frac{1}{R_c} - \frac{1}{R_{bp}^2}, \dots, -\frac{1}{R_c} - \frac{1}{R_{bp}^N} \right] \quad (\text{C-22})$$

$$Z_{12} = \begin{bmatrix} -\frac{1}{R_c} - \frac{1}{R_{bp}^1} & 0 & 0 & 0 \\ 0 & -\frac{1}{R_c} - \frac{1}{R_{bp}^n} & \ddots & \vdots \\ \vdots & \ddots & \ddots & 0 \\ 0 & \cdots & 0 & -\frac{1}{R_c} - \frac{1}{R_{bp}^N} \end{bmatrix} \quad (\text{C-23})$$

Appendix D MATRICES FOR THE ENERGY BALANCE EQUATIONS MODEL

$$\mathbf{H} = \begin{matrix} 1 \\ \vdots \\ 2N \\ 2N+1 \\ \vdots \\ 3N \\ 3N+1 \\ \vdots \\ 4N \\ 4N+1 \\ \vdots \\ 5N \\ 5N+1 \\ \vdots \\ 6N \end{matrix} \begin{bmatrix} 0 \\ \vdots \\ 0 \\ -JA_m H_v \\ \vdots \\ -JA_m H_v \\ x_l JA_m H_v \\ \vdots \\ x_l JA_m H_v \\ (1-x_l)JA_m H_v \\ \vdots \\ (1-x_l)JA_m H_v \\ 0 \\ \vdots \\ 0 \end{bmatrix} \quad (\text{D-1})$$

$$\mathbf{q}_0 = \begin{bmatrix} \frac{L_{md}\dot{m}_{bf}^1}{m_{bf}^1 dz} T_{bf}^{in} \\ 0 \\ \vdots \\ 0 \\ \frac{L_{md}\dot{m}_{bp}}{m_{bp}^N dz} T_{bp}^{in} \end{bmatrix} \quad (\text{D-2})$$

$$\text{tridiag}(D_1) = \begin{bmatrix} & -\frac{L_{md}\dot{m}_{bf}^1}{m_{bf}^1 dz} - \frac{2L_{md}W_{md}}{m_{bf}^1 cp_b^1} (h_b^1 + J^1 Cp_d) & 0 \\ \frac{L_{md}\dot{m}_{bf}^2}{m_{bf}^2 dz} & -\frac{L_{md}\dot{m}_{bf}^2}{m_{bf}^2 dz} - \frac{2L_{md}W_{md}}{m_{bf}^2 cp_b^2} (h_b^2 + J^2 Cp_d) & 0 \\ \vdots & \vdots & \vdots \\ \frac{L_{md}\dot{m}_{bf}^{N-1}}{m_{bf}^{N-1} dz} & -\frac{L_{md}\dot{m}_{bf}^{N-1}}{m_{bf}^{N-1} dz} - \frac{2L_{md}W_{md}}{m_{bf}^{N-1} cp_b^{N-1}} (h_b^{N-1} + J^{N-1} Cp_d) & 0 \\ \frac{L_{md}\dot{m}_{bf}^N}{m_{bf}^N dz} & -\frac{L_{md}\dot{m}_{bf}^N}{m_{bf}^N dz} - \frac{2L_{md}W_{md}}{m_{bf}^N cp_b^N} (h_b^N + J^N Cp_d) & \end{bmatrix} \quad (\text{D-3})$$

$$D_2 = \text{diag} \left(\frac{2L_{md}W_{md}(h_b^1 + J^1 Cp_d^1 A_m)}{m_{bf}^1 cp_b^1}, \dots, \frac{2L_{md}W_{md}(h_b^N + J^N Cp_d^N A_m)}{m_{bf}^N cp_b^N} \right) \quad (\text{D-4})$$

$$D_3 = \text{diag} \left(\frac{2L_{md}W_{md}h_p^1}{m_{bp}^1 cp_p^1}, \dots, \frac{2L_{md}W_{md}h_p^N}{m_{bp}^N cp_p^N} \right) \quad (\text{D-5})$$

$$\text{tridiag}(D_4) = \begin{bmatrix} 0 & -\frac{L_{md}\dot{m}_{pb}}{m_{pb}^1 dz} - \frac{2L_{md}W_{md}}{m_{bp}^1 cp_p^1} h_p^1 & \frac{L_{md}\dot{m}_{bp}}{m_{bp}^1 dz} \\ 0 & -\frac{L_{md}\dot{m}_{bp}}{m_{bp}^2 dz} - \frac{2L_{md}W_{md}}{m_{bp}^2 cp_p^2} h_p^2 & \frac{L_{md}\dot{m}_{bp}}{m_{bp}^2 dz} \\ \vdots & \vdots & \vdots \\ 0 & -\frac{L_{md}\dot{m}_{bp}}{m_{bp}^{N-1} dz} - \frac{2L_{md}W_{md}}{m_{bp}^{N-1} cp_p^{N-1}} h_p^{N-1} & \frac{L_{md}\dot{m}_{bp}}{m_{bp}^{N-1} dz} \\ 0 & -\frac{L_{md}\dot{m}_{bp}}{m_{bp}^N dz} - \frac{2L_{md}W_{md}}{m_{bp}^N cp_p^N} h_p^N & \frac{L_{md}\dot{m}_{bp}}{m_{bp}^N dz} \end{bmatrix} \quad (\text{D-6})$$

$$Z_1 = \text{diag}(h_{bf}^1 + J^1 Cp_d^1 A_m, \dots, h_{bf}^N + J^N Cp_d^N A_m) \quad (\text{D-7})$$

$$Z_2 = \text{diag}(-h_{bf}^1 - 2J^1 Cp_d^1 A_m - h_a^1, \dots, -h_{bf}^N - 2J^N Cp_d^N A_m - h_a^N) \quad (\text{D-8})$$

$$Z_3 = \text{diag}(h_m^1 + J^1 Cp_d^1 A_m, \dots, h_m^N + J^N Cp_d^N A_m) \quad (\text{D-9})$$

$$Z_4 = \text{diag}(h_m^1 + J^1 Cp_d^1 A_m, \dots, h_m^N + J^N Cp_d^N A_m) \quad (\text{D-10})$$

$$Z_5 = \text{diag}(-h_m^1 - 2J^1 Cp_d^1 A_m - h_a^1, \dots, -h_m^N - 2J^N Cp_d^N A_m - h_a^N) \quad (\text{D-11})$$

$$Z_6 = \text{diag}(h_a^1 + J^1 Cp_d^1, \dots, h_a^N + J^N Cp_d^N) \quad (\text{D-12})$$

$$Z_7 = \text{diag}(h_a^1 + J^1 Cp_d^1, \dots, h_a^N + J^N Cp_d^N) \quad (\text{D-13})$$

$$Z_8 = \text{diag}(-h_a^1 - J^1 Cp_d^1 A_m - h_c, \dots, -h_a^N - J^N Cp_d^N A_m - h_c) \quad (\text{D-14})$$

$$Z_9 = \text{diag}(h_c, \dots, h_c) \quad (\text{D-15})$$

$$Z_{10} = \text{diag}(h_c, \dots, h_c) \quad (\text{D-16})$$

$$Z_{11} = \text{diag}(-h_c - h_p^1, \dots, -h_c - h_p^N) \quad (\text{D-17})$$

$$Z_{12} = \text{diag}(h_p^1, \dots, h_p^N) \quad (\text{D-18})$$

Appendix E DYNAMIC TEST CONDITIONS

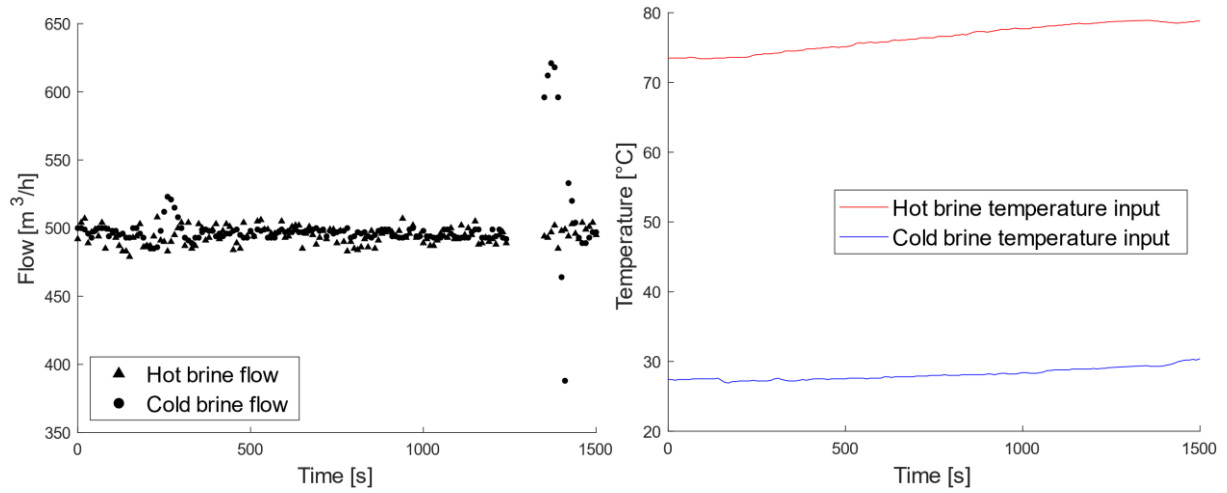


Figure E- 1 Test flow and temperatures of test 1

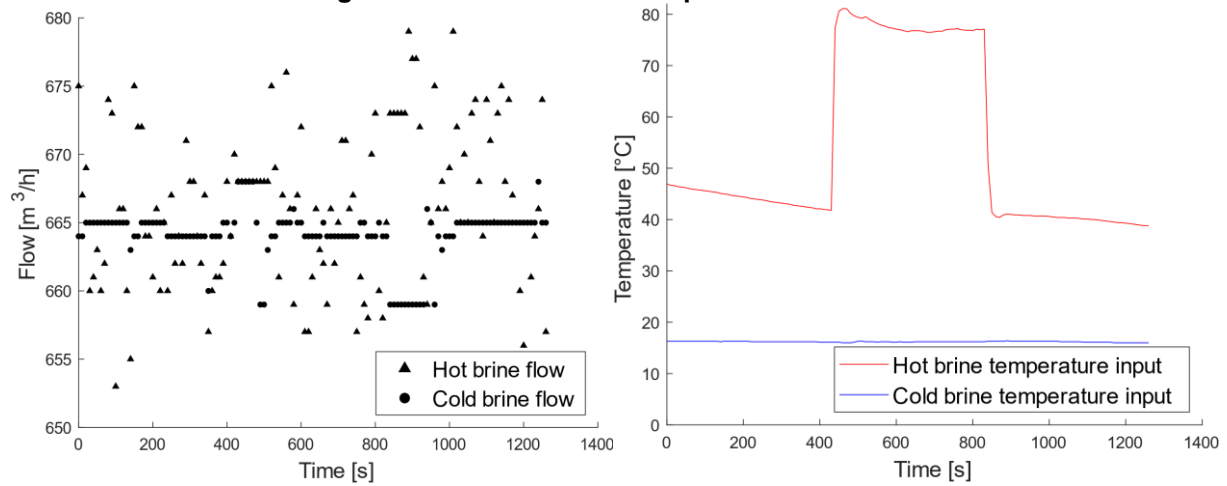


Figure E- 2 Test flow and temperatures of test 2

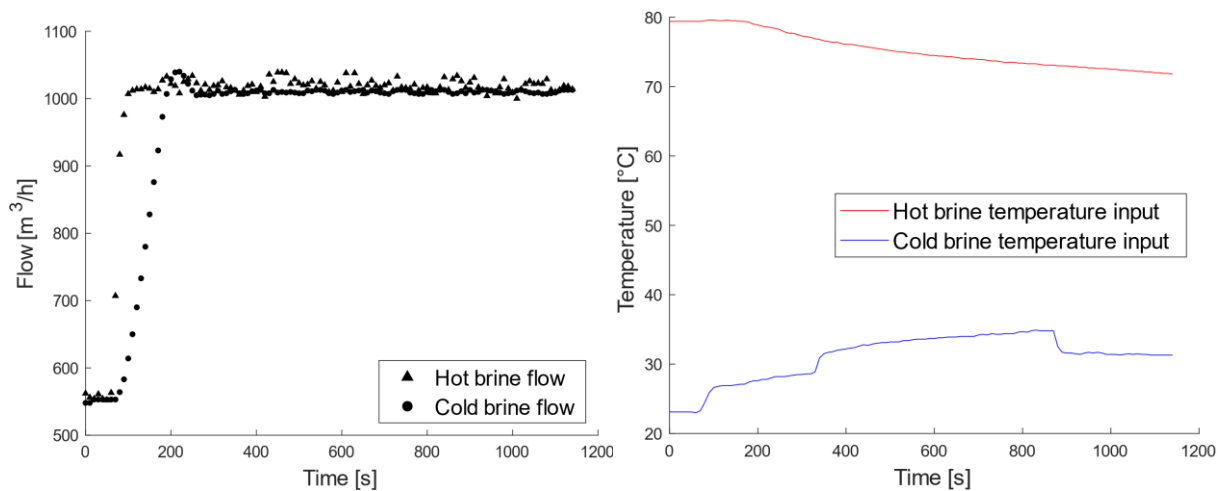


Figure E- 3 Test flow and temperatures of test 3

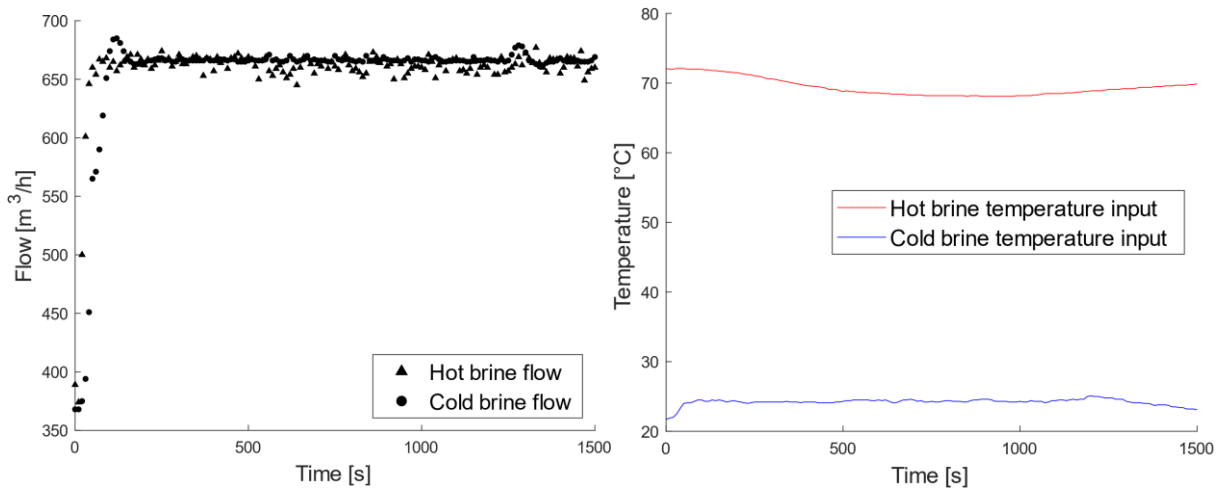


Figure E- 4 Test flow and temperatures of test 4

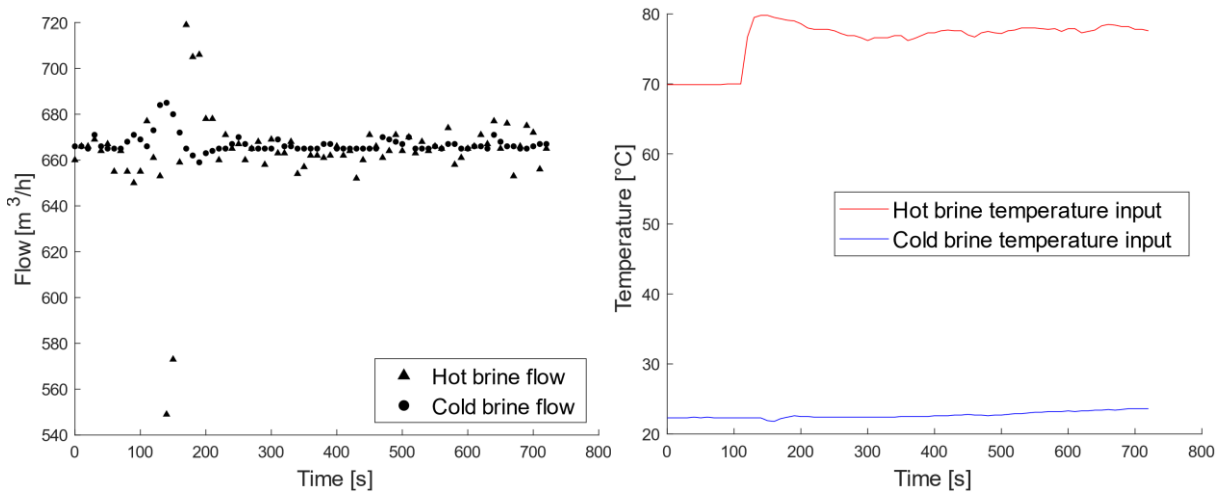


Figure E- 5 Test flow and temperatures of test 5

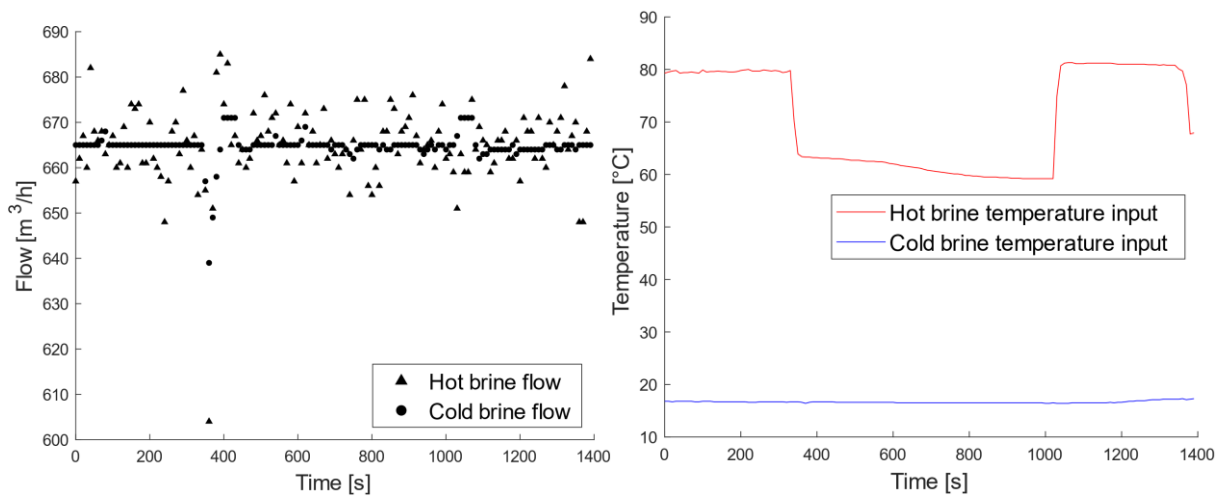


Figure E- 6 Test flow and temperatures of test 6

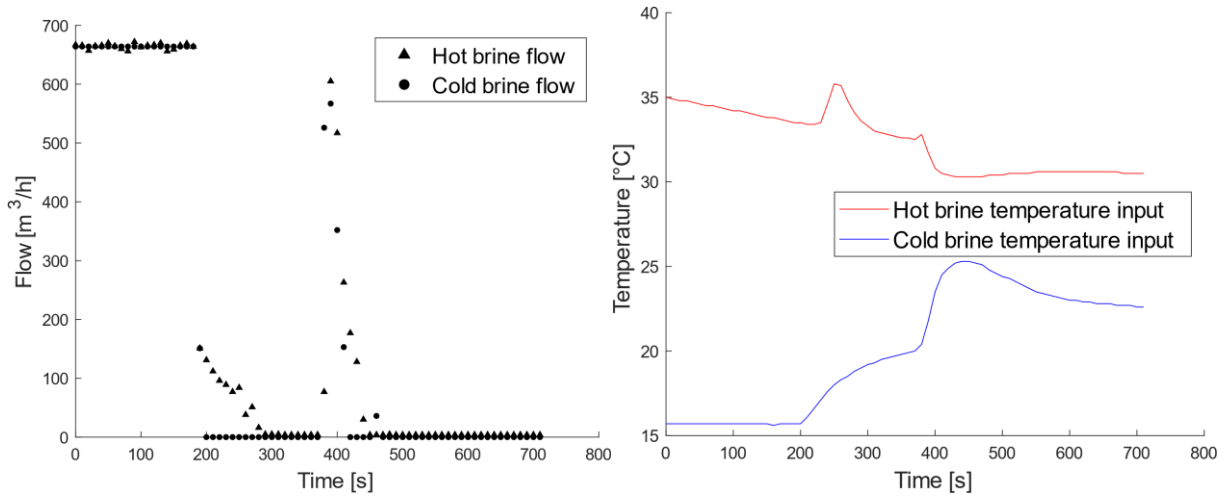


Figure E- 7 Test flow and temperatures of test 7

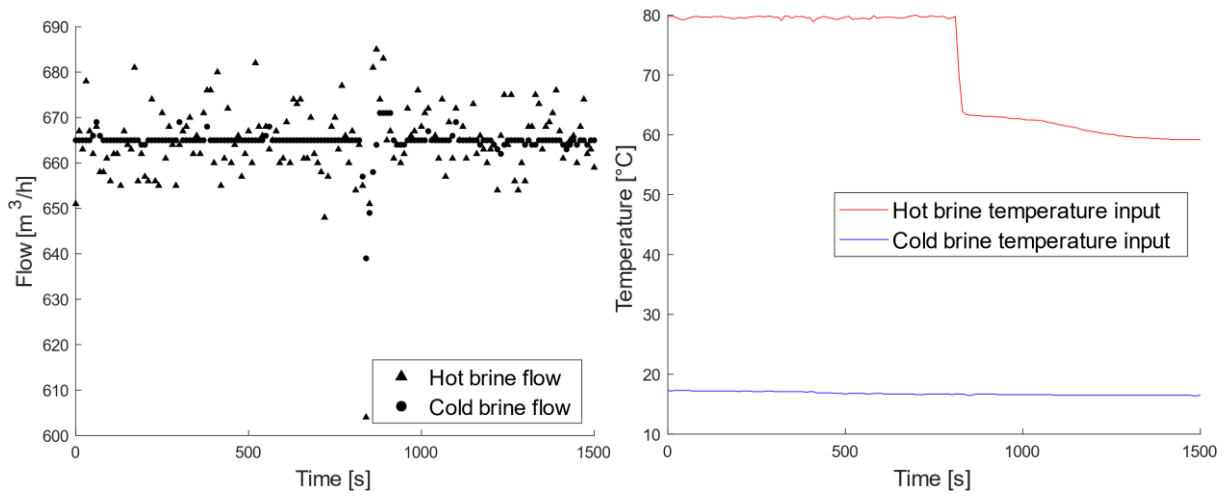


Figure E- 8 Test flow and temperatures of test 8

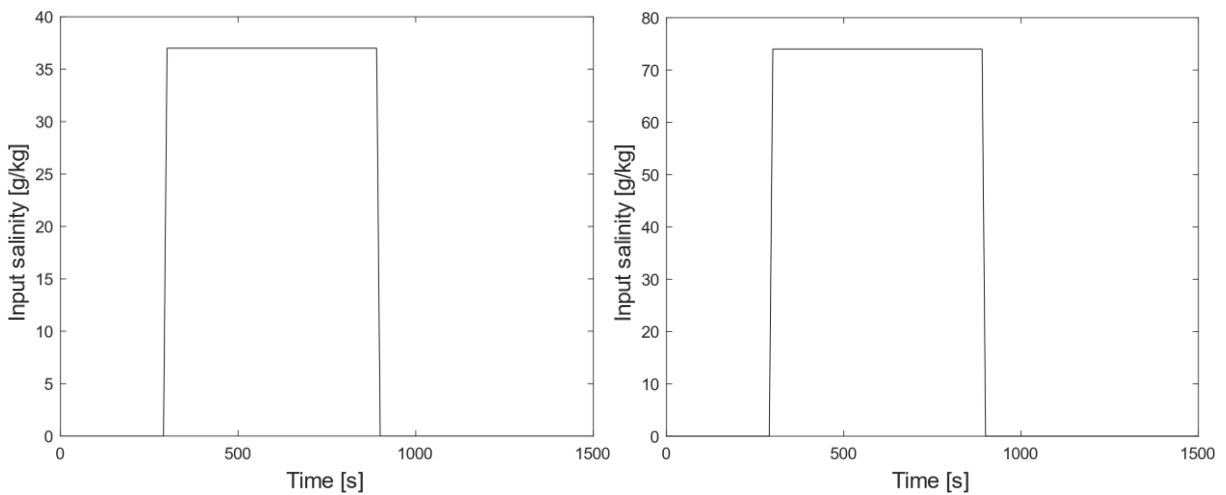


Figure E- 9 Test input salinity of test 8 on the left and test 9 on the right

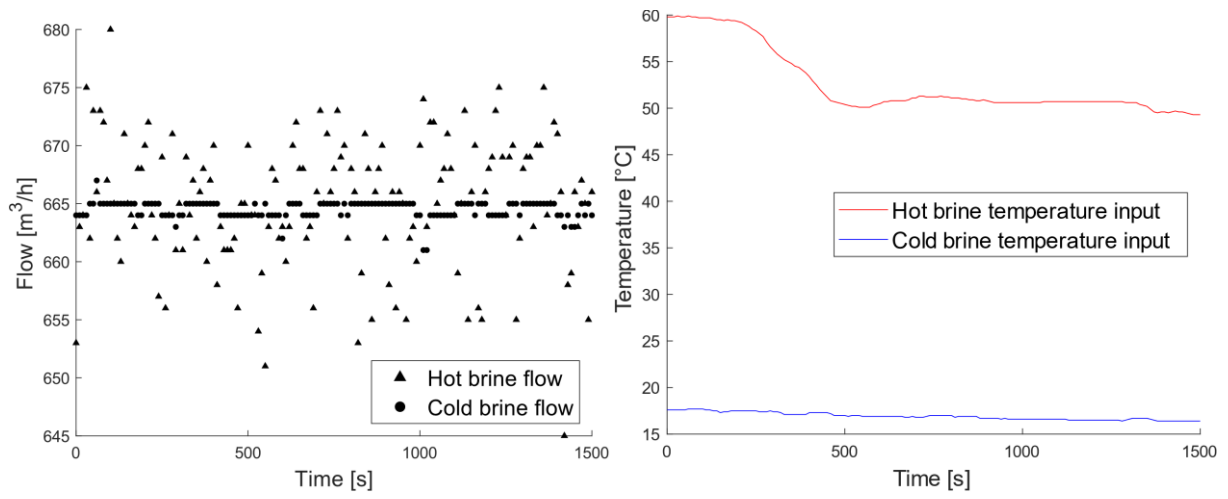


Figure E- 10 Test flow and temperatures of test 9

Appendix F DYNAMIC REGRESSION RESULTS

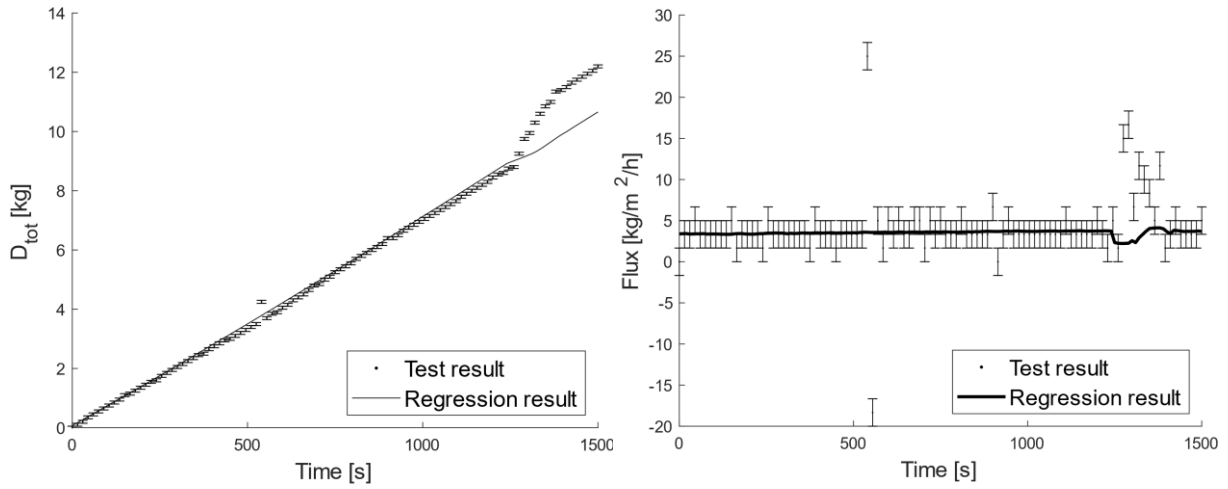


Figure F- 1 Test result of test 1. On the left the total production. On the right the flux.

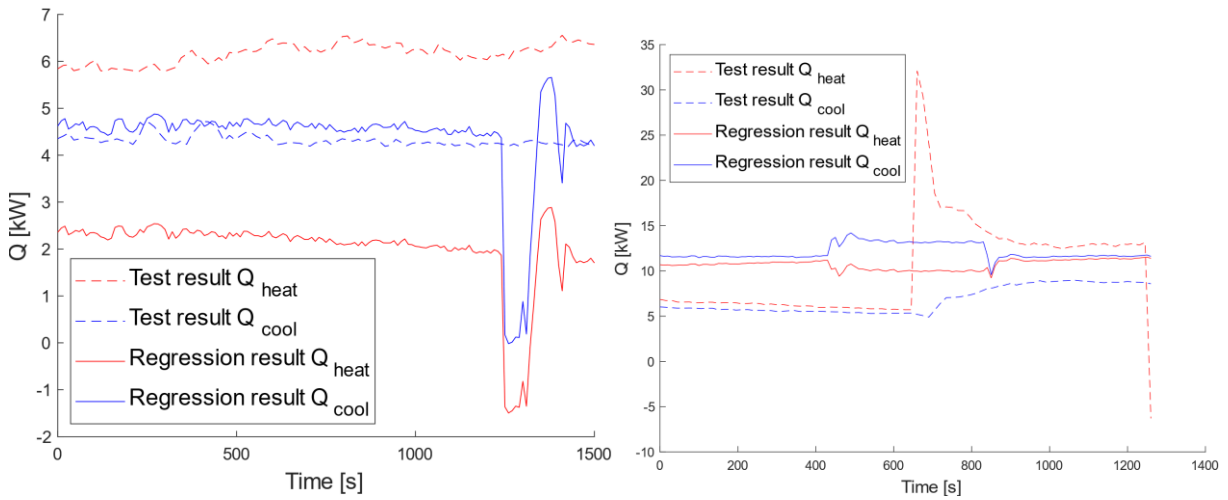


Figure F- 2 $Q_{heating}$ and $Q_{cooling}$ of test 1 the left and of test 2 on the right

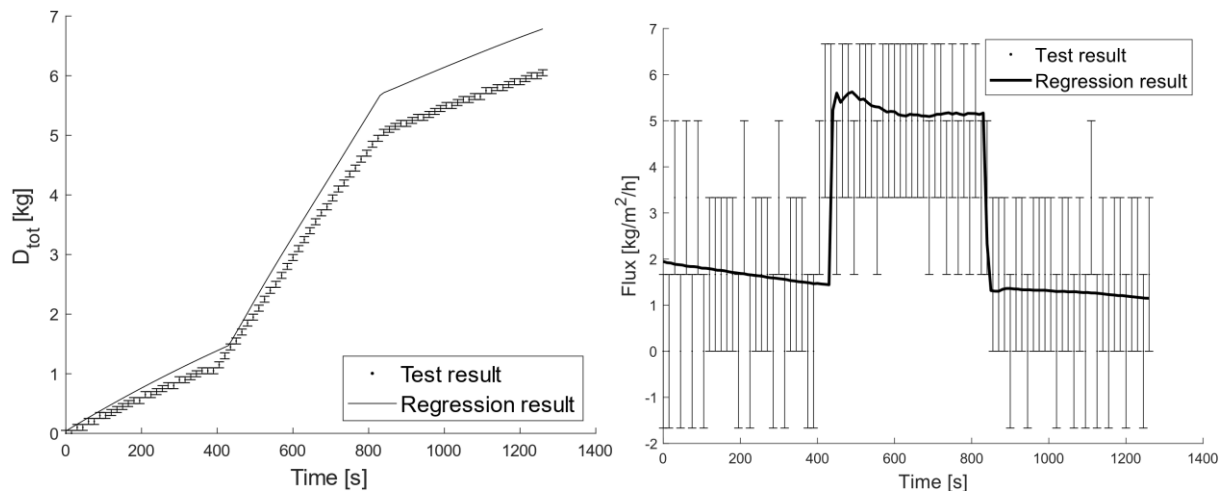


Figure F- 3 Test result of test 2. On the left the total production. On the right the flux.

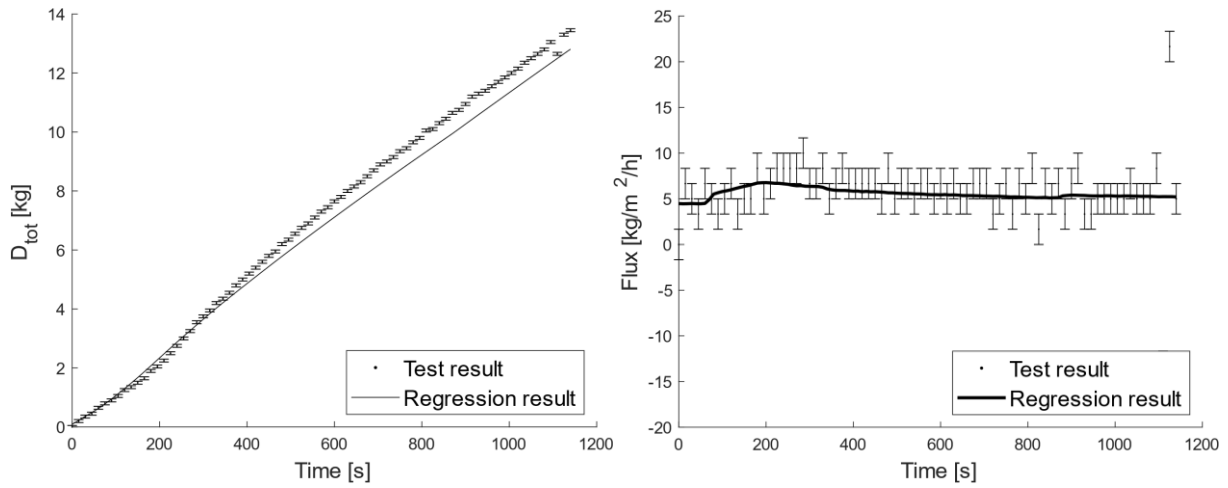


Figure F- 4 Test result of test 3. On the left the total production. On the right the flux.

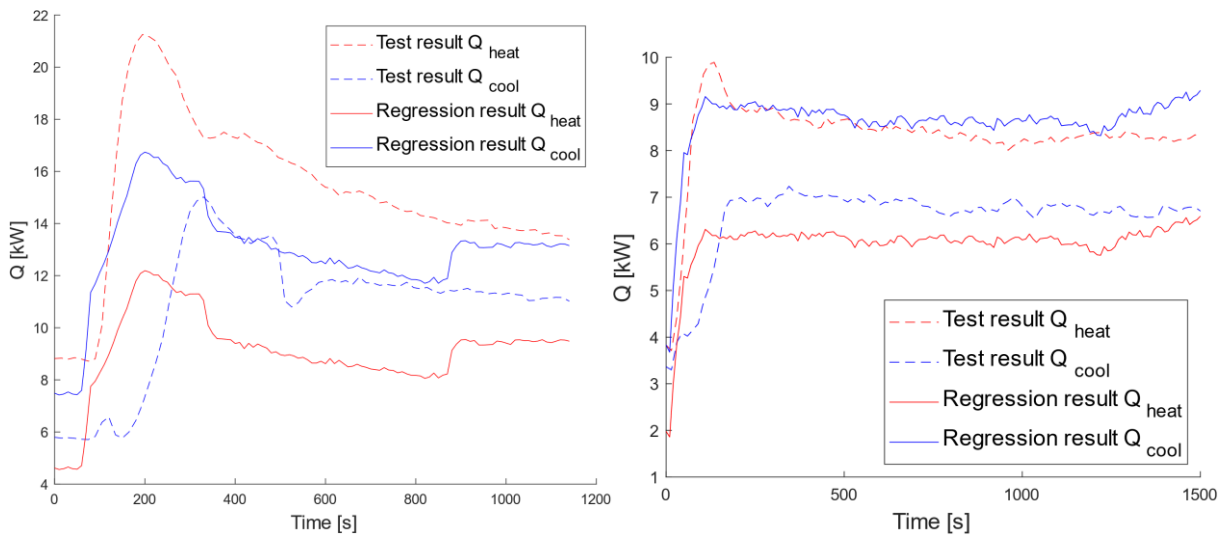


Figure F- 5 $Q_{heating}$ and $Q_{cooling}$ of test 3 the left and of test 4 on the right

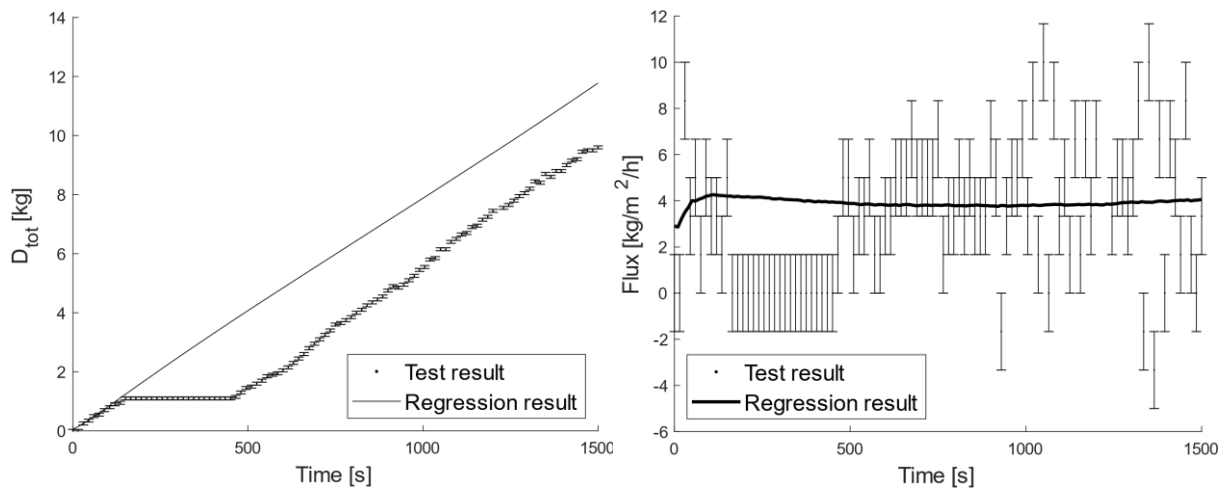


Figure F- 6 Test result of test 4. On the left the total production. On the right the flux.

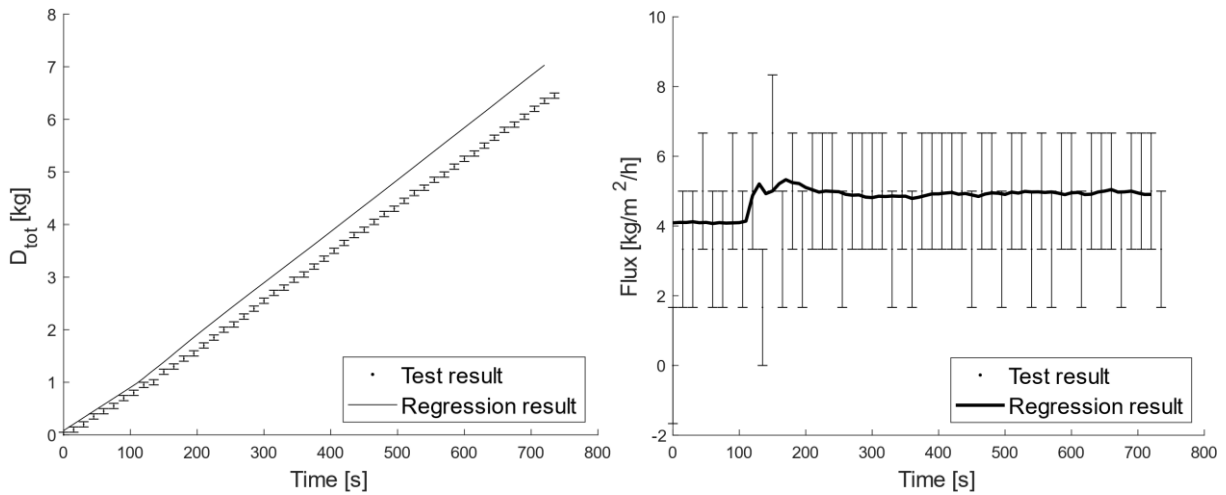


Figure F- 7 Test result of test 5. On the left the total production. On the right the flux.

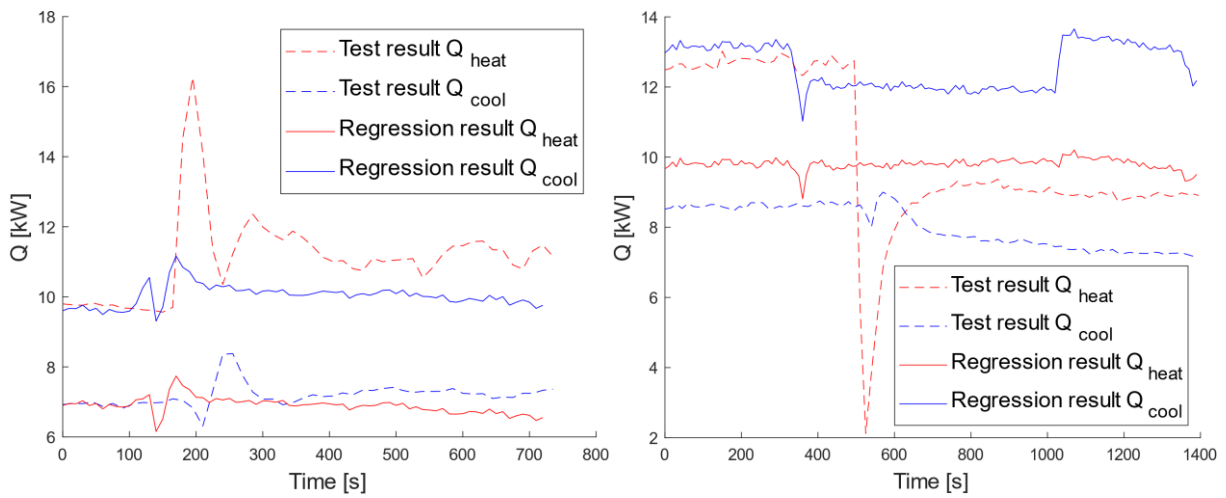


Figure F- 8 $Q_{heating}$ and $Q_{cooling}$ of test 5 the left and of test 6 on the right

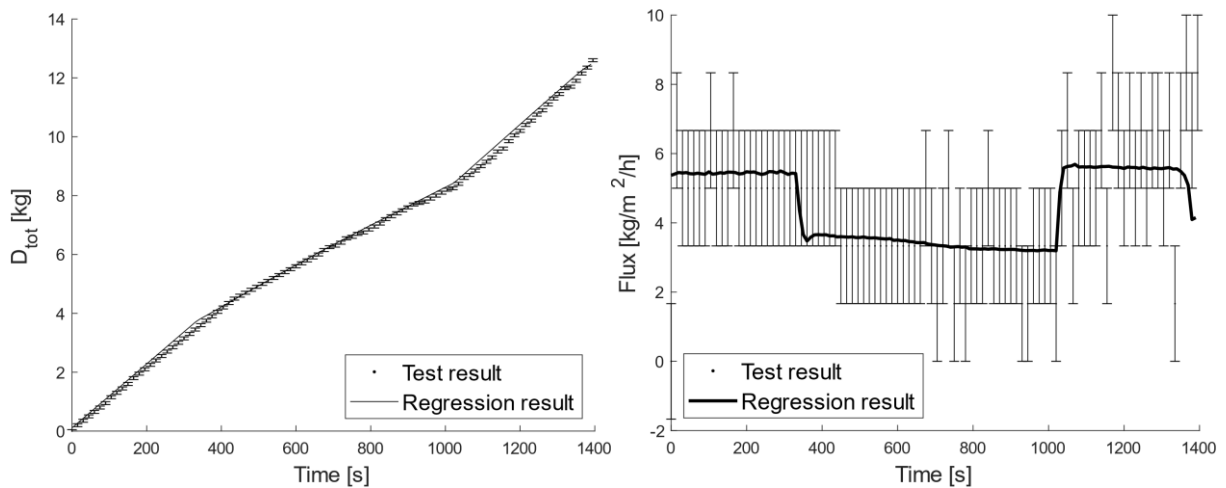


Figure F- 9 Test result of test 6. On the left the total production. On the right the flux.

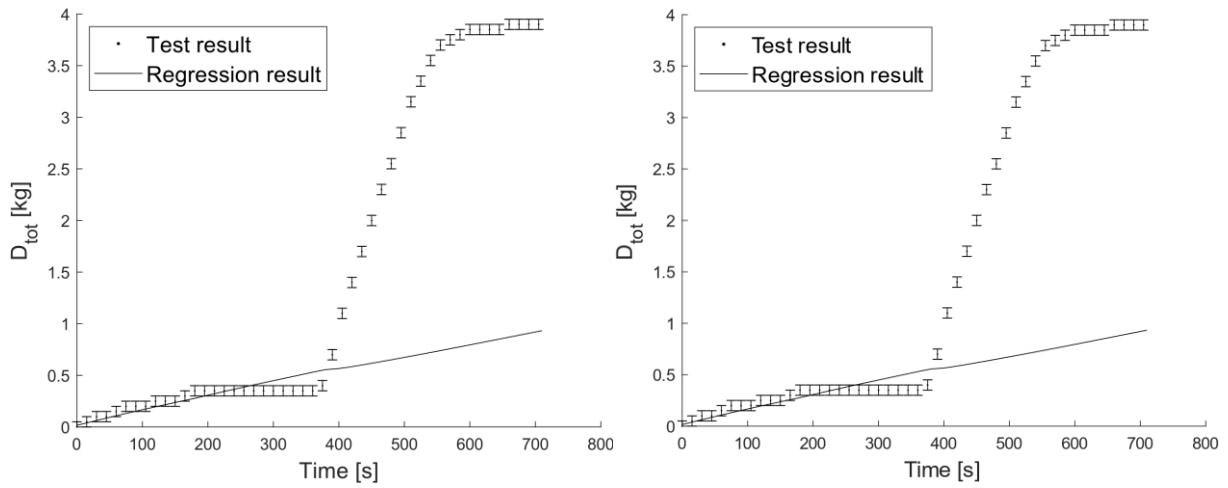


Figure F- 10 Test result of test 7. On the left the total production. On the right the flux.

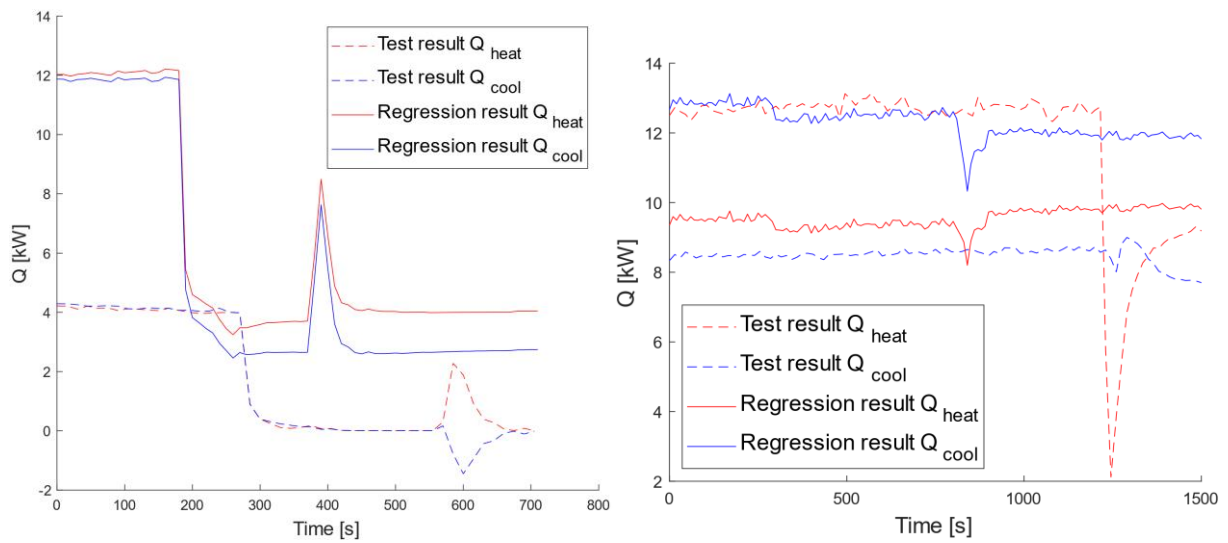


Figure F- 11 $Q_{heating}$ and $Q_{cooling}$ of test 7 the left and of test 8 on the right

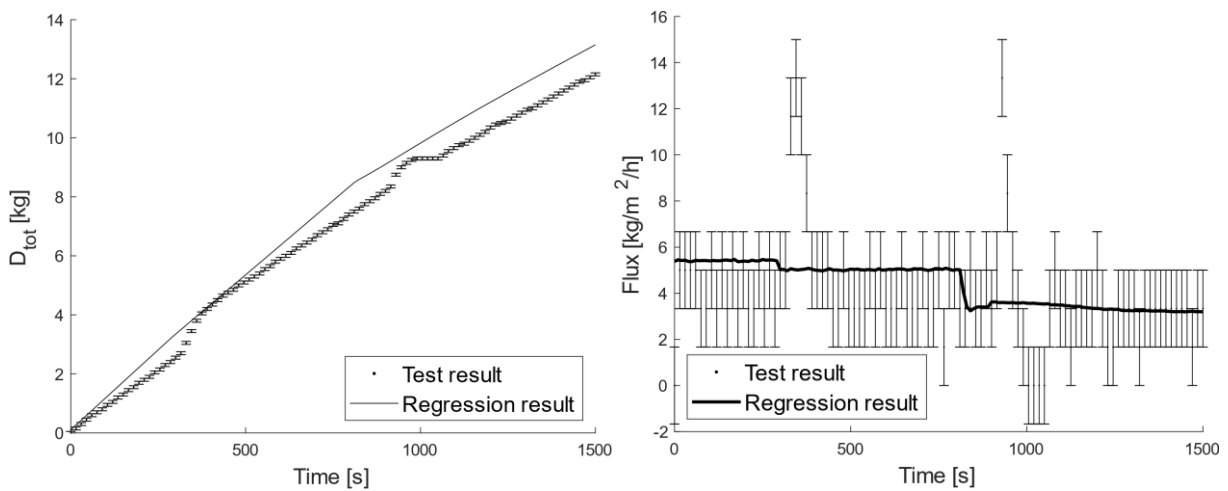


Figure F- 12 Test result of test 8. On the left the total production. On the right the flux.

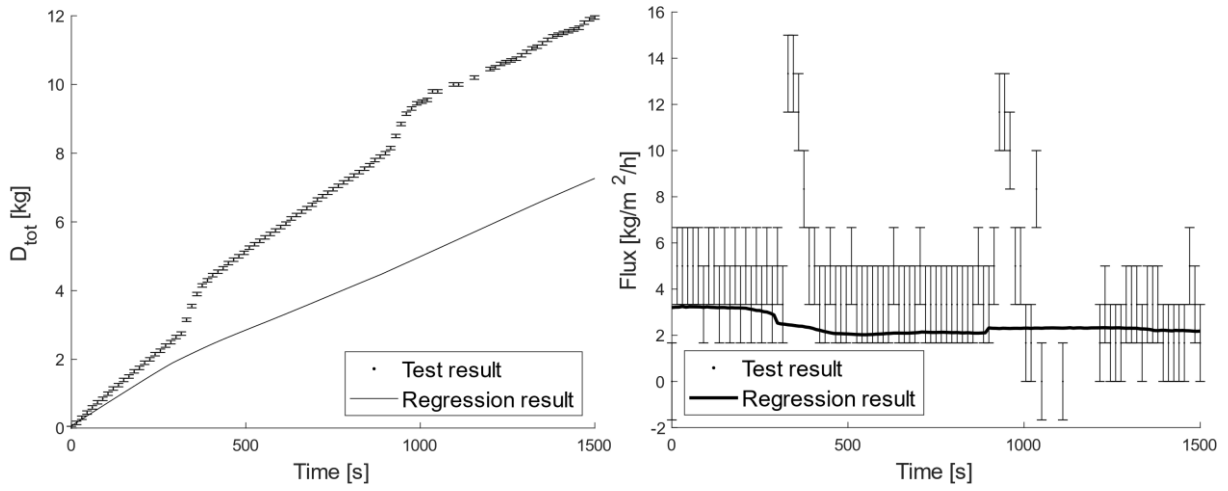


Figure D-1 Test result of test 9. On the left the total production. On the right the flux.

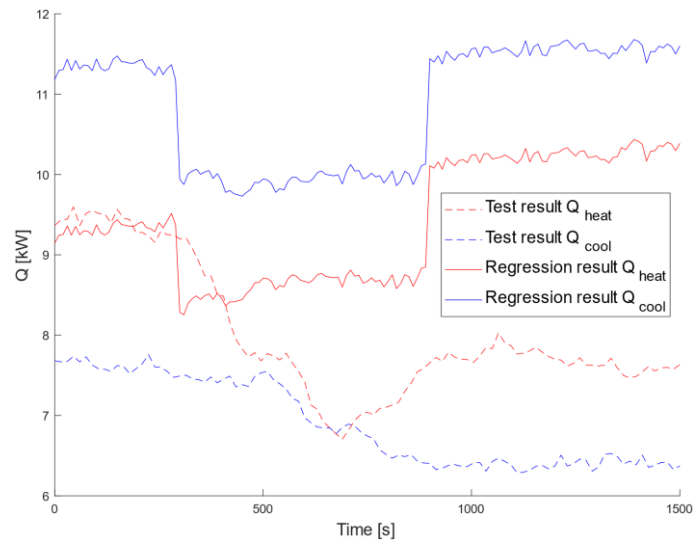


Figure F- 13 $Q_{heating}$ and $Q_{cooling}$ of test 9

Appendix G THERMAL ELECTRICAL NETWORK RESULTS

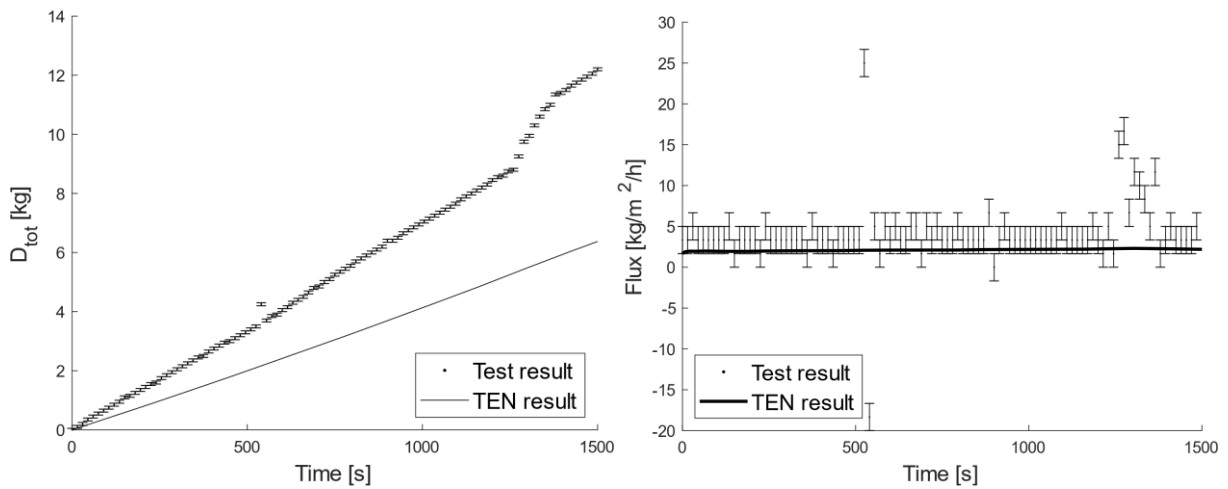


Figure G- 1 Test result of test 1. On the left the total production. On the right the flux.

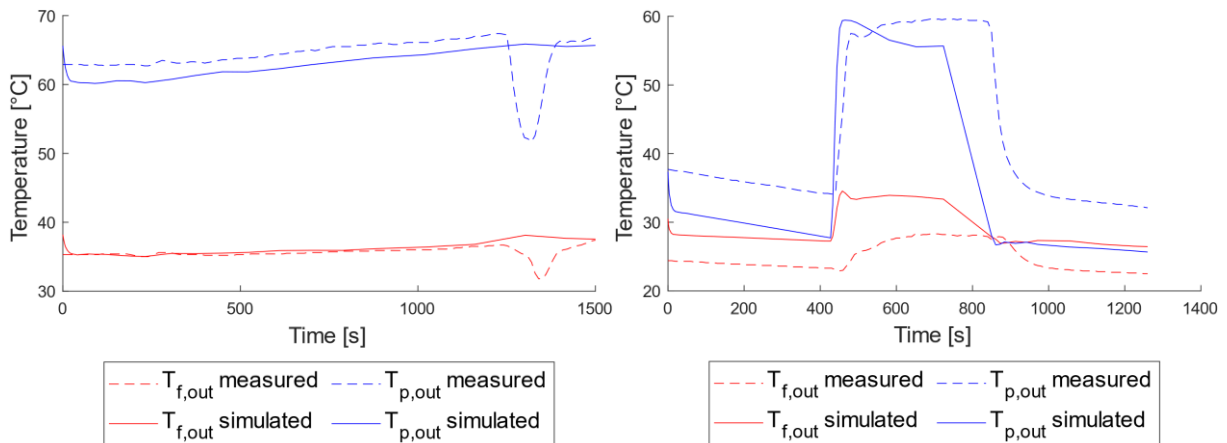


Figure G- 2 Test result of the temperatures of test 1 on the left and test 2 on the right

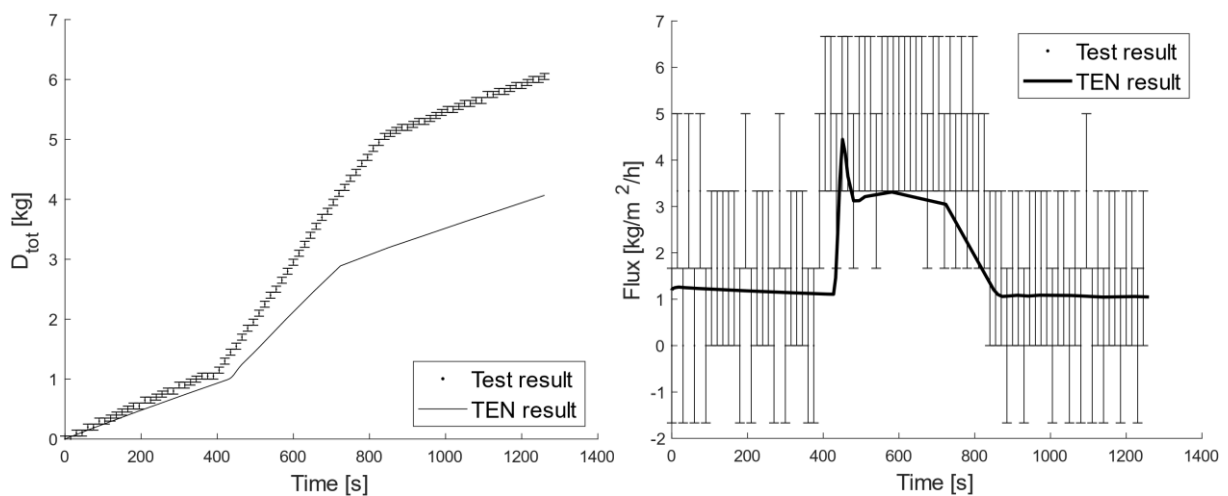


Figure G- 3 Test result of test 2. On the left the total production. On the right the flux.

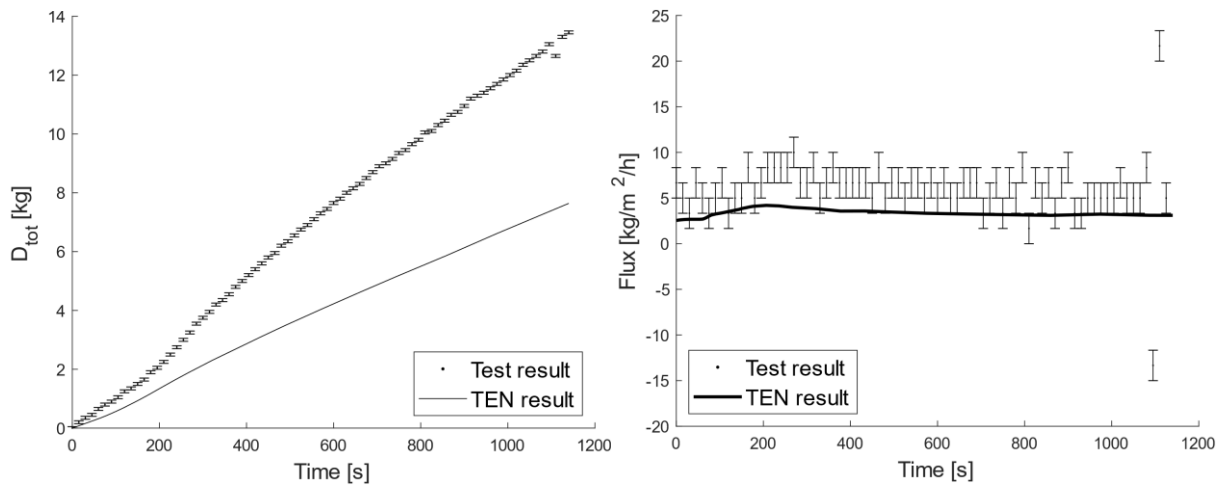


Figure G- 4 Test result of test 3. On the left the total production. On the right the flux.

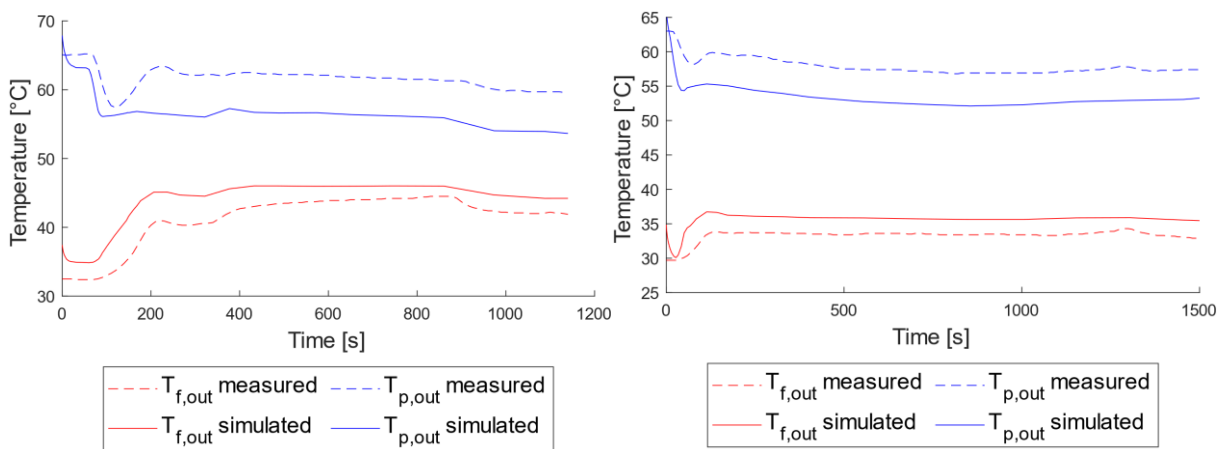


Figure G- 5 Test result of the temperatures of test 3 on the left and test 4 on the right.

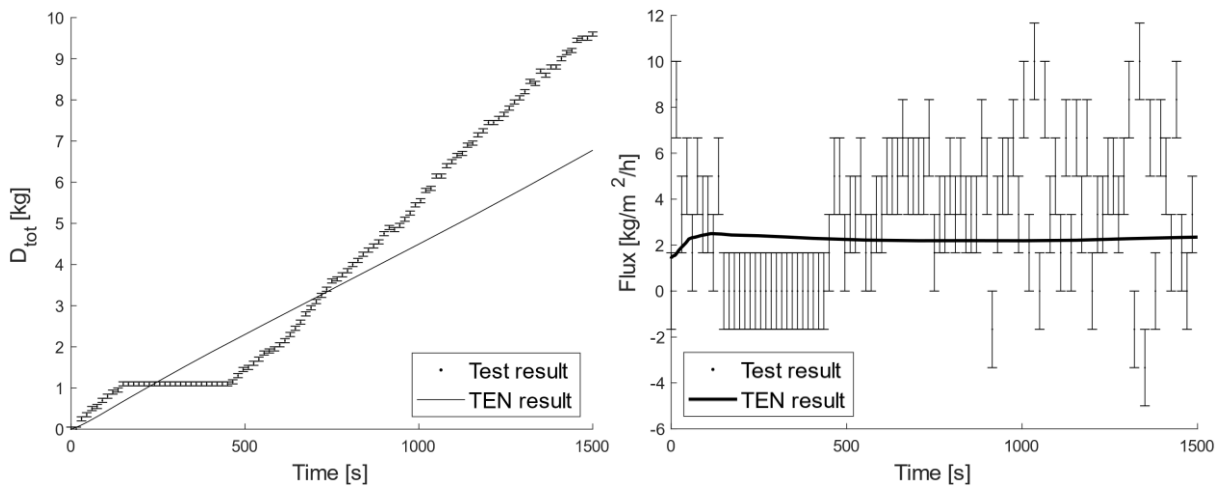


Figure G- 6 Test result of test 4. On the left the total production. On the right the flux.

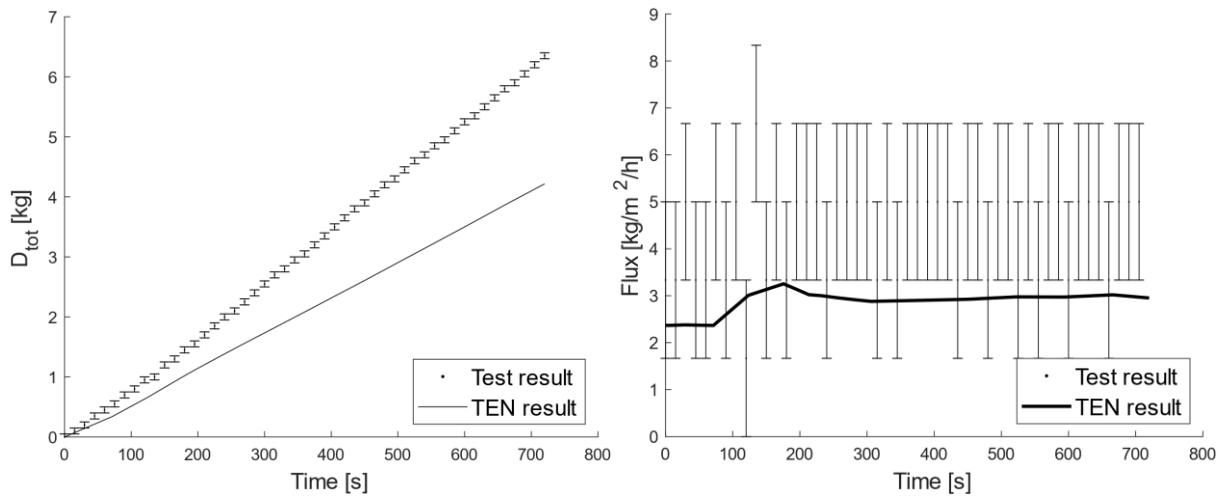


Figure G- 7 Test result of test 5. On the left the total production. On the right the flux.

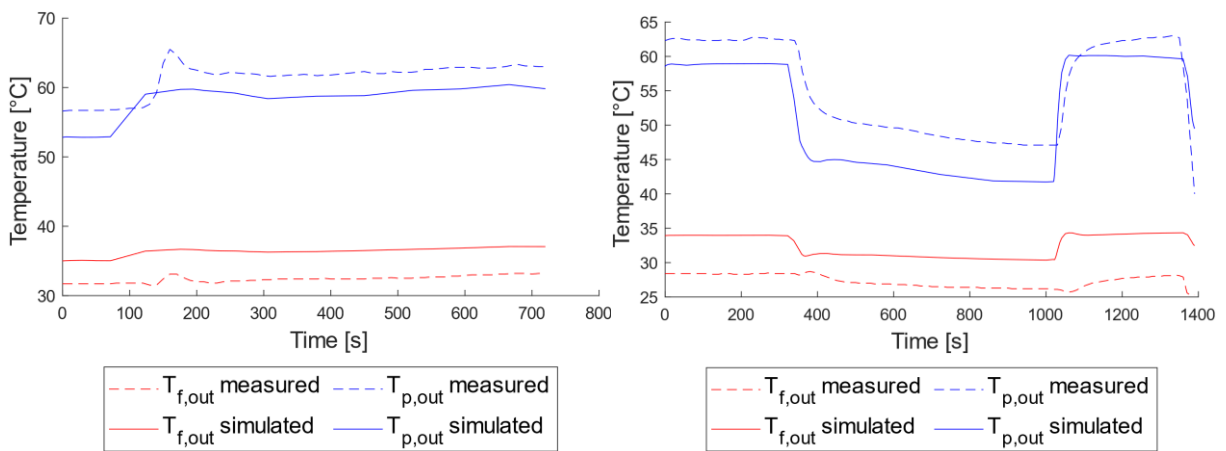


Figure G- 8 Test result of the temperatures of test 5 on the left and test 6 on the right

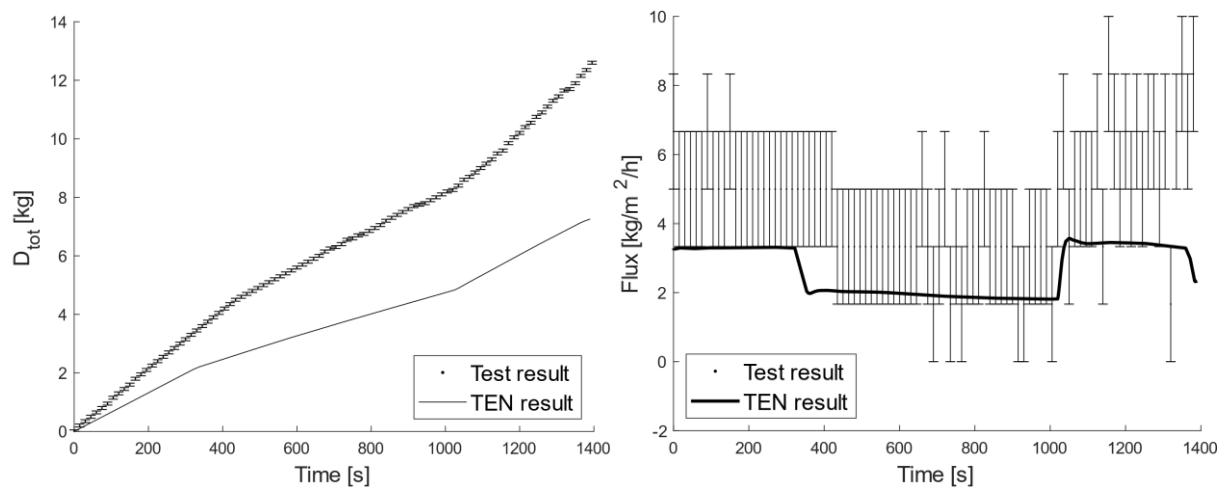


Figure G- 9 Test result of test 6. On the left the total production. On the right the flux.

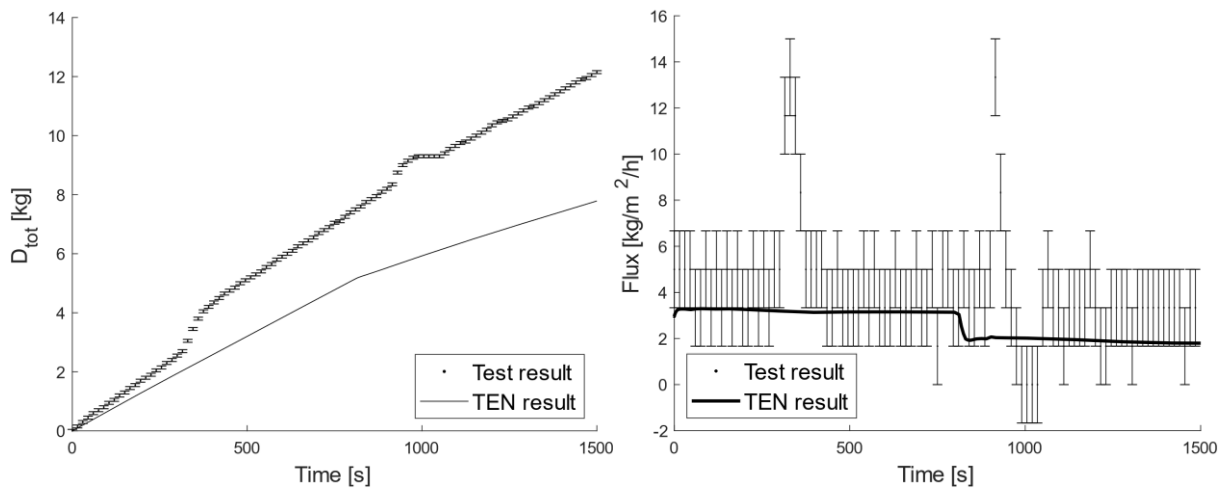


Figure G- 10 Test result of test 8. On the left the total production. On the right the flux.

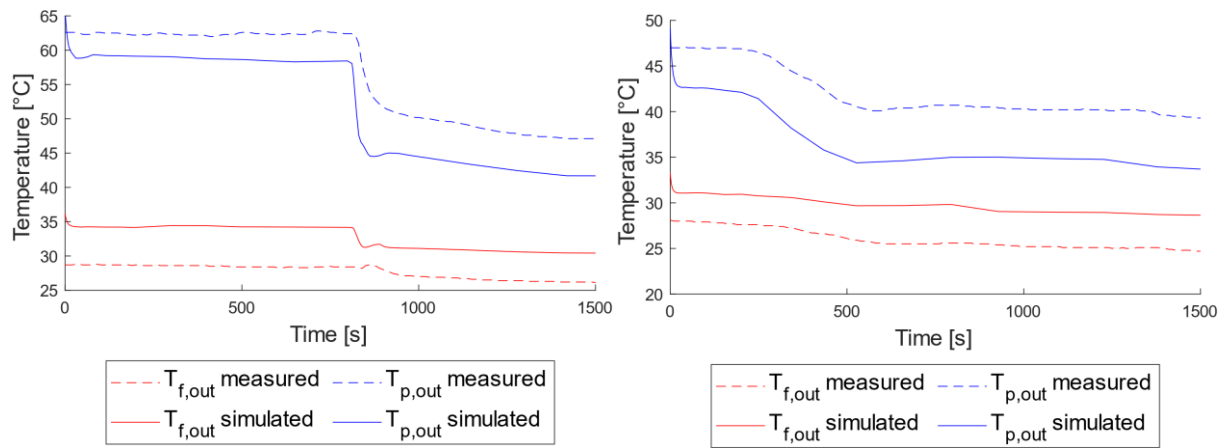


Figure G- 11 Test result of the temperatures of test 8 on the left and test 9 on the right.

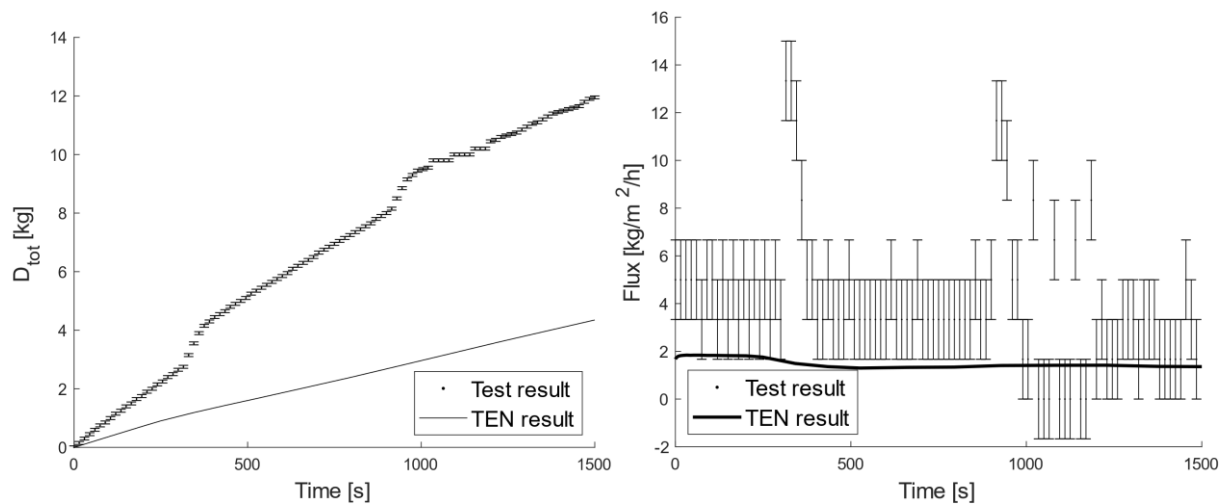


Figure E- 11 Test result of test 9. On the left the total production. On the right the flux.

Appendix H DYNAMIC ENERGY BALANCE EQUATIONS RESULTS

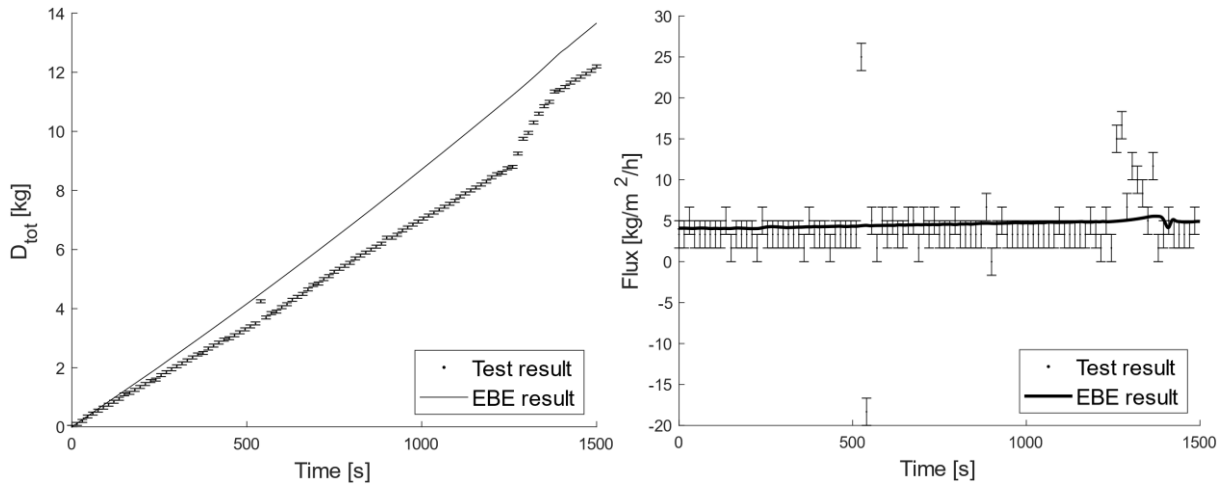


Figure H- 1 Test result of test 1. On the left the total production. On the right the flux.

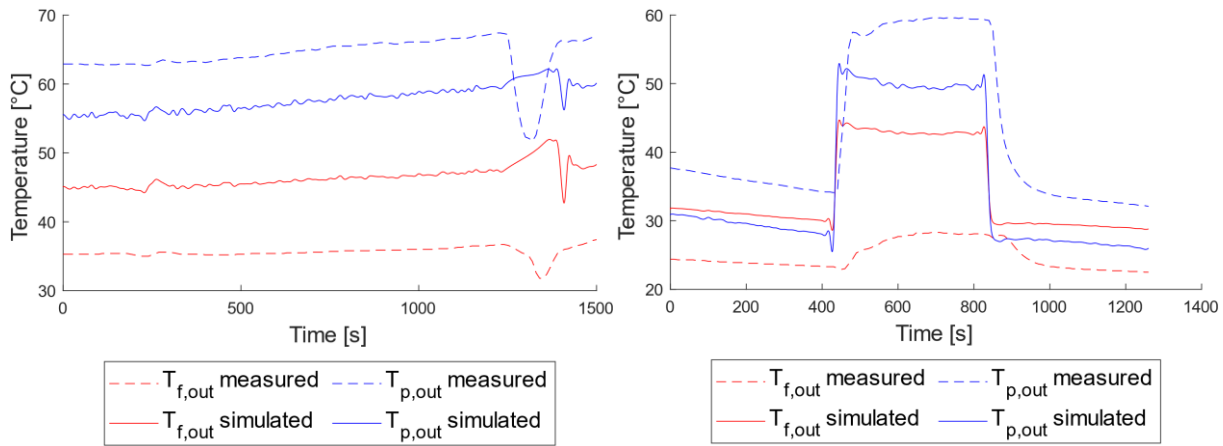


Figure H- 2 Test result of the temperatures of test 1 on the left and test 2 on the right.

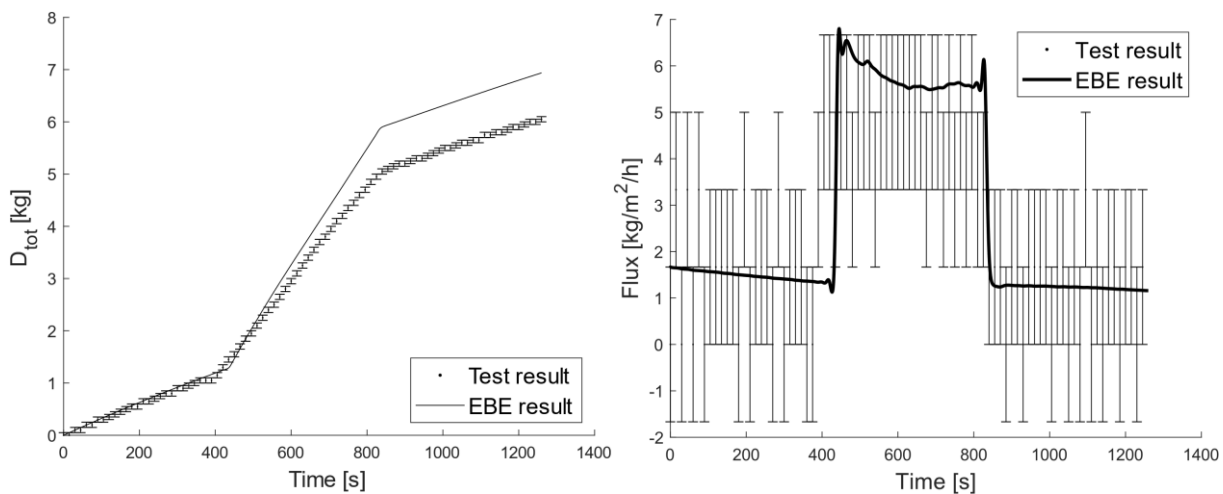


Figure H- 3 Test result of test 2. On the left the total production. On the right the flux.

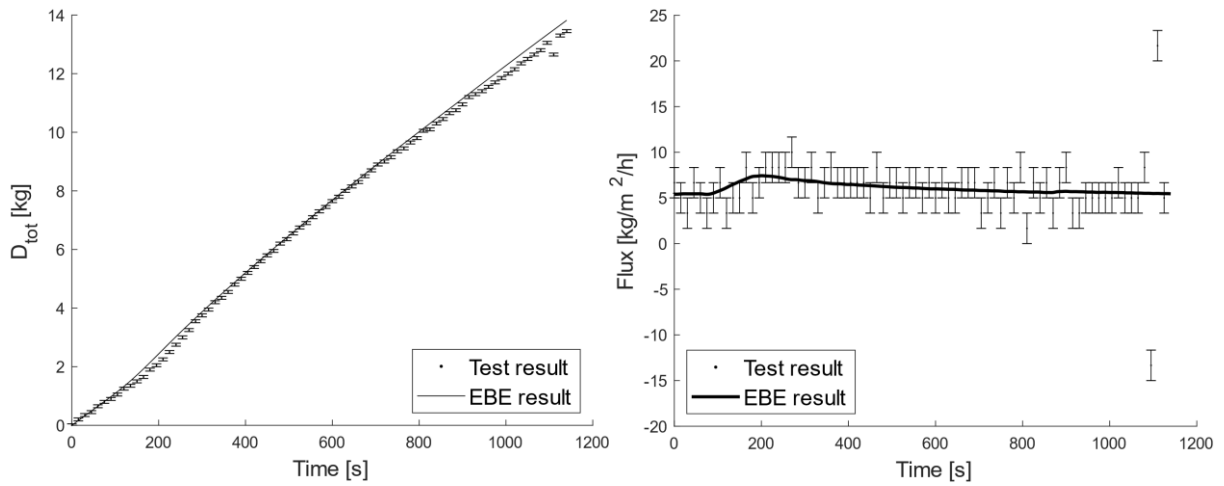


Figure H- 4 Test result of test 3. On the left the total production. On the right the flux.

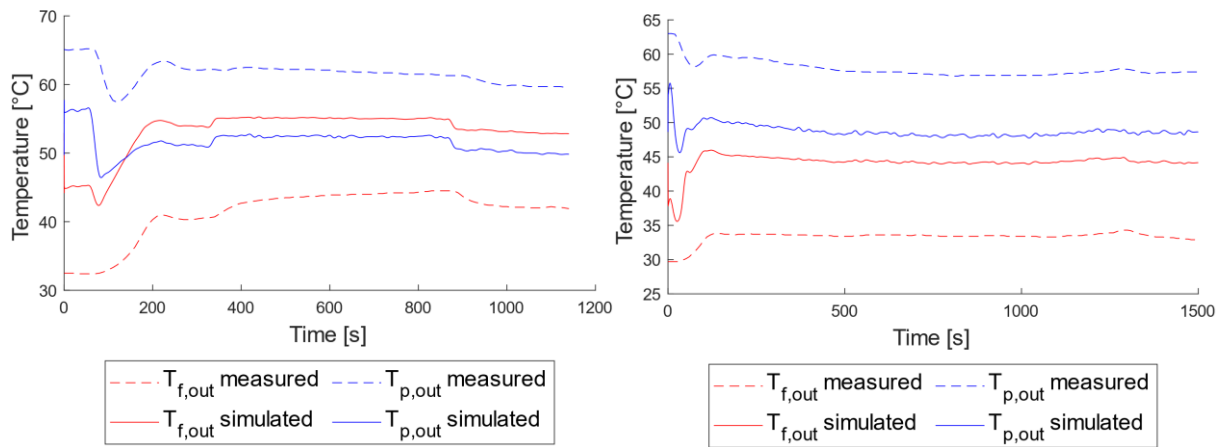


Figure H- 5 Test result of the temperatures of test 3 on the left and test 4 on the right

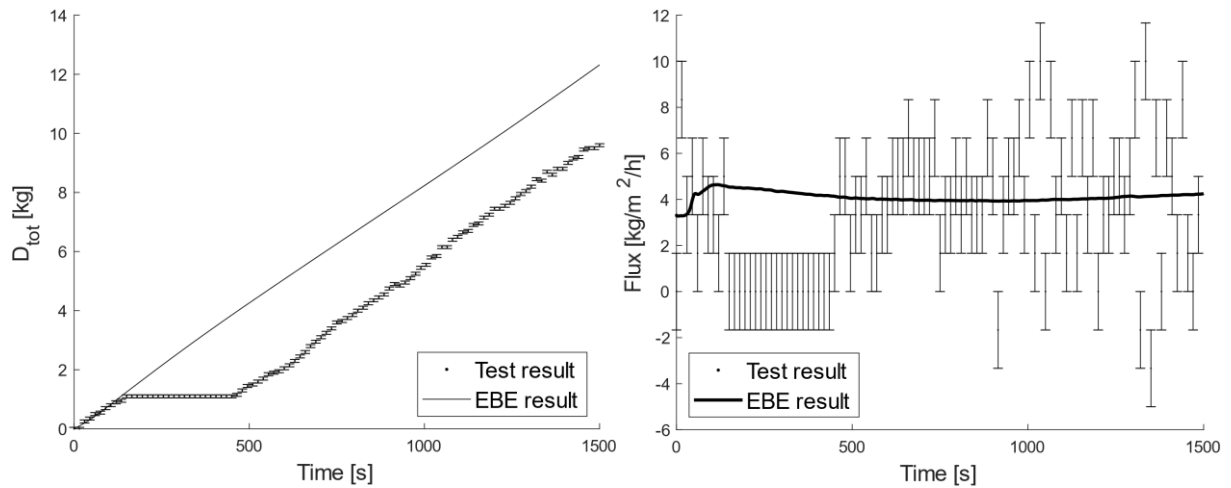


Figure H- 6 Test result of test 4. On the left the total production. On the right the flux.

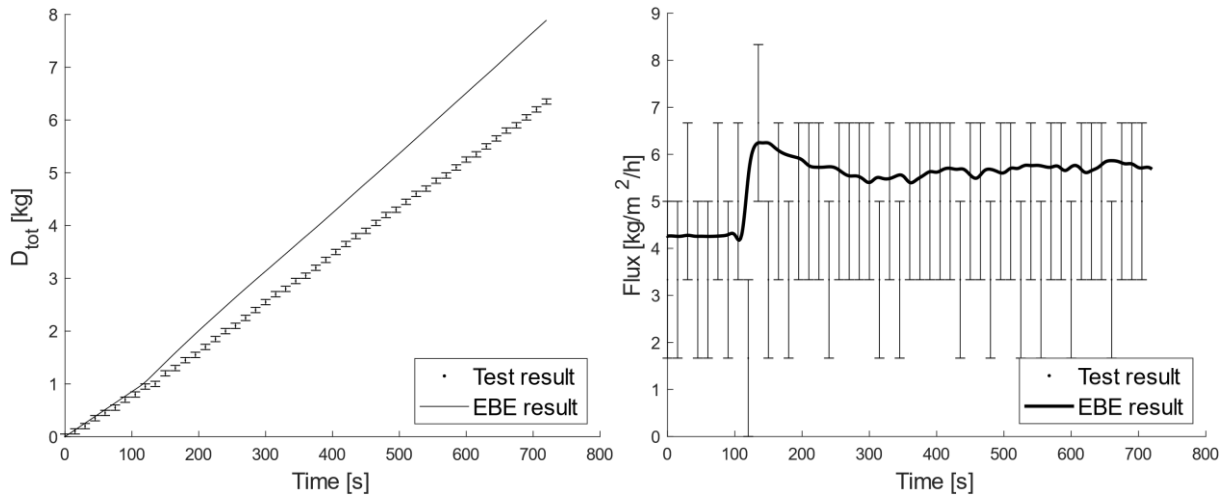


Figure H- 7 Test result of test 5. On the left the total production. On the right the flux.

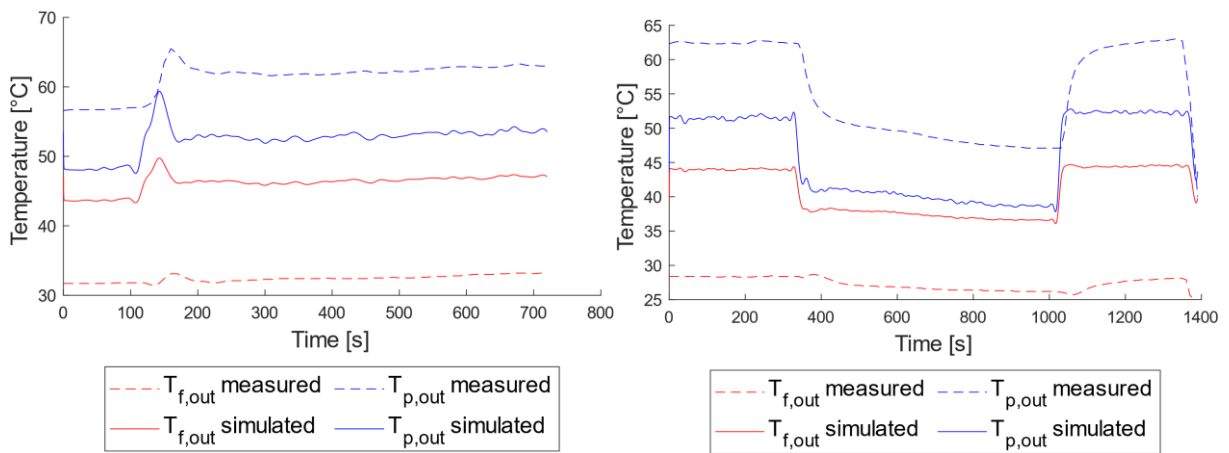


Figure H- 8 Test result of the temperatures of test 5 on the left and test 6 on the right

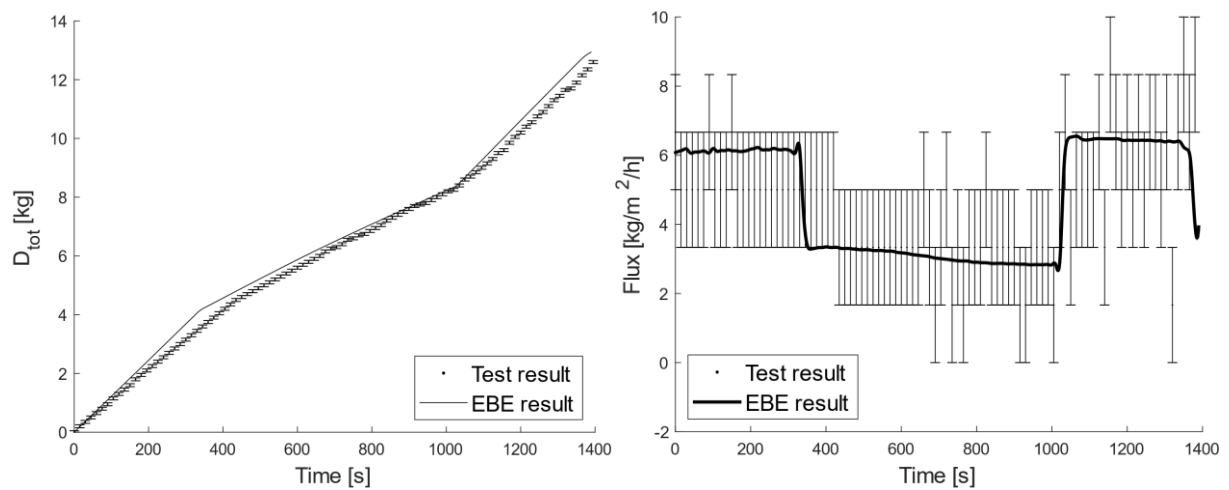


Figure H- 9 Test result of test 6. On the left the total production. On the right the flux.

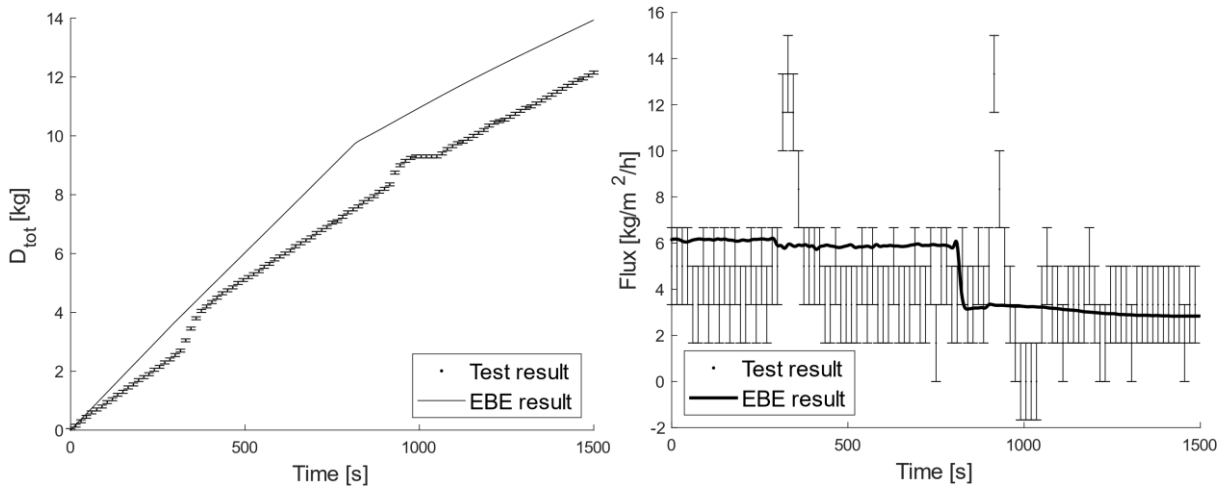


Figure H- 10 Test result of test 8. On the left the total production. On the right the flux.

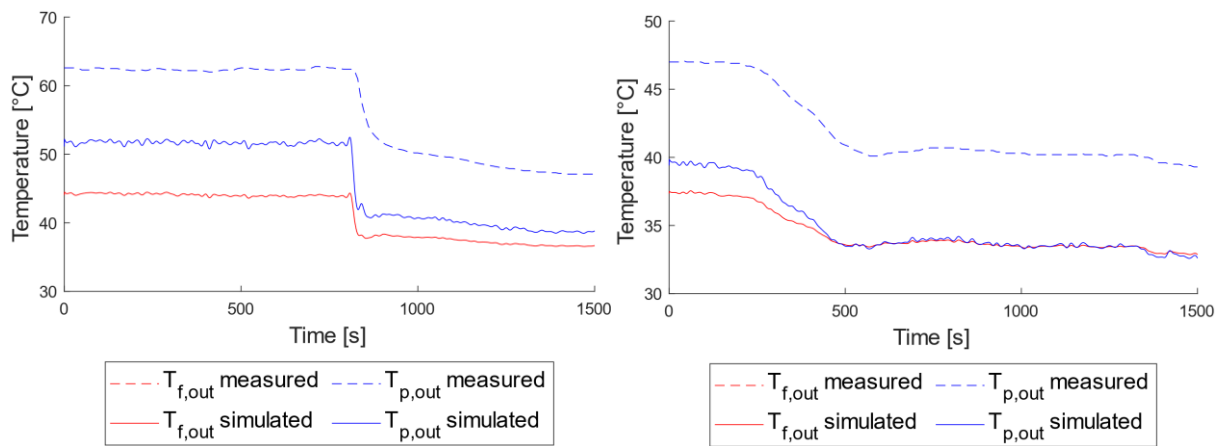


Figure H- 11 Test result of the temperatures of test 8 and test 9 on the right.

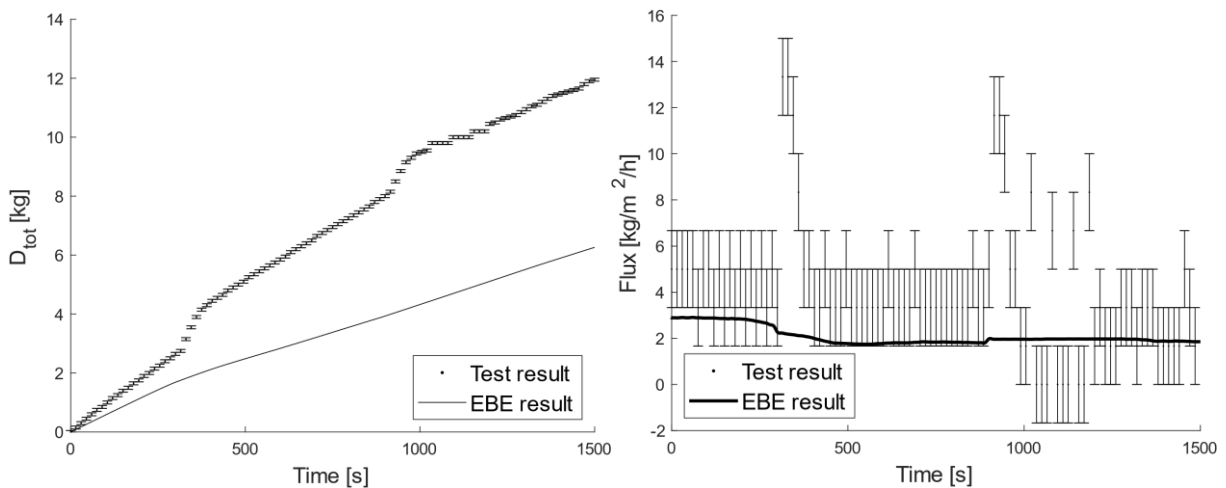


Figure H- 12 Test result of test 9. On the left the total production. On the right the flux.

FACULTY OF ENGINEERING TECHNOLOGY
GROUP T LEUVEN CAMPUS
Andreas Vesaliusstraat 13
3000 LEUVEN, België
tel. + 32 16 30 10 30
fet.groupt@kuleuven.be
www.fet.kuleuven.be

